MEASURED STATIC AND ROTORDYNAMIC CHARACTERISTICS OF A CIRCUMFERENTIALLY-GROOVED-STATOR/SMOOTH-ROTOR LIQUID ANNULAR SEAL: INFLUENCE OF VISCOSITY, ECCENTRICITY, PRESSURE, AND SPEED

A Thesis

by

Nathan David Eitrheim

Submitted to the Office of Graduate and Professional Studies of
Texas A&M University
in partial fulfillment of the requirements for the degree of

MASTER OF SCIENCE

Chair of Committee,	Dara W. Childs
Committee Members,	Luis San Andrés
	Karl Hartwig
Head of Department,	Andreas A. Polycarpou

December 2017

Major Subject: Mechanical Engineering

ABSTRACT

Circumferential grooves are often machined into annular seals to reduce leakage rates ($\dot{Q}$). For this study, a circumferentially-grooved annular seal (CGS) was tested with three different viscosity (μ) test fluids. In addition to varying μ; differential pressure (ΔP), rotor speed (ω), and static eccentricity (ε_o) were varied.

Tests are conducted to determine how static and rotordynamic characteristics of a CGS are affected by μ changes. The measured results are compared to predictions, and a smooth seal when applicable. Testing was conducted with three test fluids, ISO VG 2 (turbulent flow regime), VG 46 (laminar and turbulent flow), and VG 100 (laminar flow) oils. Speed was varied from 2-8 krpm, ΔP across the seal 2.07-8.27 bar, and ε_o from centered (0.00) to 0.80. Geometry of the CGS has a radial clearance (C_r) of 0.1905mm (7.5mils) with 15 equally spaced square grooves with a groove length and groove depth of 1.52 mm. Length to diameter ratio (L/D) is 0.5. Test fluid is supplied circumferentially and in the direction of rotor rotation to introduce pre-swirl at the seal inlet.

Increasing μ produced the following results: (1) decreasing $\dot{Q}$, (2) increasing direct and effective damping, and (3) increased direct virtual-mass. Direct stiffness was often negative. Cross-coupled stiffness was opposite in sign (destabilizing). For an ESP with CGSs, increasing μ is expected to lower the natural frequencies of the rotor system. Additionally, increasing μ is not expected to result in a rotor instability.

The VG 46 test results were significantly different from those of VG 2 and VG 100. Results for VG 46 at low ω, consisted of a low phase angle (angle between the applied static load vector and $\boldsymbol{\varepsilon_o}$), small cross-coupled stiffness, and small whirl frequency ratio. While these VG 46 results are consistent with themselves, this behavior was not observed in the VG 2 and VG 100 test results.

For the turbulent flow seal, grooves have the effect of reducing the rotordynamic coefficients, and reducing the dependence of the rotordynamic coefficients on ε_o (changes were generally small with changing ε_o) when compared to a smooth seal.

Static and rotordynamic characteristics were poorly predicated by the available turbulent-flow seal analysis code. For the laminar flow seal code used, $\dot{Q}$, cross-coupled stiffness (k), and

direct damping (*C*) were reasonably predicted. Direct stiffness (*K*), cross-coupled damping (*c*), and static load were poorly predicted.

ACKNOWLEDGEMENTS

I would like to thank all of the faculty, staff, and graduate students of the Texas A&M Turbomachinery Laboratory. The help received was invaluable and too extensive to thank everyone individually.

CONTRIBUTORS AND FUNDING SOURCES

Contributors

This work was supported by a thesis committee consisting of Professor Dara Childs and Professor Luis San Andrés of the Department of Mechanical Engineering and Professor Karl Hartwig of the Department of Material Science and Engineering.

Funding Sources

Funding for this research was provided by the Texas A&M Turbomachinery Laboratory.

NOMENCLATURE

$\boldsymbol{A_{ij}}$	Stator acceleration in frequency domain [L/T^2]
B	Depth of groove [L]
C	Direct Damping [FT/L]
c	Cross-coupled Damping [FT/L]
C_{eff}	Effective Damping [FT/L]
C_{ij}	Seal Damping Coefficient [FT/L]
C_r	Seal radial clearance [L]
D	Seal diameter [L]
$\boldsymbol{D_{ij}}$	Stator displacement in frequency domain [L]
e_o	Eccentricity [L]
F_s	Applied static force [F]
F_{sX}, F_{sY}	Applied static force components [F]
f_{rX}, f_{rY}	Fluid film dynamic reaction force components [F]
f_X, f_Y	Applied dynamic excitation force components [F]
$\boldsymbol{F_X}$, $\boldsymbol{F_Y}$	Dynamic excitation force components in frequency domain [F]
$\boldsymbol{H_{ij}}$	Dynamic stiffness in frequency domain[F/L]
$\boldsymbol{j}$	Complex number: $\sqrt{-1}$ [-]
K	Direct Stiffness [F/L]
k	Cross-coupled Stiffness [F/L]
K_{eff}	Effective Stiffness [F/L]
K_{eq}	Equivalent stiffness [F/L]
K_{ij}	Seal Stiffness Coefficient [F/L]
L	Seal axial length [L]
M	Direct Virtual-mass [M]
m	Cross-coupled Virtual-mass [M]
M_{ij}	Seal Virtual-mass Coefficient [M]
M_s	Stator mass [M]
$\dot{Q}$	Volumetric flow rate per seal [L^3/T]

R	Rotor Radius [L]
Re	Reynolds number [-]
Re_z	Axial Reynolds number [-]
Re_Θ	Circumferential Reynolds number [-]
v_{inlet}	Measured circumferential fluid velocity at a location upstream of the seal inlet [L/T]

Greek Symbols

ΔT	Temperature rise across the seal [Θ]
ΔP	Pressure Drop across the seal [F/L^2]
ΔX, ΔY	Relative displacement between rotor and stator [L]
ε_o	Eccentricity ratio, $\boldsymbol{e_o}/C_r$ [-]
ϕ	Applied static force phase angle [-]
μ	Dynamic fluid viscosity [FT/ L^2]
ρ	Fluid Density [M/L^3]
ω	Angular shaft speed [1/T]
Ω	Excitation frequency [1/T]

Abbreviations

CGS	Circumferentially Grooved Seal
ESP	Electric Submersible Pump
GS/SR	(Circumferentially) Grooved Stator / Smooth Rotor
PSR	Pre-Swirl Ratio, defined in Eq. (8)
SS/GR	Smooth Stator / (Circumferentially) Grooved Rotor
SS/SR	Smooth Stator / Smooth Rotor
WFR	Whirl Frequency Ratio

TABLE OF CONTENTS

Page

LIST OF FIGURES

Page

LIST OF TABLES

Page

1. INTRODUCTION

Pumps are used in many industries to move liquids from a relatively low pressure source to a more useful location through the use of a pressure gradient, which is supplied by the pump. Since fluid moves from regions of high to low pressure, sealing mechanisms are required to reduce backflow within the pump, which reduces the pump's efficiency. The simplest seal design is a plain annular seal and is commonly used as neck or wear ring, interstage, and balance piston seals [1]. While annular seals are similar in design to a plain journal bearing, their clearances are much larger than bearings. Typical journal bearings have clearance to radius ratios (C_r/R) of around 0.001 while annular seals are around 0.003-0.005 [1]. This larger clearance dramatically reduces the generation of forces due to the hydrodynamic effect (viscous fluid between two converging surfaces with relative motion between them). Henry Black was among the first to study the reaction forces generated by annular seals and show that these forces can affect rotor stability and response [2].

The hydrodynamic effect contributes to the generation of forces which results from viscous fluid flow between a rotating eccentric shaft and an annular clearance such as a bearing or seal. A high-pressure region develops in the converging section as fluid is "dragged" into a converging wedge. A low-pressure region develops in the diverging section (cavitation generally does not occur here in seals as it does in bearings).

In addition to the hydrodynamic effect, a centering force known as the Lomakin Effect acts on the rotor [3]. As depicted in Fig. 1, the Lomakin Effect results from an eccentric rotor where an increased clearance on one side results in an increased entrance pressure loss, with a smaller friction loss along the seal; the opposite side with the smaller clearance has a smaller entrance loss and a larger friction loss. The Pressure difference across the seal results in a centering force on the eccentric rotor [3].

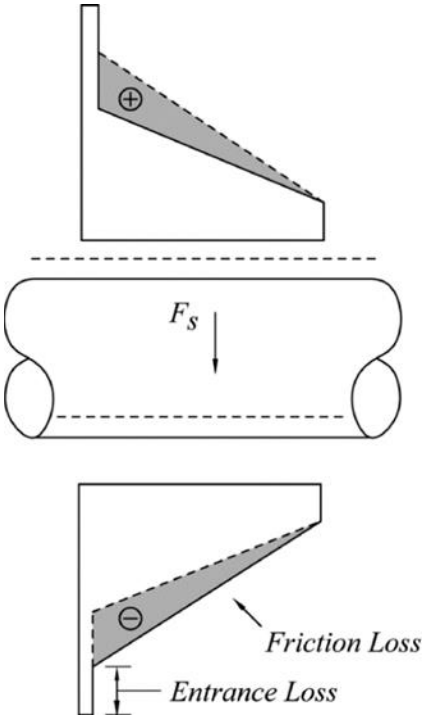

Figure 1 Depiction of the Lomakin Effect [1]

Most pumps are designed for a single operating condition and viscosity (μ) liquid. However, an ESP may see a wide range of μ over its useful life. ESPs are down-hole pumps used to lift oil to the surface and can have 20 or more stages. While seal reaction forces can be relatively weak, the long flexible shaft and large number of seals in ESPs means that the seals have a profound impact on pump rotordynamics. Reliability can be improved by reducing rotor vibration levels, which requires a better understanding of the forces generated by seals and their effect on rotor stability and response. The primary objective is to determine how static and rotordynamic characteristics of a circumferentially grooved seal (CGS) are affected by changing μ. This objective is achieved by measuring static and rotordynamic characteristics of a CGS at varying μ and operating conditions.

For small perturbations about an equilibrium position, reaction forces on the shaft can be modeled as

$$-\begin{Bmatrix} f_{rX} \\ f_{rY} \end{Bmatrix} = \begin{bmatrix} K_{XX}(\varepsilon_o) & K_{XY}(\varepsilon_o) \\ K_{YX}(\varepsilon_o) & K_{YY}(\varepsilon_o) \end{bmatrix} \begin{Bmatrix} \Delta X \\ \Delta Y \end{Bmatrix} + \begin{bmatrix} C_{XX}(\varepsilon_o) & C_{XY}(\varepsilon_o) \\ C_{YX}(\varepsilon_o) & C_{YY}(\varepsilon_o) \end{bmatrix} \begin{Bmatrix} \Delta \dot{X} \\ \Delta \dot{Y} \end{Bmatrix} + \begin{bmatrix} M_{XX}(\varepsilon_o) & M_{XY}(\varepsilon_o) \\ M_{YX}(\varepsilon_o) & M_{YY}(\varepsilon_o) \end{bmatrix} \begin{Bmatrix} \Delta \ddot{X} \\ \Delta \ddot{Y} \end{Bmatrix} \quad (1)$$

which was developed by Nelson and Nquyen [4,5] for a smooth seal and is an improvement on the work by Childs [6] for a smooth centered seal. The reaction force in the X direction is f_{rX} and

in Y is f_{rY}. Stiffness (K_{ij}), damping (C_{ij}), and Virtual-Mass (M_{ij}) coefficients are a function of the eccentricity ratio

$$\varepsilon_o = \frac{e_o}{C_r} \tag{2}$$

where e_o is the static eccentricity of the rotor. Diagonal terms of the coefficient matrices are the direct coefficients, the off diagonal terms are the cross-coupled coefficients. ΔX, ΔY; $\Delta \dot{X}$, $\Delta \dot{Y}$; $\Delta \ddot{X}$, and $\Delta \ddot{Y}$ are components of the relative displacement, velocity, and acceleration vectors between rotor and stator.

At the centered position, $\varepsilon_o = 0$, direct stiffness, $K_{XX} = K_{YY} = K$, and cross-coupled stiffness, $K_{XY} = -K_{YX} = k$. This same definition is applied to the direct and cross-coupled damping (C, c), and direct and cross-coupled virtual-mass (M, m) terms.

Whirl frequency ratio (WFR) is commonly used in both seals and journal bearings to characterize bearing and annular seal rotordynamic behavior and was first formulated by Lund [7] as

$$WFR^2 = \frac{(K_{eq}-K_{XX})(K_{eq}-K_{YY})-K_{XY}K_{YX}}{\omega^2(C_{XX}C_{YY}-C_{XY}C_{YX})}, \tag{3}$$

where ω is the shaft running speed, and the equivalent stiffness (K_{eq}) is

$$K_{eq} = \frac{K_{XX}C_{YY}+K_{YY}C_{XX}-K_{XY}C_{YX}-K_{YX}C_{XY}}{C_{XX}+C_{YY}}. \tag{4}$$

For a flexible rotor supported by hydrodynamic bearings, the WFR is used to find the onset speed of instability (OSI) by

$$OSI = \frac{\omega_{n1}}{WFR} \tag{5}$$

where ω_{n1} is the first natural frequency of the system.

San Andrés [8] formulated a WFR definition that includes cross-coupled virtual-mass terms (M_{XY}, M_{YX}) when they are not negligible. Measured results for the seal tested here found M_{XY} and M_{YX} to be opposite in sign (destabilizing). As a result, the WFR definition formulated by San Andrés is used. San Andrés's definition for WFR is given in Appendix B.

WFR does not provide a good comparison of stability characteristics between seals of different geometries. For this comparison, effective damping (C_{eff}) is often used and is defined as

$$C_{eff} = C - \frac{k}{\omega} + \frac{m}{\omega^2}. \tag{6}$$

This equation is only valid at the centered position, $\varepsilon_o = 0$. Direct damping resists rotor motion and therefore has a stabilizing effect. The destabilizing effect of *k* is subtracted from *C* to give a measure of total stabilizing/destabilizing forces in C_{eff}.

At $\varepsilon_o = 0$, the centering forces from both the Lomakin effect and Hydrodynamic effect is characterized by the effective stiffness

$$K_{eff} = K + c\omega - M\omega^2. \tag{7}$$

An increase in K_{eff} increases the pump rotor's natural frequencies.

Fluid rotation at the inlet of a seal has a significant impact on the destabilizing cross-coupled forces [9]. With circumferential fluid velocity at the seal inlet defined as v_{inlet}, and the rotor radius as *R*, the Pre-Swirl Ratio (PSR) is

$$PSR = \frac{v_{inlet}}{\omega R}. \tag{8}$$

In 1989 Iwatsubo et al. [10] developed a test rig for liquid annular seals and measured static and dynamic characteristics of several plain annular seals as well as the PSR. Iwatsubo et al. found that increasing PSR increased *k* and had a profound destabilizing effect on the system, which was consistent with the analysis of Black et al. in 1981 [9].

Many pump manufacturers machine circumferential grooves in annular seals to reduce seal leakage [11]. These grooves can be machined into either the rotor or stator. Marquette et al. [12] in 1997 measured flow rate ($\dot{Q}$) and rotordynamic coefficients for a high ΔP, high ω, grooved stator, smooth rotor (GS/SR) annular seal. They found that smooth stator, smooth rotor (SS/SR) seals have significantly better stability characteristics based on the C_{eff}, have higher K_{eff}, and leak more (particularly at lower speeds) than GS/SR seals. Moreland [13] measured static and rotordynamic characteristics, and PSR for a smooth stator, grooved rotor (SS/GR) liquid annular seal. Torres [14] measured static and rotordynamic characteristics, and PSR for a GS/SR liquid annular seal. Both Moreland and Torres found the CGS reduced all rotordynamic coefficients with the exception of cross-coupled damping and cross-coupled virtual-mass when compared to an equivalent SS/SR seal. Additionally, both Moreland and Torres often found negative direct stiffness coefficients for the CGS.

Florjancic and McCloskey [15] developed a three-control volume model for turbulent flow in 1990 to predict GS/SR static and rotordynamic characteristics and compared the predictions to measured results, finding that the model gave reasonable predicted values. In 1996, Marquette and Childs [16] improved on the three-control volume model by Florjancic by

accounting for diverging flow in the groove of the seal. Arghir and Frene [17] in 2004 developed a three-control volume bulk flow model that could be used to predict static and rotordynamic characteristics of a GS/SR at eccentric rotor positions. The models developed by [15–17] are for turbulent flow seals. Seals tested here in the turbulent flow regime are compared to predictions based on a bulk flow model by San Andrés et. al.[18].

Semanate and San Andrés [19] developed a grooved seal model for locked floating oil ring seals in 1994. This model was valid for laminar (as well as turbulent) flow in the seal. Unfortunately, the fundamental assumption of deep grooves that they employed has been shown not to be valid [20] by test results. In 2012, San Andrés and Delgado [21] improved on the analysis by Semanate and San Andrés by taking into account the effect of the groove by using an effective groove depth. Their model is only valid for laminar flow seals. Seals tested here in the laminar flow regime are compared to predictions based on the model by San Andrés and Delgado [21]. The code gave reasonable predictions, particularly at low ε_o.

2. STATEMENT OF WORK

The main object is to measure static and rotordynamic characteristics of a GS/SR liquid annular seal as μ of the working fluid is varied. Three test fluids are used; ISO VG 2, ISO VG 46, and ISO VG 100. The seal is tested at four speeds; 2, 4, 6, and 8 krpm. Each ω case is tested at four Δ*Ps*; 2.07, 4.14, 6.21, and 8.27 bar. Each Δ*P* case is tested at four ε_o values; 0.00 (centered), 0.27, 0.53, and 0.80. This results in a total of 192 test points. Static measurements include; $\dot{Q}$, e_o, applied static load, and PSR. Dynamic measurements include; excitation forces, acceleration, and relative displacement. These dynamic measurements are used to calculate rotordynamic coefficients (K_{ij}, C_{ij}, and M_{ij}), WFR, K_{eff}, and C_{eff}.

Geometry of the test seal can be seen in Fig. 2. Fifteen equally spaced square grooves are machined into the annular seal with an *L*/*D* (length/diameter) ratio of 0.5. The seal has a (minimum) nominal radial clearance (C_r) of 0.2032mm (8mils).

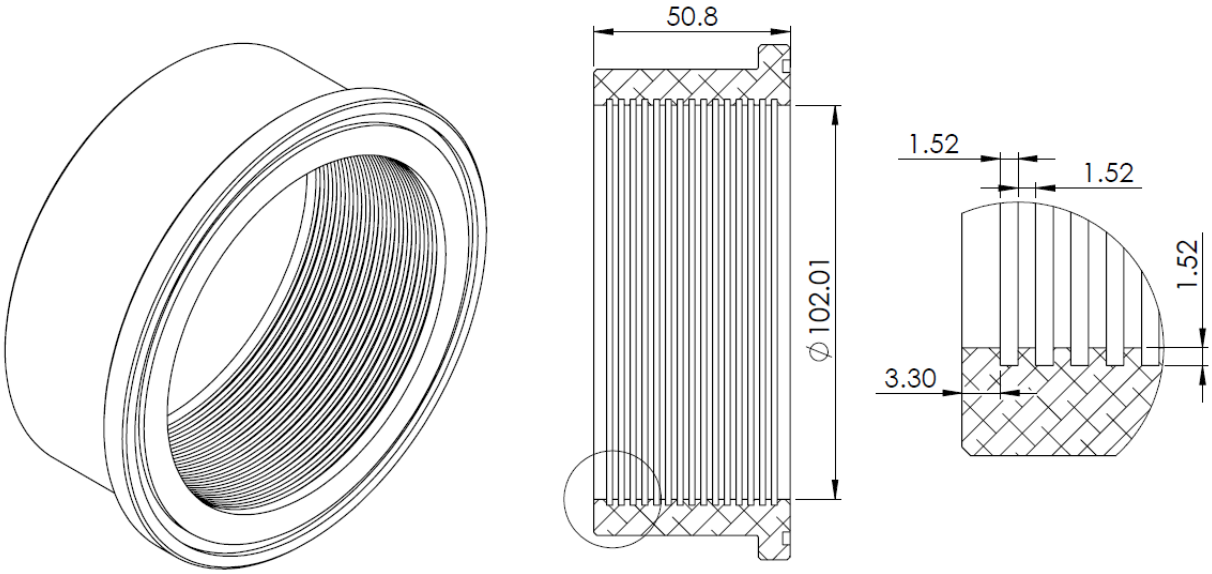

Figure 2 Test seal geometry and cross section, dimensions in mm

In ESPs, grooves in the seals are used to reduce $\dot{Q}$ and increase efficiency, however, this may be detrimental to rotor stability and pump reliability. In an ESP, grooves are generally

machined into the stator. ESPs are uncommon in that the pumped liquid may vary over the life of the pump [11].

This study intends to determine how seal static and rotordynamic characteristics are affected by changes in μ in a GS/SR. To the author's knowledge, the impact of changing μ on the characteristics of a GS/SR have not been previously reported.

3. TEST RIG DESCRIPTION

3.1 Test Rig Assembly

The test rig was originally designed for measuring rotordynamic coefficients of annular bushing oil seals by Kaul [22]. The rig uses the "shake the stator" design developed by Glienicke in 1966 [23]. Fig. 3 shows a cross section of the test rig which is driven by a variable frequency drive electric motor. Hydraulic shakers are used to adjust the static position as well as dynamically excite the stator (discussed further in section 5).

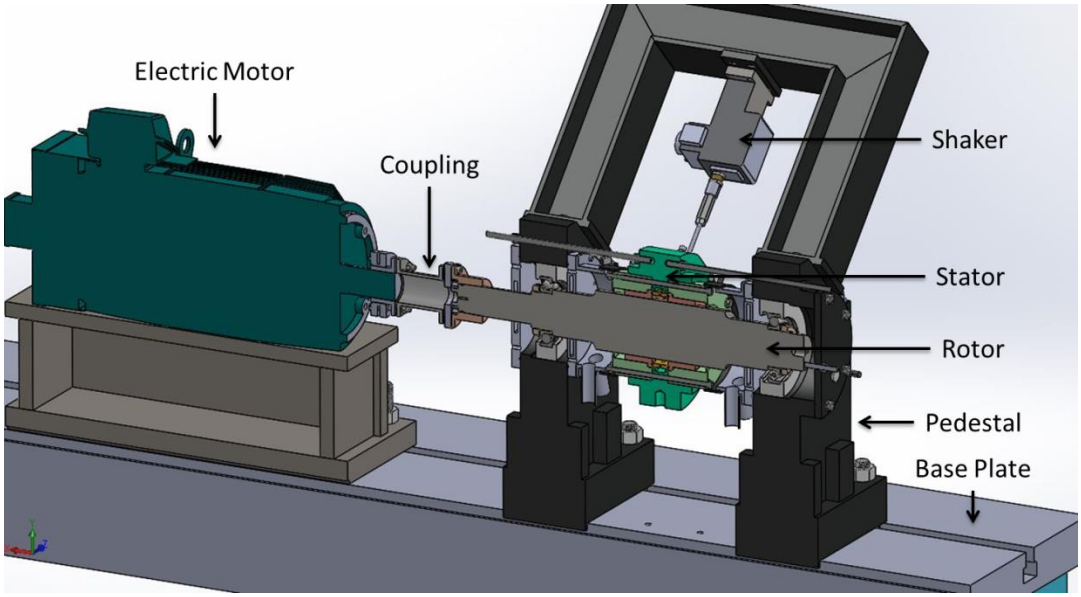

Figure 3 Test rig cross section

A cross section of the stator section can be seen in Fig. 4. Two hybrid ceramic ball bearings support the rotor to minimize rotor movement, and pitch stabilizers are used to keep the stator centerline parallel to the rotor centerline [22].

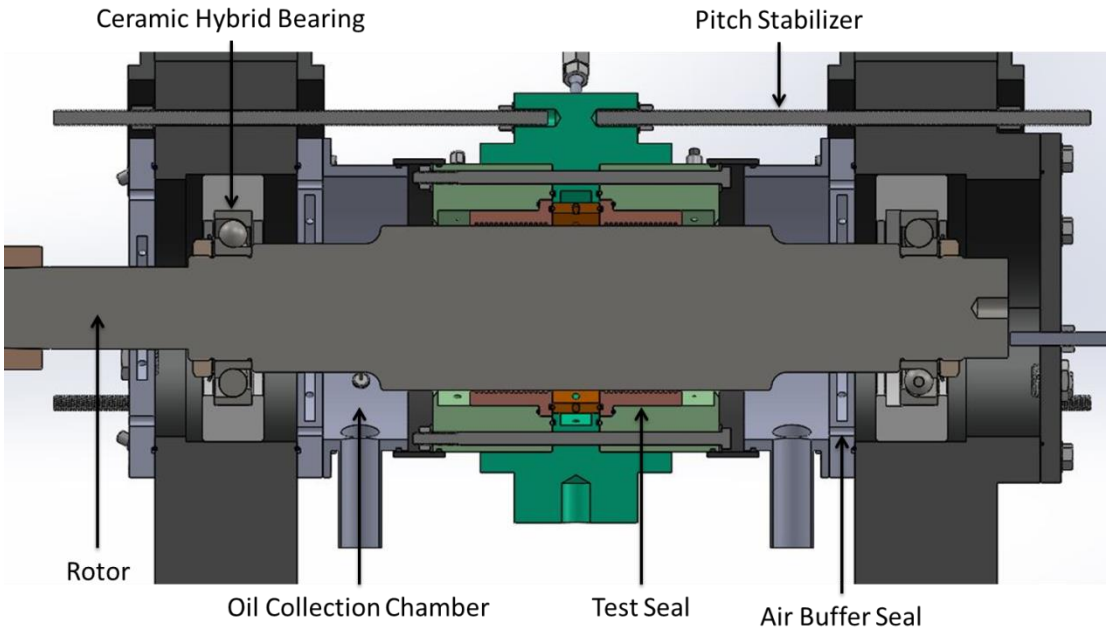

Figure 4 Test rig stator cross section

As seen in Fig. 5, the seal holder uses a swirl insert to inject the test fluid tangentially and in the direction of rotor rotation. Test fluid then flows across the two test seal sections, past a single tooth labyrinth seal to prevent air entering the seal, and then into the oil collection chamber. The stator housing floats and is moved by the shaker assembly. The oil collection chamber is stationary, and a flexible rubber gasket is used to seal between the two components.

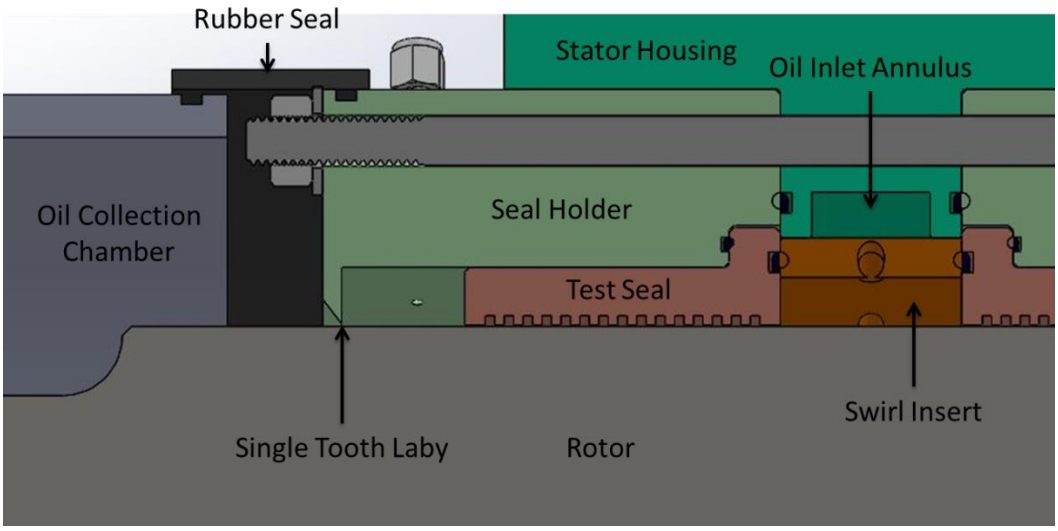

Figure 5 Test rig seal housing cross section

As seen in Fig. 6, the swirl insert has 12 holes with diameters of 4.1 mm and are at an angle of 30° from the tangent. The swirl insert has a diameter of 117 mm and a width of 29 mm.

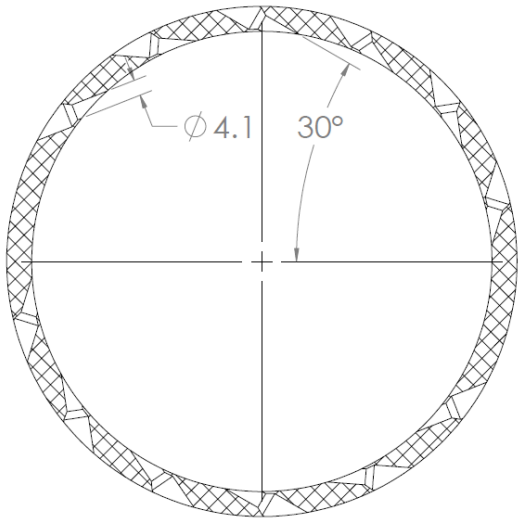

Figure 6 Swirl insert cross-sectional view, dimensions in mm

3.2 Test Rig Instrumentation

Rotor speed is measured with a proximity probe, which detects the passing of a notch machined into the rotor. Pressure transducers at the inlet and both outlets are used to calculate the ΔP across the test seal. Thermocouples at the inlet and outlet are used to measure the test fluid temperature. Proximity probes measure the relative displacement between the stator and rotor to calculate the ε_o of the rotor relative to the stator.

Accelerometers, load cells, and proximity probes in the *X* and *Y* direction measure stator acceleration, reaction forces, and relative displacements in their respective coordinates as the stator is excited. Fig. 7 depicts instrumentation on the stator and their locations.

Instrumentation uncertainty values are given in Table 1.

Table 1 Instrumentation measurement uncertainties

Instrument	Uncertainty
Thermocouple	±0.75%
Pressure Transducer	±1%
Accelerometer	±1%
Proximity Probes	±0.4%
Load Cells	±0.5%
Pitot Tube Differential Pressure	±0.15%

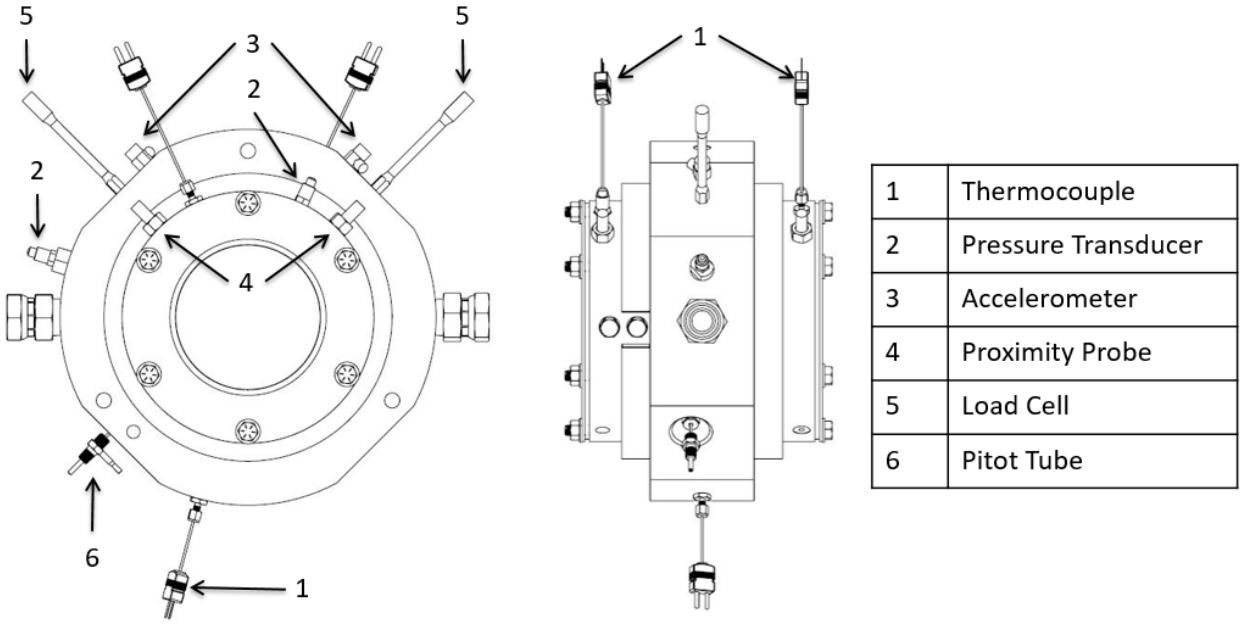

1	Thermocouple
2	Pressure Transducer
3	Accelerometer
4	Proximity Probe
5	Load Cell
6	Pitot Tube

Figure 7 Stator instrumentation locations viewed from the non-drive end and side

Circumferential fluid velocity is measured with the differential pressure of a pitot tube as seen in Fig. 8. The pitot tube is tangential to the rotor, flush with the seal (such that the distance between the pitot tube and the rotor is C_r), and located 2.54 mm upstream from the inlet of the seal, which is off the centerline of the swirl insert. v_{inlet} is calculated from this differential pressure and used to calculate PSR in Eq. (8).

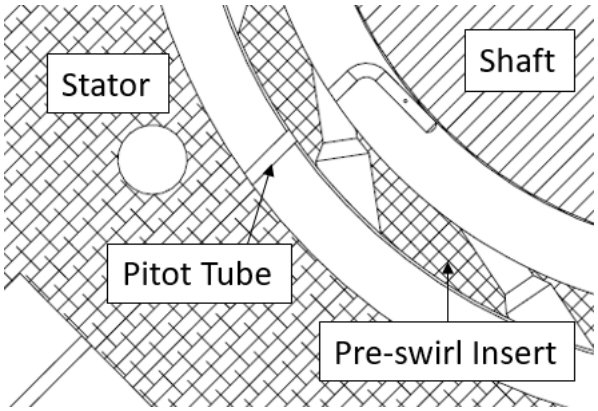

Figure 8 Pitot tube pre-swirl measurement

4. PRELIMINARY MEASUREMENTS

4.1 “Cold” Clearance

At ambient temperature, the stator is moved in a circular orbit around the shaft with the seal in contact with the rotor at all times for a complete precession circle. This circular path as measured by the proximity probes is used to find the relative center of the seal.

4.2 “Hot” Clearance

The test fluid is heated to the test temperature of 46.1°C (115°F) and run through the test rig until thermal equilibrium is reached between the test fluid and test section. Temperature of the oil at the inlet is controlled to within ±1.1°C (±2°F). Oil is shutoff, and a clearance measurement is taken immediately after shutdown using the same procedure as the cold clearance. This measured C_r is used for defining rotor ε_o and accounts for thermal growth of the test rig.

4.3 Baseline Dynamic Measurements

Before any oil has been run through the system, a baseline measurement is taken to find the mass, stiffness, and damping characteristics of the test rig assembly (alone, without seal forces). The stator is excited at approximately 10% of the C_r at multiple frequencies (see section 5.2 for a further discussion). The initial dry measured properties are later subtracted from the wet test measurements in the data analysis step, producing only the fluid-film reaction forces.

5. STATIC AND DYNAMIC TEST MEASUREMENTS

5.1 Static Measurements

With test fluid flowing through the test section, the desired ω is set. Using the hydraulic shaker system, the rotor is brought to the desired ε_o based on the hot clearance measurements. Desired ΔP is obtained by adjusting $\dot{Q}$. Once steady state for the desired test point is obtained, ω, X and Y relative stator displacement, inlet and outlet pressure, inlet and outlet temperature, applied static forces (f_{sX} and f_{sY}), and υ_{inlet} are recorded by the data acquisition system (DAQ).

5.2 Dynamic Measurements

Using the method outlined by Rouvas and Childs [24], the stator is excited with a pseudo-random periodic signal that has been optimized to minimize the peak excitation force required. The stator is excited at 10% of C_r in two orthogonal directions independently; the excitation lasts 0.1024 seconds and is repeated 32 times in each direction. $\Delta\ddot{X}$, $\Delta\ddot{Y}$; ΔX, ΔY; and dynamic excitation forces (f_X and f_Y) are measured and sampled by the DAQ at 10kHz. Dynamic data is broken into and stored as four separate, equal duration, sets of data; which are used for a repeatability analysis.

6. STATIC DATA ANALYSIS

For both static and rotordynamic characteristics, uncertainty in the measurement is calculated with the method discussed in detail in Appendix C. In the uncertainty analysis, only repeatability of the measurement is calculated, instrumentation error is assumed to be negligible. For the static measurements (with the exception of static forces), uncertainties were at least an order of magnitude lower than the measured value. As a result, only static force uncertainties are presented for the static measurements.

6.1 Temperature Rise

Temperature rise (ΔT) due to viscous heating of the fluid is calculated as

$$\Delta T = \frac{T_{out1}+T_{out2}}{2} - T_{in} \tag{9}$$

where T_{out1} and T_{out2} are the seal outlet temperatures and T_{in} is the seal inlet temperature as measured by thermocouples at these locations.

6.2 Reynolds Number

To determine the flow regime of the test fluid in the seal, the Reynolds Number is calculated. Axial Reynolds Number (Re_z) is calculated from

$$Re_z = \rho 2(C_r + B)w/\mu \, , \tag{10}$$

where ρ is the fluid density, B is the groove depth, and

$$w = \dot{Q}/A \, . \tag{11}$$

Here, A is the cross-sectional area of the annulus

$$A = 2\pi R(B + C_r) \, . \tag{12}$$

Circumferential Reynolds Number (Re_Θ) is calculated from

$$Re_\theta = \rho R\omega(C_r + B)/\mu \, . \tag{13}$$

Magnitude of the resultant Reynolds Number (Re) is

$$Re = \sqrt{{Re_z}^2 + {Re_\theta}^2} \, . \tag{14}$$

This formulation of Re applies for flow within the groove, and not the lands of the seal. The fluid properties μ and ρ are determined by the average fluid temperature in the seal.

6.3 Pre-swirl Ratio

A pitot tube and differential pressure transducer is used to measure the differential pressure between the static and dynamic pressure of the fluid at the inlet of the seal in the circumferential direction. The fluid velocity is calculated using

$$v_{inlet} = \sqrt{\frac{2\Delta P_u}{\rho}} \tag{15}$$

where ΔP_u is the differential pressure of the pitot tube.

7. DYNAMIC DATA ANALYSIS

7.1 Rotordynamic Coefficients

Rotordynamic coefficients are calculated using a method outlined by Childs and Hale [25]. Beginning with the equations of motion (EOM) for the system,

$$M_s \begin{Bmatrix} \ddot{X}_s \\ \ddot{Y}_s \end{Bmatrix} = \begin{Bmatrix} f_X \\ f_Y \end{Bmatrix} + \begin{Bmatrix} f_{rX} \\ f_{rY} \end{Bmatrix} \tag{16}$$

where M_s is the mass of the stator, and $\ddot{X}_s$ and $\ddot{Y}_s$ are the measured stator accelerations. Combining Eqs. (1) and (16) gives

$$\begin{Bmatrix} f_X \\ f_Y \end{Bmatrix} - M_s \begin{Bmatrix} \ddot{X}_s \\ \ddot{Y}_s \end{Bmatrix} = \begin{bmatrix} K_{XX}(\varepsilon_o) & K_{XY}(\varepsilon_o) \\ K_{YX}(\varepsilon_o) & K_{YY}(\varepsilon_o) \end{bmatrix} \begin{Bmatrix} \Delta X \\ \Delta Y \end{Bmatrix} + \begin{bmatrix} C_{XX}(\varepsilon_o) & C_{XY}(\varepsilon_o) \\ C_{YX}(\varepsilon_o) & C_{YY}(\varepsilon_o) \end{bmatrix} \begin{Bmatrix} \Delta \dot{X} \\ \Delta \dot{Y} \end{Bmatrix} + \begin{bmatrix} M_{XX}(\varepsilon_o) & M_{XY}(\varepsilon_o) \\ M_{YX}(\varepsilon_o) & M_{YY}(\varepsilon_o) \end{bmatrix} \begin{Bmatrix} \Delta \ddot{X} \\ \Delta \ddot{Y} \end{Bmatrix}. \tag{17}$$

Measured time domain data is converted to the frequency domain using a Discrete Fourier Transform to produce

$$\begin{Bmatrix} \boldsymbol{F_X - M_S A_X} \\ \boldsymbol{F_Y - M_S A_Y} \end{Bmatrix} = \begin{bmatrix} \boldsymbol{H_{XX}} & \boldsymbol{H_{XY}} \\ \boldsymbol{H_{YX}} & \boldsymbol{H_{YY}} \end{bmatrix} \begin{Bmatrix} \boldsymbol{D_X} \\ \boldsymbol{D_Y} \end{Bmatrix} \tag{18}$$

where $\boldsymbol{F_X}$ and $\boldsymbol{F_Y}$ are the excitation force components, $\boldsymbol{A_X}$ and $\boldsymbol{A_Y}$ are the acceleration components, and $\boldsymbol{D_X}$ and $\boldsymbol{D_Y}$ are the displacement components in the frequency domain. The dynamic stiffness' ($\boldsymbol{H_{ij}}$) are related to the rotordynamic coefficients by

$$\boldsymbol{H_{ij}} = K_{ij} - \Omega^2 M_{ij} + \boldsymbol{j}(\Omega C_{ij}) \tag{19}$$

where Ω is the excitation frequency, and $\boldsymbol{j} = \sqrt{-1}$.

For excitations in two orthogonal directions, the EOM can be written in matrix form as

$$\begin{bmatrix} \boldsymbol{F_{XX} - M_S A_{XX}} & \boldsymbol{F_{XY} - M_S A_{XY}} \\ \boldsymbol{F_{YX} - M_S A_{YX}} & \boldsymbol{F_{YY} - M_S A_{YY}} \end{bmatrix} = \begin{bmatrix} \boldsymbol{H_{XX}} & \boldsymbol{H_{XY}} \\ \boldsymbol{H_{YX}} & \boldsymbol{H_{YY}} \end{bmatrix} \begin{bmatrix} \boldsymbol{D_{XX}} & \boldsymbol{D_{XY}} \\ \boldsymbol{D_{YX}} & \boldsymbol{D_{YY}} \end{bmatrix}. \tag{20}$$

From here, $\boldsymbol{H_{ij}}$ can be calculated from Eq. (20). The baseline $\boldsymbol{H_{ij}}$ is subtracted from the calculated $\boldsymbol{H_{ij}}$ of the test point to give just the dynamic stiffness of the fluid film. This result is then divided by two to get the result for an individual seal. A repeatability analysis of the data is discussed further in Appendix C.

7.2 Curve Fit and Rotordynamic Coefficients

Rotordynamic coefficients are calculated by using a least-squares regression curve fit of the $\boldsymbol{H_{ij}}$ data. First, the $\boldsymbol{H_{ij}}$ data is broken into the real and imaginary components where

$$\mathrm{Re}\left(\boldsymbol{H_{ij}}\right) = K_{ij} - \Omega^2 M_{ij} = K_{ij} - \Lambda M_{ij} \qquad \mathrm{Im}(\boldsymbol{H_{ij}}) = \Omega C_{ij}\ . \tag{21}$$

Next, a linear curve fit as described by Beckwith et al. [26] is applied to the real and imaginary components individually in the form

$$y(x_i) = a + bx_i \tag{22}$$

where (x_i) is the measured inputs and $y(x_i)$ are the calculated outputs. The coefficients a and b are defined as

$$a = \frac{\sum y_i \sum x_i^2 - \sum x_i \sum x_i y_i}{n\sum x_i^2 - (\sum x_i)^2} \qquad b = \frac{n\sum x_i y_i - \sum x_i \sum y_i}{n\sum x_i^2 - (\sum x_i)^2}\ . \tag{23}$$

As seen in Figs. 9 and 10, the curve fit is in close agreement with the measured data. High frequency points with excessive uncertainties were dropped from the analysis (such as the points at 170Hz). The range of frequencies used for the curve fit was at least 1.5 times the running speed depending on the test point. K_{ij} is obtained from the y-intercept, and M_{ij} is obtained from the curvature of Re($\boldsymbol{H_{ij}}$).

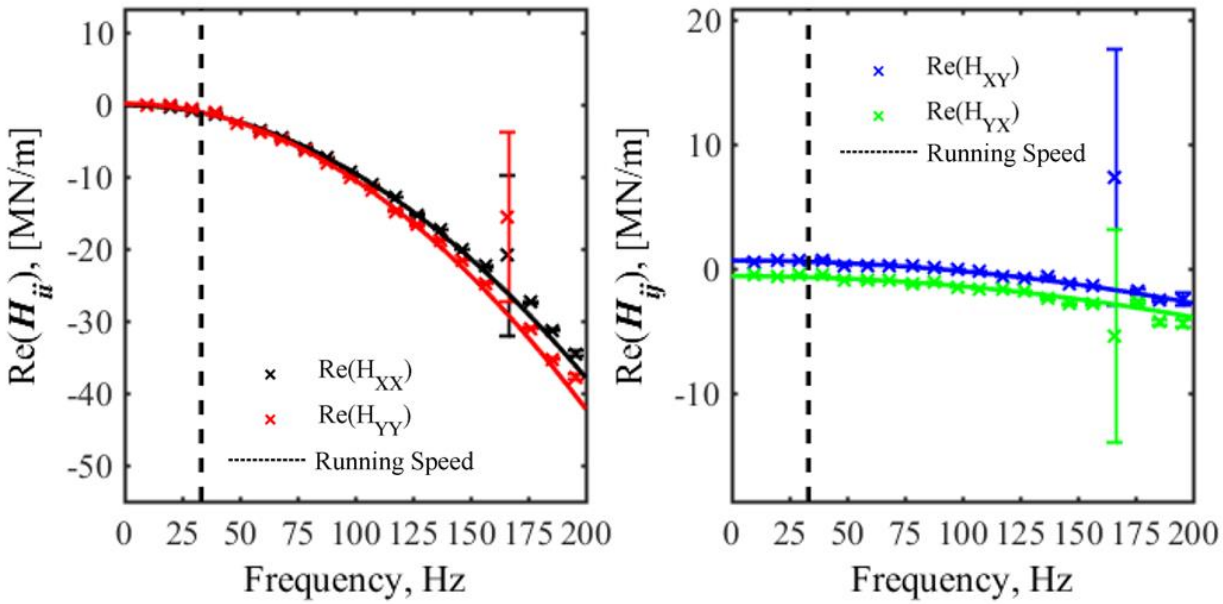

Figure 9 Real part of (a) H_{ii} (b) H_{ij} for VG 100 at 2 krpm, 4.14 bar, and ε_o = 0.80

C_{ij} is obtained from the *y*-intercept of Im($\boldsymbol{H_{ij}}$).

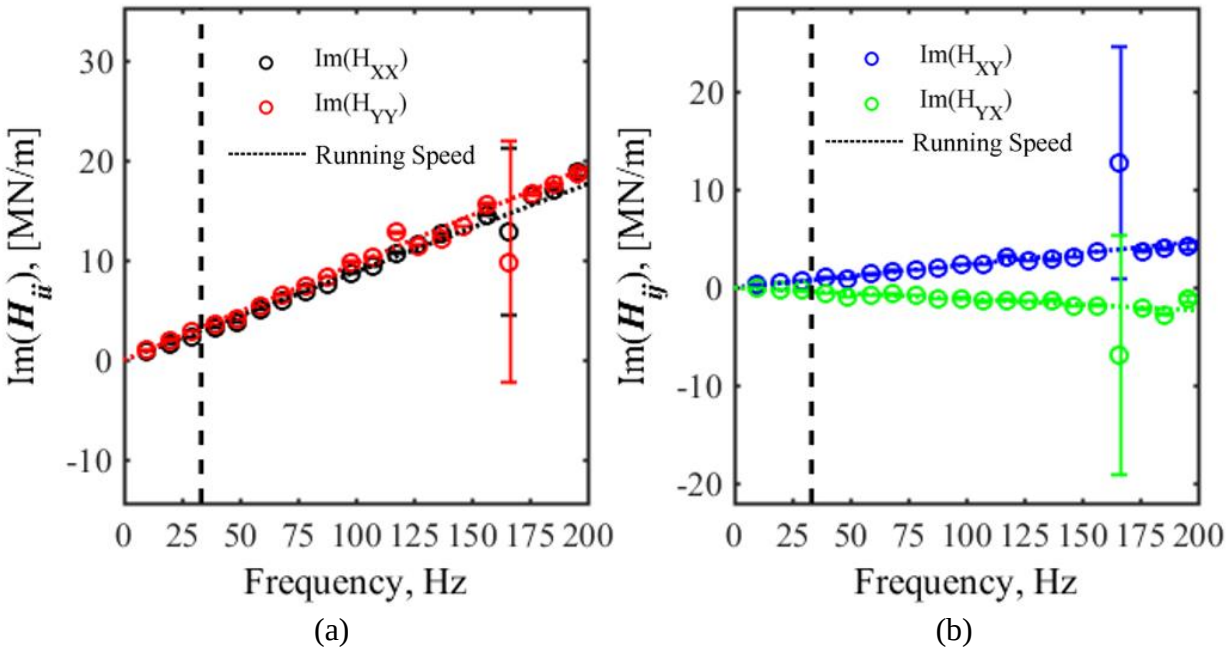

Figure 10 Imaginary part of (a) H_{ii} (b) H_{ij} for VG 100 at 2 krpm, 4.14 bar, and ε_o = 0.80

7.3 Coordinate System Transformation

The customary rotordynamic analysis coordinate system where the rotor is statically loaded along the -*Y* axis as the rotor is turning counter-clockwise is shown in Fig. 11. This coordinate system is used with "force control". Applied static load in *X* is zero.

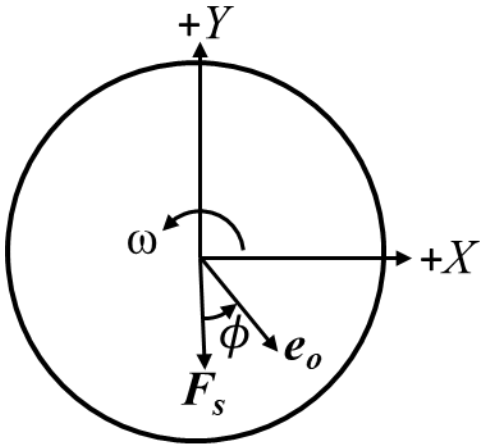

Figure 11 Non-drive end view of traditional *X-Y* coordinate system (force control)

The traditional *X-Y* coordinate system was not used as a result of test difficulties, arising from the negative direct stiffness of the seal. Position, rather than load, was adjusted to control rotor eccentricity. Fig. 12 shows the radial-tangential (*r-t*) coordinate system used to present the rotordynamic coefficients. In this coordinate system, *r* is the direction of rotor displacement along the vector $\boldsymbol{e_o}$ which extends from the center of the seal to the center of the journal. This coordinate system is used with "position control". Displacement of the rotor in *t* is zero. Test results presented here use the *r-t* coordinate system with a counter-clockwise shaft rotation as shown in Fig. 12.

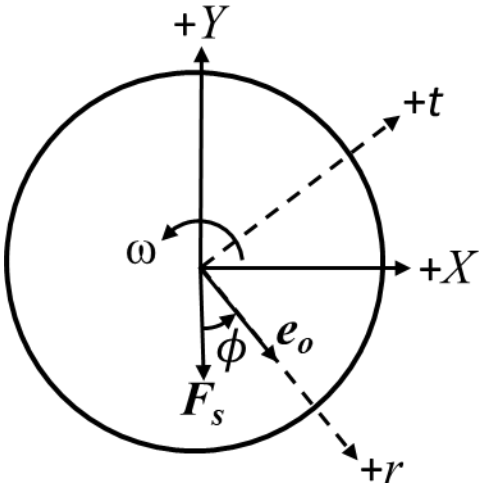

Figure 12 Non-drive end view of *r-t* coordinate system (position control)

Results are transformed from the *X*-*Y* coordinate system of Fig. 11 to the *r*-*t* coordinate system used here in Fig. 12, by the linear transformation

$$\begin{Bmatrix} f_{rX} \\ f_{rY} \end{Bmatrix} = \begin{bmatrix} \sin(\phi) & \cos(\phi) \\ -\cos(\phi) & \sin(\phi) \end{bmatrix} \begin{Bmatrix} f_{rr} \\ f_{rt} \end{Bmatrix}. \tag{24}$$

The reaction force in the *r* direction is f_{rr} and in *t* is f_{rt}. After the linear transformation, Eq. (1) becomes

$$-\begin{Bmatrix} f_{rr} \\ f_{rt} \end{Bmatrix} = \begin{bmatrix} K_{rr}(\varepsilon_o) & K_{rt}(\varepsilon_o) \\ K_{tr}(\varepsilon_o) & K_{tt}(\varepsilon_o) \end{bmatrix} \begin{Bmatrix} \Delta X_r \\ \Delta X_t \end{Bmatrix} + \begin{bmatrix} C_{rr}(\varepsilon_o) & C_{rt}(\varepsilon_o) \\ C_{tr}(\varepsilon_o) & C_{tt}(\varepsilon_o) \end{bmatrix} \begin{Bmatrix} \Delta \dot{X}_r \\ \Delta \dot{X}_t \end{Bmatrix} + \begin{bmatrix} M_{rr}(\varepsilon_o) & M_{rt}(\varepsilon_o) \\ M_{tr}(\varepsilon_o) & M_{tt}(\varepsilon_o) \end{bmatrix} \begin{Bmatrix} \Delta \ddot{X}_r \\ \Delta \ddot{X}_t \end{Bmatrix}. \tag{25}$$

At the centered position, $\varepsilon_o = 0$, direct stiffness, $K_{XX} = K_{YY} = K_{rr} = K_{tt} = K$ and cross-coupled stiffness, $K_{XY} = -K_{YX} = K_{tr} = -K_{rt} = k$. This same definition is applied to the direct and cross-coupled damping (C, c), and direct and cross-coupled virtual-mass (M, m) terms.

8. STATIC RESULTS

8.1 Clearance

Although the same seal was tested three times, a new hot clearance was taken for each assembly and those results are presented in Table 2. The percent difference between the minimum and maximum C_r measured while at operating temperature was 0.6%. Thermal growth of the rotor and stator reduced the nominal C_r of 0.2032 mm to an average hot clearance of 0.1905 mm for the three assemblies.

Table 2 Radial hot clearance for each test assembly

Test Assembly	Radial Hot Clearance, C_r [mm]
ISO VG 2	0.1899
ISO VG 46	0.1911
ISO VG 100	0.1905
Average	**0.1905**

8.2 Temperature Rise

As seen in Fig. 13(a), ΔT increases with increasing ω because of increasing shearing of the viscous fluid, which generates heat. As seen in Fig. 13(b), average fluid μ decreases with increasing ω due to the temperature change. The average μ change is significant for VG 100 and small for VG 2.

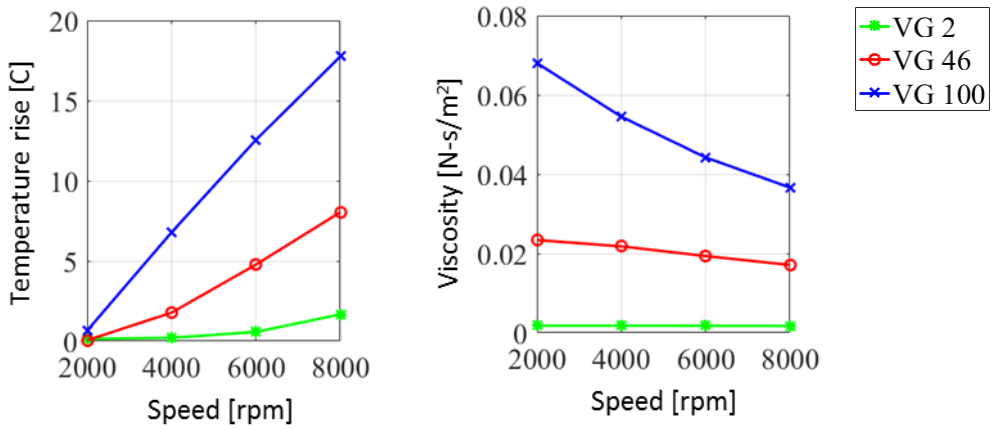

(a) (b)

Figure 13 (a) ΔT and (b) average μ vs ω at 6.21 bar and ε_o = 0.00

In Fig. 14(a), ΔT decreases with increasing ΔP, which is the result of increased $\dot{Q}$ which removes heat energy in the seal. In Fig. 14(b), ΔT decreases with increasing ε_o; this is from the increased $\dot{Q}$. As μ increases ΔT increases because viscous heating is proportional to μ.

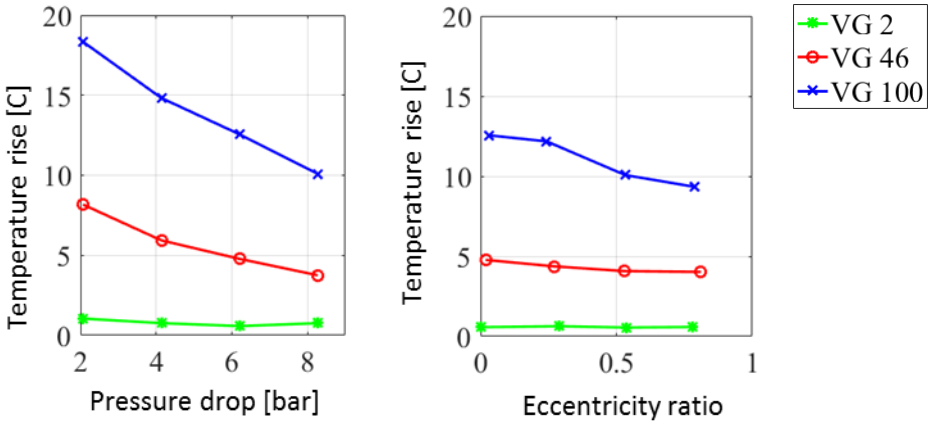

(a) (b)

Figure 14 ΔT vs (a) ΔP at 6 krpm and ε_o = 0.00, and (b) ε_o at 6 krpm and 6.21 bar

8.3 Leakage Rates

As seen in Fig. 15(a), with VG 2, $\dot{Q}$ decreases with an increasing ω. With VG 46 and VG 100, $\dot{Q}$ increases with increasing ω due to viscous heating of the liquid which reduces the effective μ. In Fig. 15(b), $\dot{Q}$ increases with increasing ΔP as the driving force for axial flow is increased. As seen in Fig. 15(c), $\dot{Q}$ increases with increasing ε_o. Leakage decreases with increasing μ.

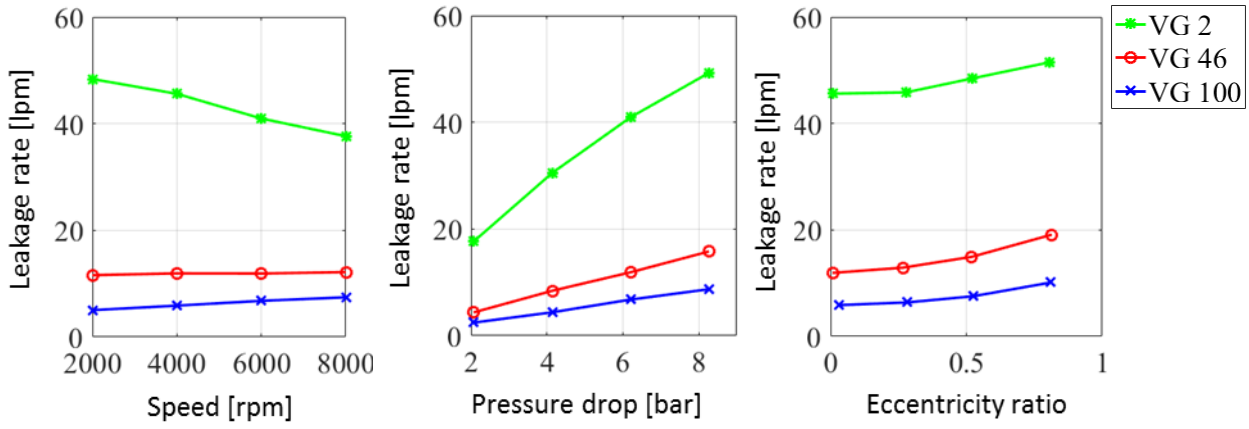

(a) (b) (c)

Figure 15 $\dot{Q}$ vs (a) ω at 6.21 bar and ε_o = 0.00, (b) ΔP at 4 krpm and ε_o = 0.00, and (c) ε_o at 2 krpm and 2.07 bar

8.4 Reynolds Number

In Table 3, the range of *Re* for each test assembly is shown. For all ISO VG 2 tests, the flow with in the seal is turbulent. The ISO VG 46 test *Re* ranges from laminar, to turbulent flow. ISO VG 100 flow is laminar for all test points. The *Re* is calculated with fluid properties based on the average fluid temperature in the seal.

Table 3 Range of *Re* in test seal for each test fluid

Test Fluid:	Minimum *Re*	Maximum *Re*
ISO VG 2	7,847	33,354
ISO VG 46	618	3,785
ISO VG 100	215	1,809

Figure 16 shows that circumferential flow dominates for all test conditions. In Fig. 16(a), Re_Θ/Re_z increases with increasing ω. This is the result of circumferential fluid velocity increasing with increasing ω. In Fig. 16(b), Re_Θ/Re_z decreases with increasing ΔP because the axial fluid velocity increases with increasing ΔP. As seen in Fig. 16(c), Re_Θ/Re_z decreases with increasing ε_o, because the axial fluid velocity increases with increasing ε_o. Increasing μ increases Re_Θ/Re_z because axial fluid velocity decreases with increasing μ. The lowest ratio of 2.7 was measured at the 2 krpm, 8.27bar, ε_o = 0.8, and VG 2 test point.

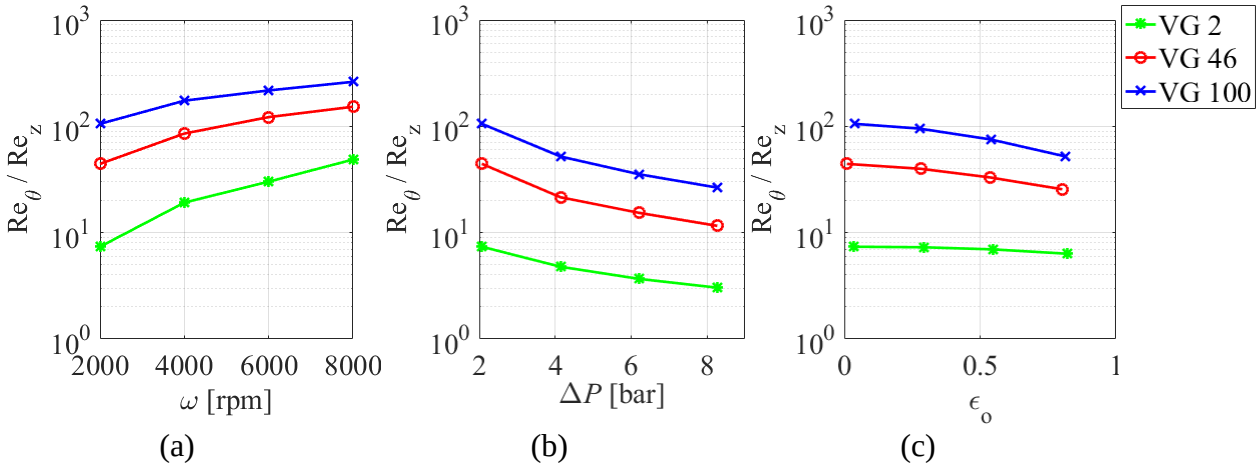

Figure 16 Re_Θ/Re_z vs (a) ω at 2.07 bar and ε_o = 0.00, (b) ΔP at 2 krpm and ε_o = 0.00, and (c) ε_o at 2 krpm and 2.07 bar

8.5 Pre-swirl Ratio

As seen in Fig. 17(a), v_{inlet} increases with increasing ω for VG 2. This is expected as circumferential flow at the inlet increases with ω due to shear driven flow from the shaft. As seen in Fig. 17(b), for VG 2, PSR decreases with increasing ω which is expected as PSR = $v_{inlet}/R\omega$.

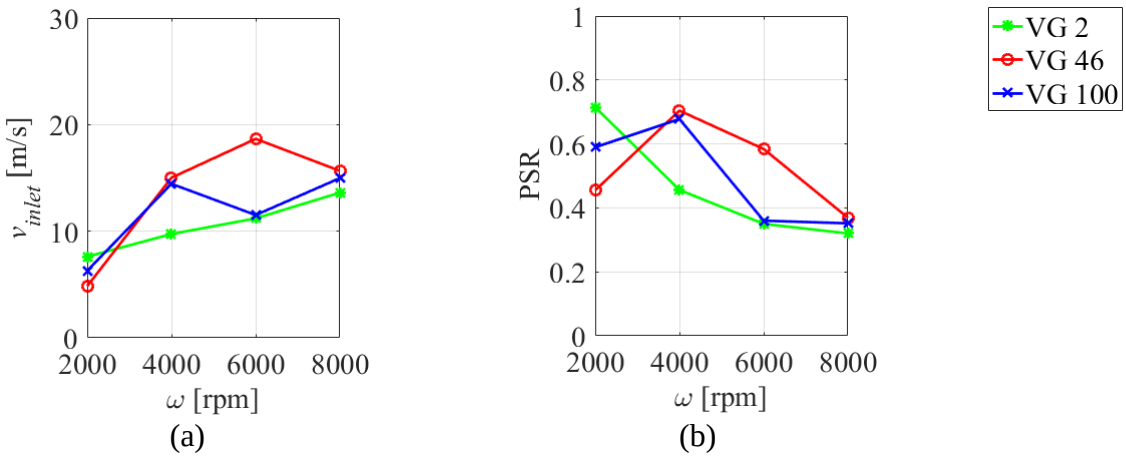

Figure 17 (a) v_{inlet} and (b) PSR at 4.14 bar and ε_o = 0.00 vs ω

As seen in Fig. 18, v_{inlet} generally increases with increasing ΔP. The increase of v_{inlet} with increasing ΔP is the result of increasing $\dot{Q}$.

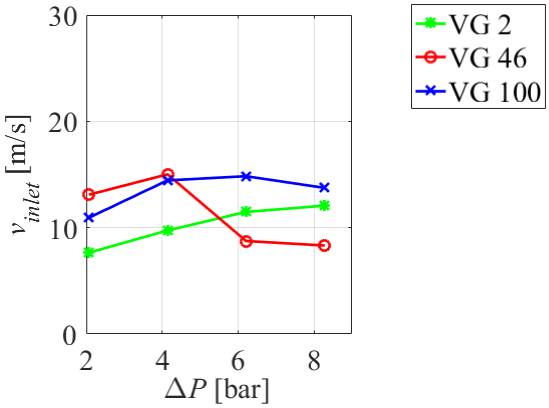

Figure 18 v_{inlet} vs ΔP at 4 krpm and ε_o = 0.00

The VG 46 and VG 100 liquids have PSR and v_{inlet} measurements that do not follow a consistent trend with respect to changing ω or ΔP. This is suspected to be from the pitot tube measuring boundary layer flow on the shaft, as well as the injected pre-swirl velocity. It is not clear if the measured values of v_{inlet} are representative of the average value entering the seal with VG 46 and VG 100 or, if the v_{inlet} (and PSR) is not well controlled by the swirl insert for these fluids.

8.6 Static Forces

Applied static force phase angle (ϕ) in the *r-t* coordinate system is defined as

$$\phi = -\tan^{-1}(F_{st}/F_{sr}) \tag{26}$$

Where F_{st} and F_{sr} are the tangential and radial components of the applied static force (F_s) as shown in Fig. 19. Results are presented with a counter-clockwise shaft rotation.

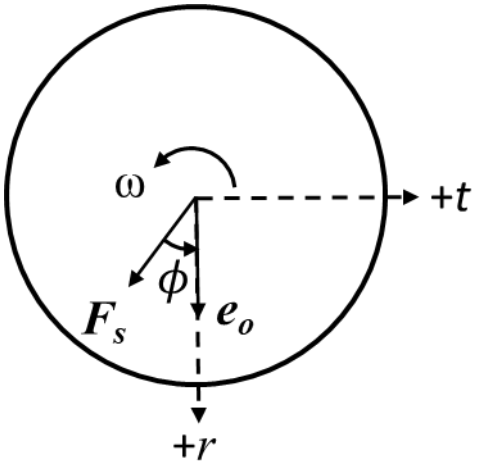

Figure 19 Applied static force and phase angle in the *r-t* coordinate system

The magnitude of F_s is defined as

$$F_s = \sqrt{F_{st}^2 + F_{sr}^2} \tag{27}$$

A ϕ between 0° and 90° indicates F_r (reaction force to the applied static force F_s) is toward the center of the seal (centering force). Similarly, a ϕ outside of this range indicates F_r is away from the seal center (decentering).

As seen in Fig. 20, ϕ generally does not change significantly with increasing ε_o.

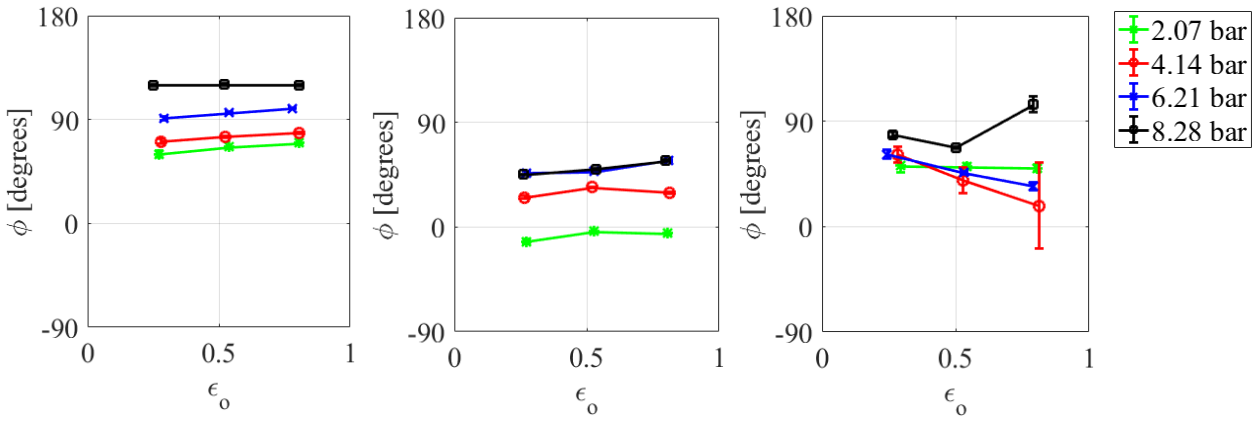

(a) VG 2 (b) VG 46 (c) VG 100

Figure 20 ϕ vs ε_o at 6 krpm for (a) VG 2 (b) VG 46 and (c) VG 100

As seen in Fig. 21(a), for VG 2, ϕ generally increases with increasing ΔP. In Fig. 21(b), for VG 46, ϕ does not change significantly with increasing ΔP. As seen in Fig. 21(c), for VG 100, ϕ generally decreases with increasing ΔP. This implies F_r becomes decentering as ΔP increases for VG 2 and becomes centering as ΔP increases for VG 100.

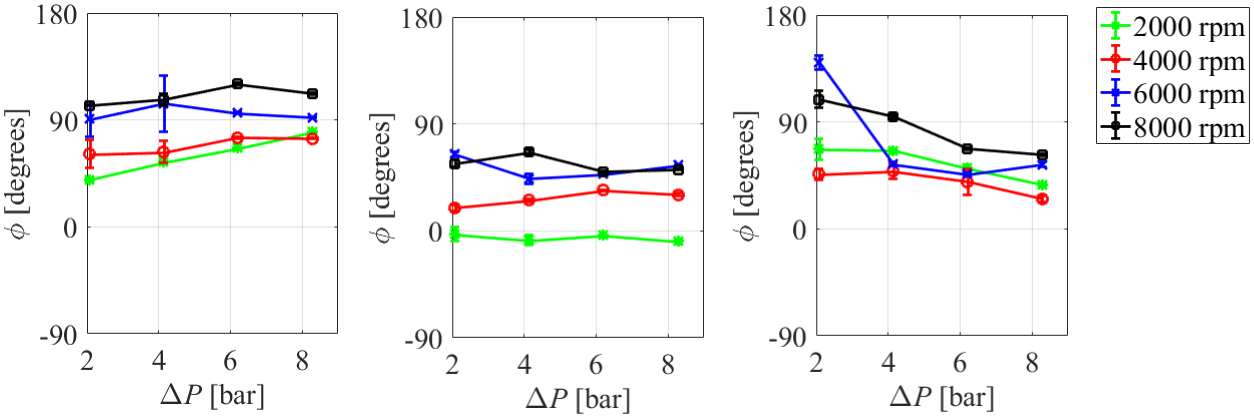

(a) VG 2 (b) VG 46 (c) VG 100

Figure 21 ϕ vs ΔP at ε_o = 0.53 for (a) VG 2 (b) VG 46 and (c) VG 100

As seen in Fig. 22, ϕ generally increases with increasing ω. This implies F_r becomes decentering as ω increases.

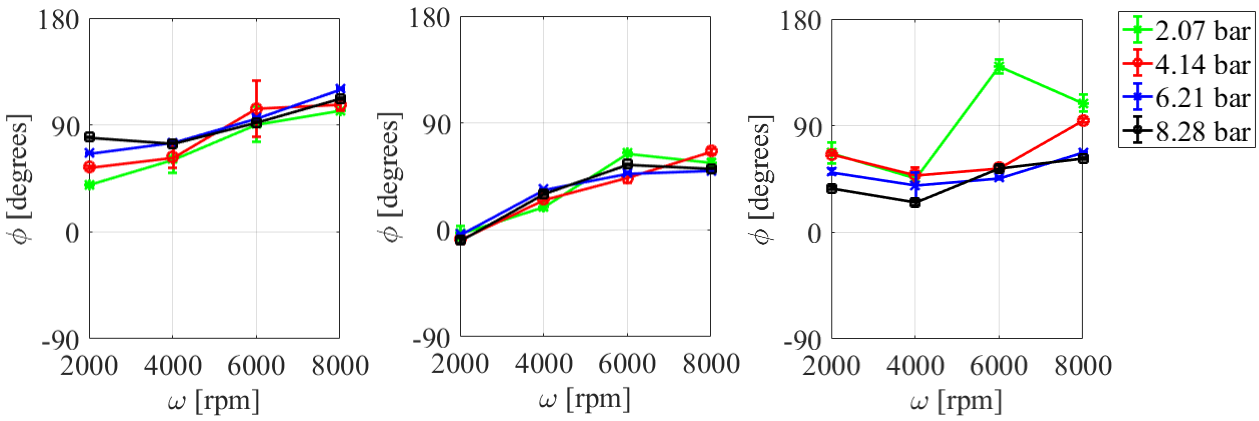

(a) VG 2 (b) VG 46 (c) VG 100

Figure 22 ϕ vs ω at ε_o = 0.53 for (a) VG 2 (b) VG 46 and (c) VG 100

No clear trend could be found between ϕ and μ, and no conclusions are made. A ϕ outside of the 0° to 90° range did not correlate to a negative K_{rr}.

As seen in Fig. 23(a and b), for VG 2 and VG 46, F_s increases with increasing ε_o. In Fig. 23(c), for VG 100, F_s generally increases then decreases with increasing ε_o. This is likely due to the significant amount of cross-coupled stiffness and often negative direct stiffness.

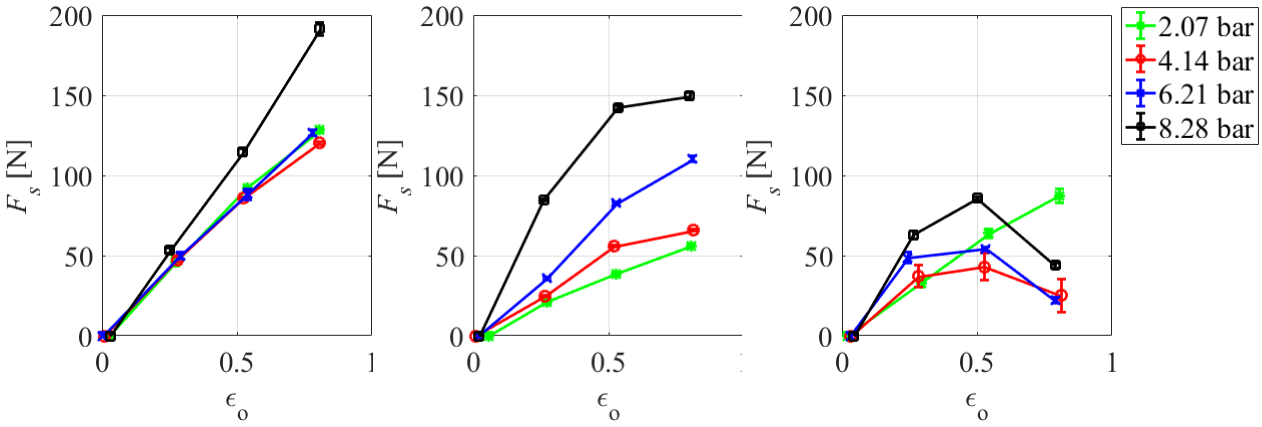

(a) VG 2 (b) VG 46 (c) VG 100

Figure 23 F_s vs ε_o at 6 krpm for (a) VG 2 (b) VG 46 and (c) VG 100

9. DYNAMIC RESULTS

Results in this section are from the curve fit analysis of $\boldsymbol{H_{ij}}$ in section 7.2. K_{ij}, C_{ij}, and M_{ij} are presented with uncertainties of the measured coefficients.

9.1 Direct Stiffness

As seen in Fig. 24, K_{rr} and K_{tt} changes are small as ε_o increases. K_{rr} and K_{tt} are often negative. Uncertainty values for K_{rr} and K_{tt} are generally on the same order, or one order of magnitude smaller than the measured value. Negative K_{rr} values do not correlate with a $\phi > 90°$.

K_{rr} and K_{tt} are often negative which is detrimental to rotor performance as the natural frequency drops with decreasing K_{rr} and K_{tt}. No clear trend could be found between K_{rr} and K_{tt}, and μ.

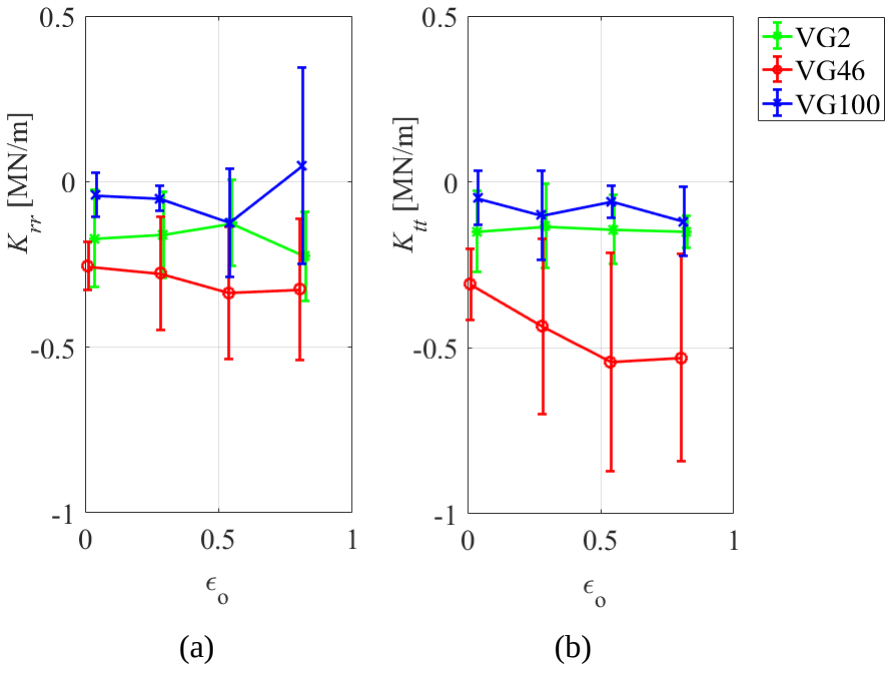

Figure 24 (a) K_{rr} and (b) K_{tt} vs ε_o at 2 krpm and 2.07 bar

As seen in Fig. 25(a), no clear trend could be found between ΔP and K. As seen in Fig. 25(b), changes are small for K as ω increases.

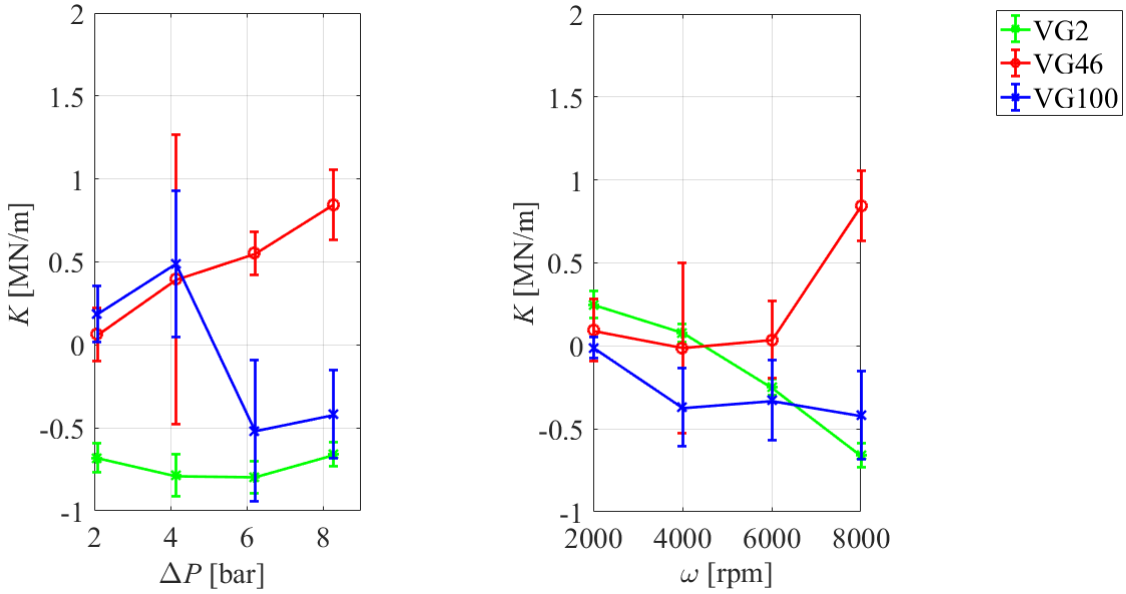

Figure 25 *K* vs (a) Δ*P* at 8 krpm and (b) ω at 8.27 bar

9.2 Cross-Coupled Stiffness

As seen in Fig. 26, changes to K_{rt} and K_{tr} are small as ε_o increases. K_{rt} and K_{tr} are generally opposite in sign (destabilizing, within the uncertainty of the measured values).

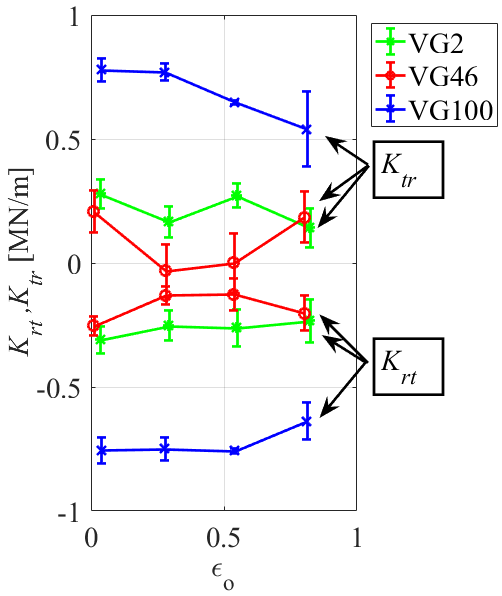

Figure 26 K_{rt} and K_{tr} vs ε_o at 2 krpm and 2.07 bar

As seen in Fig. 27(a), no trend could be found between ΔP and k. As seen in Fig. 27(b), k increases in magnitude with increasing ω. The results of Fig. 27(b) are consistent with those of Fig. 22(b), VG 46 has a low ϕ and small k at low ω. As ω increases, both ϕ and k increase. At the centered position, k is approximately equal in magnitude and opposite in sign.

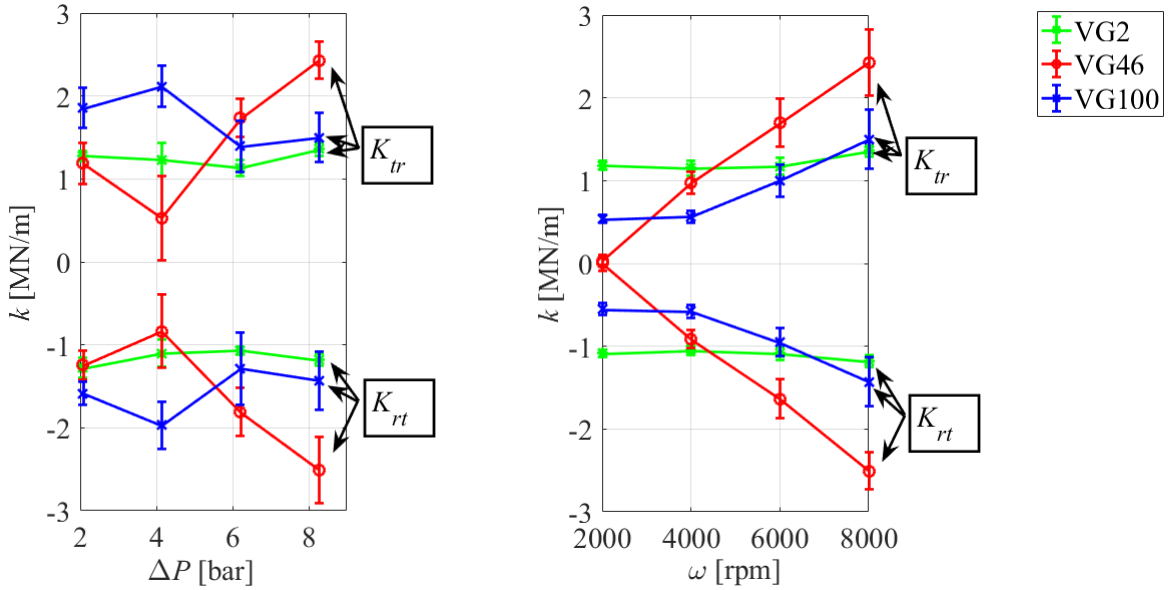

Figure 27 *k* vs (a) Δ*P* at 8 krpm and (b) ω at 8.27 bar

No clear trend could be found between K_{rt} and K_{tr} and μ. Destabilizing forces arise when K_{rt} and K_{tr} have opposite signs which is detrimental to rotor performance. These forces are counteracted by damping which is discussed further in section 9.8.

9.3 Direct Damping

Figure 28 shows C_{rr} and C_{tt} vs ε_o. For VG 2, C_{rr} and C_{tt} generally decrease with increasing ε_o. C_{rr} and C_{tt} increase with an increasing ε_o for VG 100.

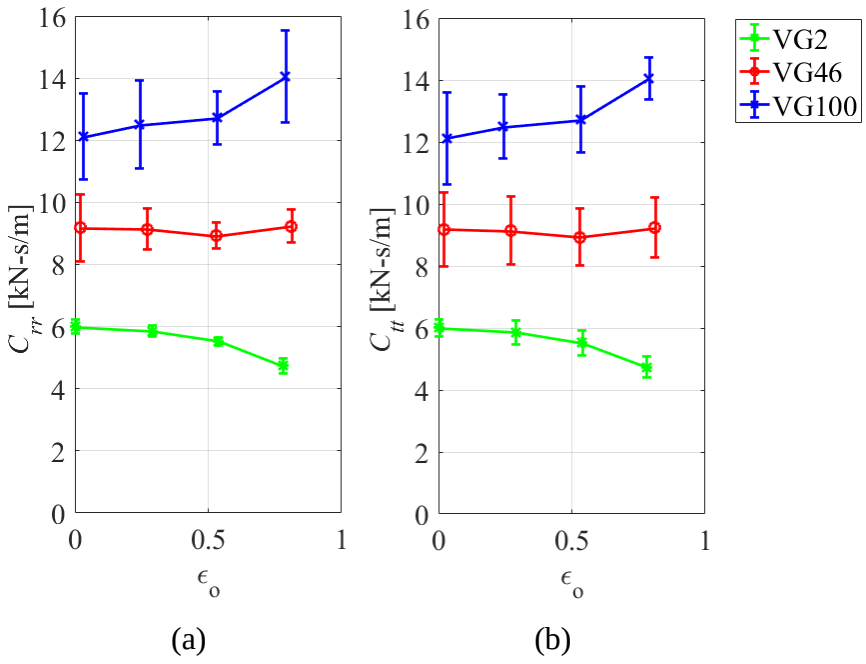

Figure 28 (a) C_{rr} and (b) C_{tt} vs ε_o at 6 krpm and 6.21 bar

As seen in Fig. 29(a), C increases with an increasing ΔP. As seen in Fig. 29(b), C increases with ω for VG 2 and decreases with ω for VG 100. This decrease for VG 100 is likely the result of viscous heating in the seal which drops the average μ within the seal.

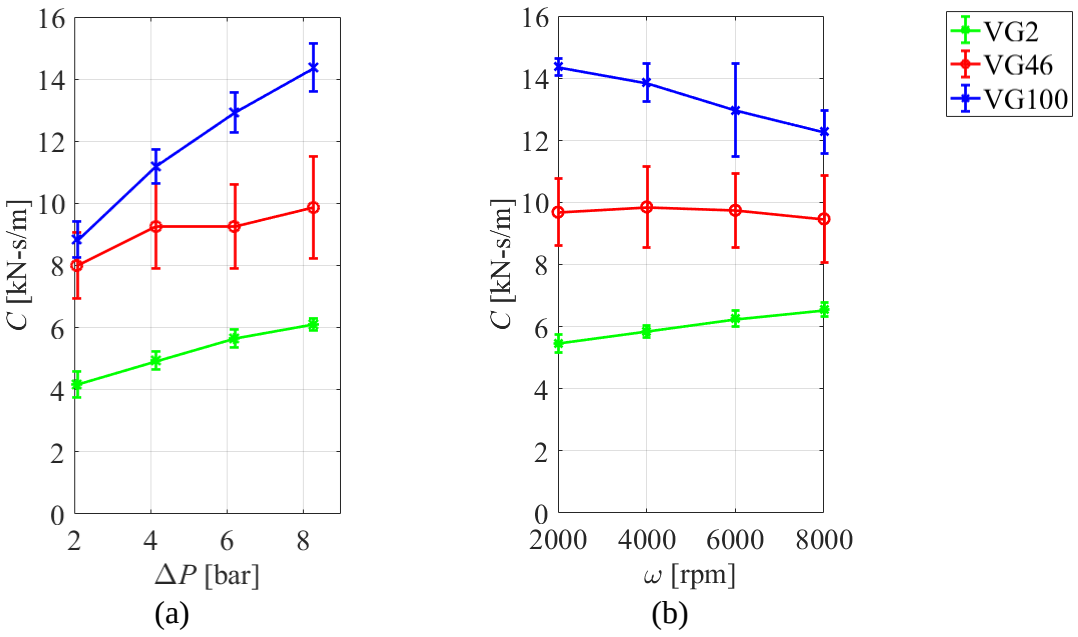

Figure 29 *C* vs (a) Δ*P* at 4 krpm and (b) ω at 6.21 bar

Increasing μ increased *C* significantly. Damping resists rotor perturbations which has a stabilizing effect. Comparison of destabilizing and stabilizing forces is discussed in section 9.8.

9.4 Cross-Coupled Damping

As seen in Fig. 30, C_{rt} and C_{tr} have opposite signs and generally increases in magnitude with increasing ε_o.

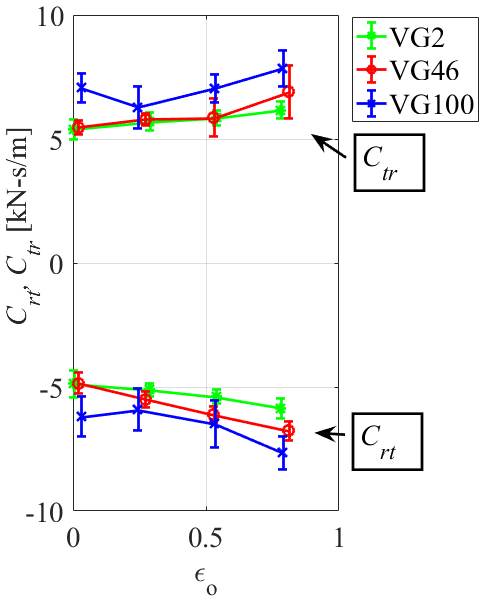

Figure 30 C_{rt} and C_{tr} vs ε_o at 6 krpm and 6.21 bar

Figure 31(a) shows no clear trend between c and ΔP, however, changes were small. As seen in Fig. 31(b), c increases in magnitude with increasing ω. At the centered position, C_{rt} and C_{tr} is equal in magnitude and opposite in sign.

An increase in μ slightly increases the magnitude of C_{rt} and C_{tr}, this result however was not the case for all test points and changes were small.

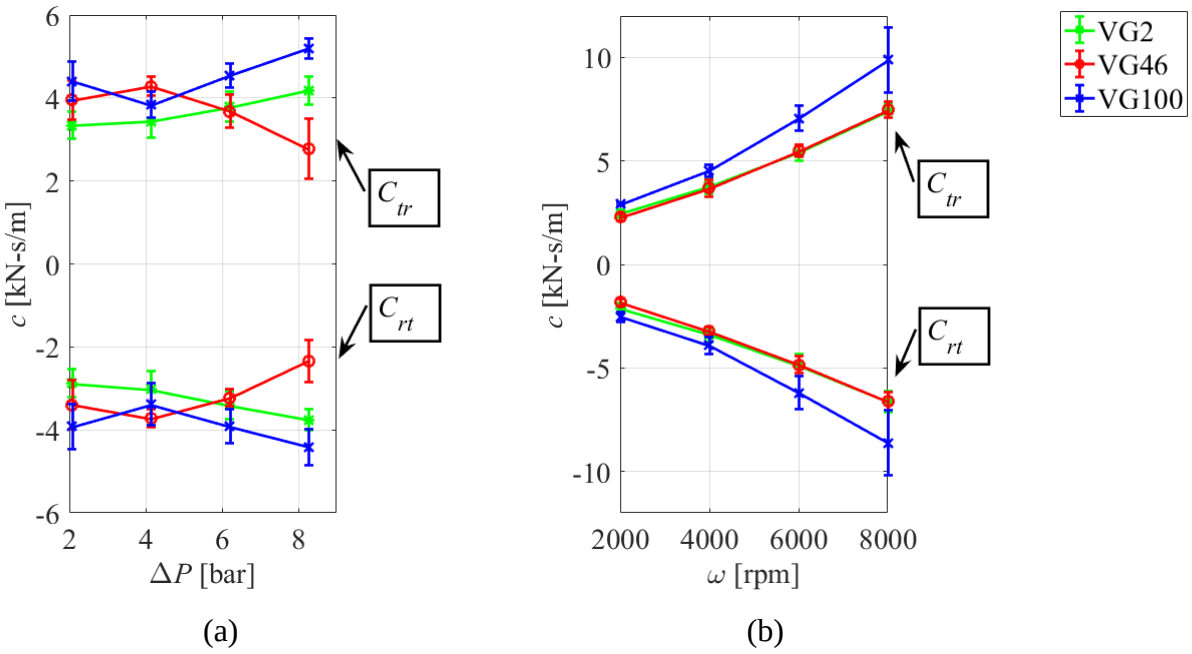

Figure 31 *c* vs (a) Δ*P* for 4 krpm and (b) ω at 6.21 bar

9.5 Direct Virtual-Mass

As seen in Fig. 32, M_{rr} increases with increasing ε_o. M_{tt} has a small change with increasing ε_o.

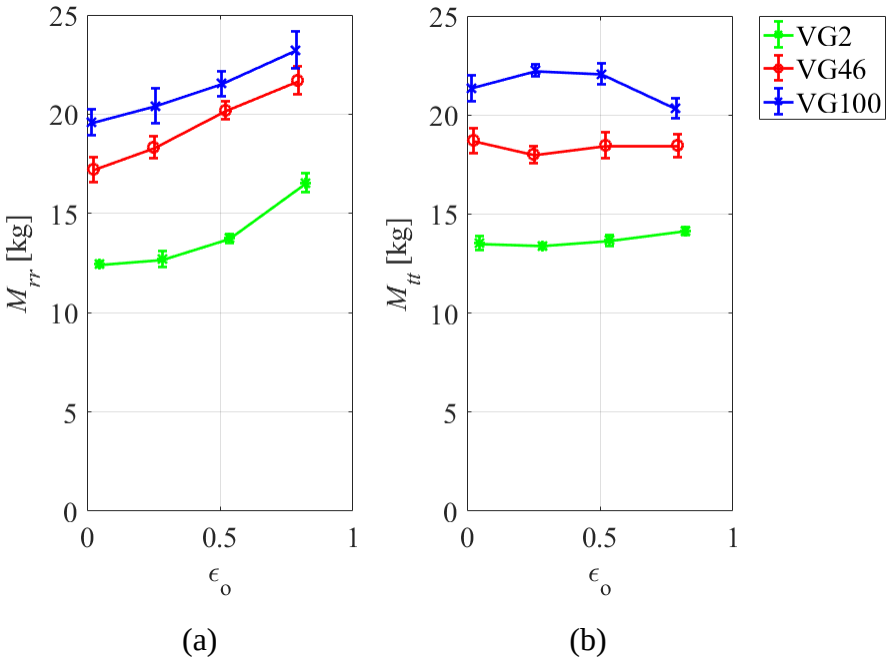

Figure 32 (a) M_{rr} and (b) M_{tt} vs ε_o at 6 krpm and 4.14 bar

Increasing μ increased M_{rr} and M_{tt}. Increasing M_{rr} and M_{tt} has the effect of lowering the natural frequency of the rotor system. For ESP's with CGS, increasing μ will lower the natural frequencies of the rotor system.

Figure 33(a) shows that M generally increases with increasing ΔP. This is not always the case for VG 100 where changes are small. As seen in Fig. 33(b), M decreases with increasing ω.

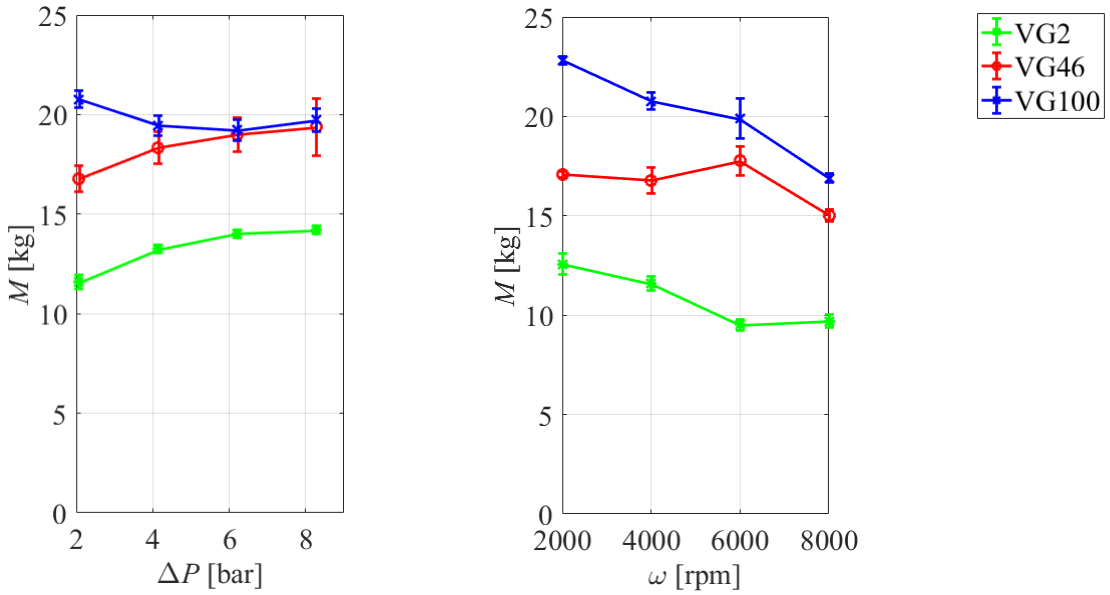

Figure 33 *M* vs (a) Δ*P* at 4 krpm and (b) ω at 2.07 bar

9.6 Cross-Coupled Virtual-Mass

As seen in Fig. 34, M_{rt} and M_{tr} typically have opposite signs (destabilizing). Uncertainty values were often on the order of the measured values for M_{rt} and M_{tr}.

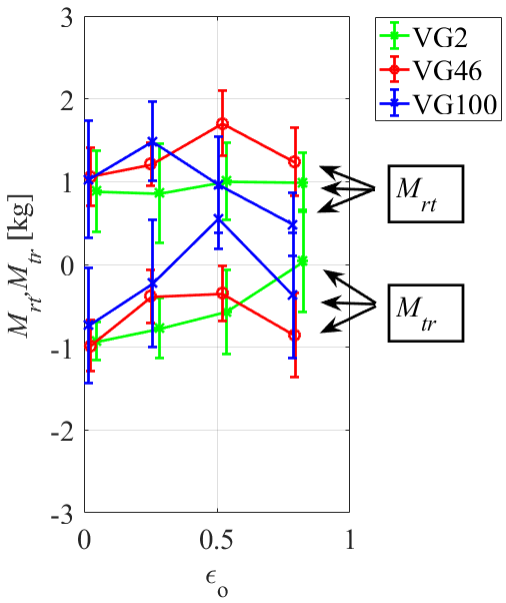

Figure 34 M_{rt} and M_{tr} vs ε_o at 6 krpm and 4.14 bar

9.7 Effective Stiffness

As shown in Fig. 35, K_{eff} is generally negative, and $|K_{eff}|$ increases with increasing ω. This will lower the natural frequencies of the pump rotor.

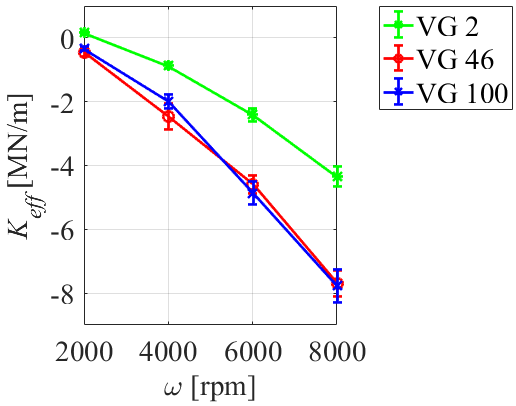

Figure 35 K_{eff} vs ω at 8 bar

As seen in Fig. 36, K_{eff} decreases with increasing ΔP. As μ increases, K_{eff} generally decreases.

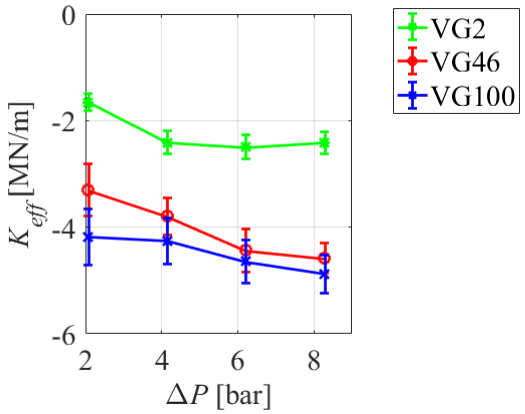

Figure 36 K_{eff} vs ΔP at 6 krpm

The generally negative K_{eff} indicates these seals can lower the natural frequencies of the pump. The decreasing K_{eff} with increasing μ shows that increasing μ in an ESP with CGS will lower natural frequencies.

9.8 Effective Damping

As seen in Fig. 37(a), C_{eff} generally increases with increasing ΔP. In Fig. 37(b), C_{eff} increases with increasing ω for VG 2 and decreases with increasing ω for VG 46 and VG 100, which is likely the result of viscous heating. As μ increases, C_{eff} increases. This result indicates total destabilizing forces decrease with increasing μ and a seal will be more stable at higher μ.

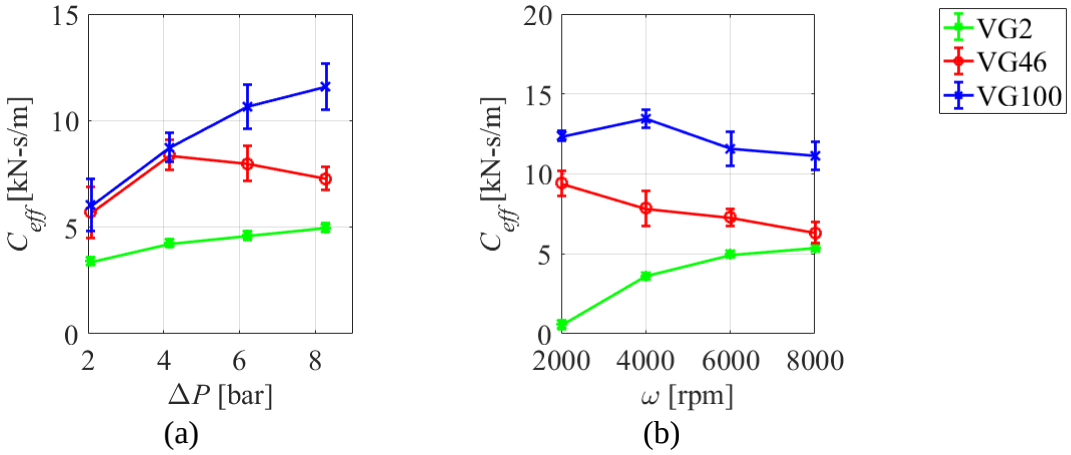

Figure 37 C_{eff} vs (a) ΔP at 6 krpm and (b) ω at 8.27 bar

9.9 Whirl Frequency Ratio

As mentioned in Section 1, WFR does not give a good comparison of stability characteristics for different seal geometries and that C_{eff} should be used for this. For a CGS, WFR does give insight into the physical interpretation of the fluid film behavior.

As seen in Fig. 38, as ω increases, the WFR tends towards a value of ~0.2. For a GS/SR geometry it is expected the WFR would trend towards a value less than 0.5 as the circumferential fluid velocity is reduced in the grooved stator due to the no slip condition inside the groove. The results of Fig. 38 are consistent with the results of Fig. 27(b), for VG 46; k and WFR are small at low ω. As ω increases, k and WFR also increase.

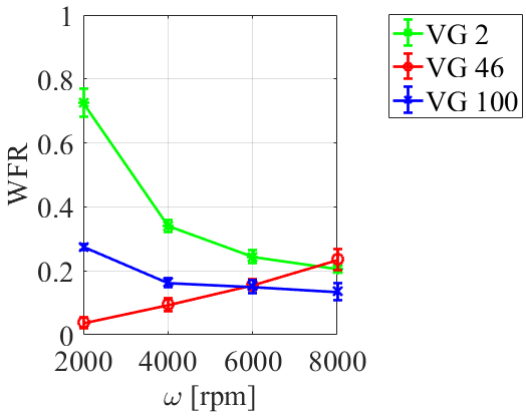

Figure 38 WFR vs ω at 6.21 bar and ε_o = 0.00

This result is different from that of Childs et al. [20] which found grooving in a CGS compared to a SS/SR does not reduce the WFR. This result was based on a short ($L/D \approx 0.21$) seal test with ~24.6% of the seals surface grooved with three grooves and a C_r/R of ~0.001; compared to the seal tested for this report which has an L/D of 0.5, 45% of the seal surface grooved with 15 grooves, and a C_r/R of 0.004. This significant difference between the two seal geometries account for the difference in results and conclusions.

10. SMOOTH STATOR/SMOOTH ROTOR COMPARISON

In this section, the turbulent flow (VG 2) test results from the GS/SR seal are compared to a SS/SR seal of comparable geometry, and at the same operating conditions. The SS/SR has the same L/D of 0.5 and C_r/R of 0.004 as the GS/SR. The SS/SR results are from as yet to be published test results at the Texas A&M Turbomachinery Laboratory. Comparable SS/SR data are not available for ISO VG 46 and ISO VG 100.

10.1 Direct Stiffness

As seen in Fig. 39, K_{rr} and K_{tt} for the SS/SR are generally larger in magnitude (and positive) than those of a GS/SR (generally negative). For a turbulent flow seal, grooves have the effect of creating negative K_{rr} and K_{tt}. Additionally, grooves make K_{rr} and K_{tt} significantly less dependent on ε_o.

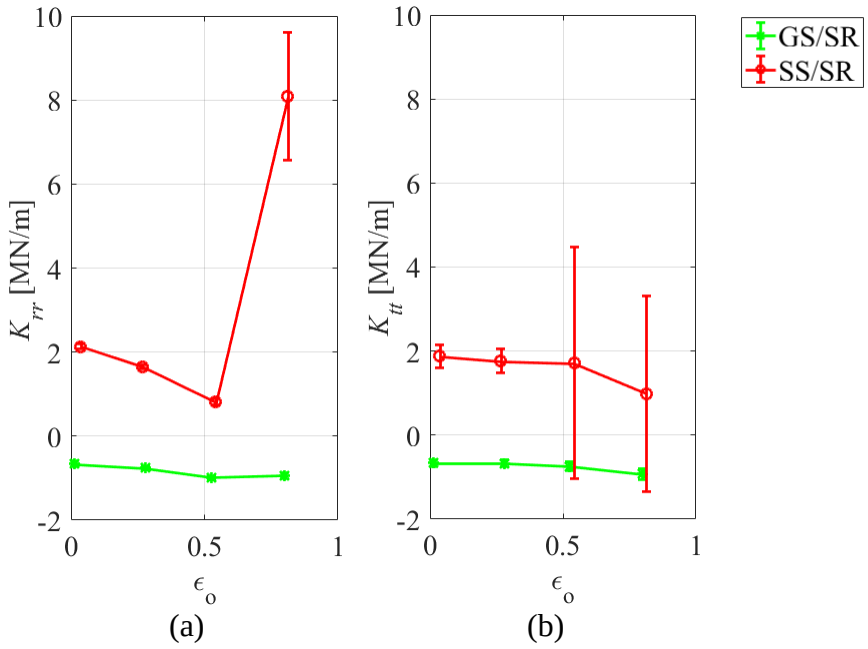

Figure 39 GS/SR and SS/SR; (a) K_{rr} and (b) K_{tt} vs ε_o at 8 krpm, 8.28 bar, and ISO VG 2

10.2 Cross-Coupled Stiffness

As seen in Fig. 40, K_{rt} and K_{tr} for the SS/SR increase in magnitude with increasing ε_o and are larger than those of a GS/SR. For a turbulent flow seal, grooves have the effect of reducing the magnitude of K_{rt} and K_{tr}. Additionally, grooves make K_{rt} and K_{tr} significantly less dependent on ε_o.

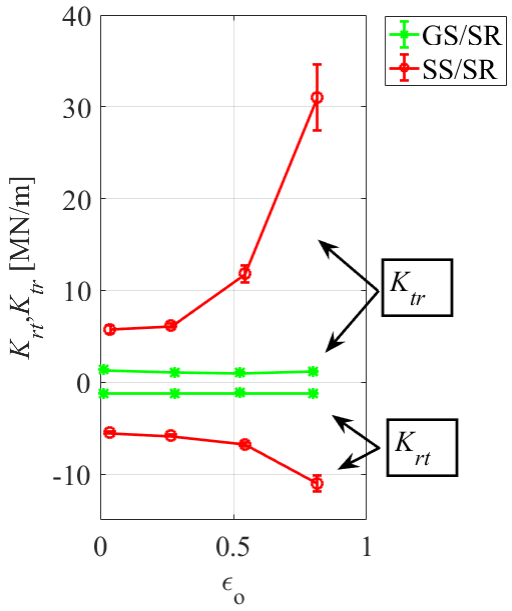

Figure 40 GS/SR and SS/SR; K_{rt} and K_{tr} vs ε_o at 8 krpm, 8.28 bar, and ISO VG 2

10.3 Direct Damping

As seen in Fig. 41, C_{rr} and C_{tt} for the SS/SR seal increase with increasing ε_o and are larger than those of a GS/SR. For a turbulent flow seal, grooves have the effect of reducing the magnitude of C_{rr} and C_{tt}. Additionally, grooves make C_{rr} and C_{tt} less dependent on ε_o.

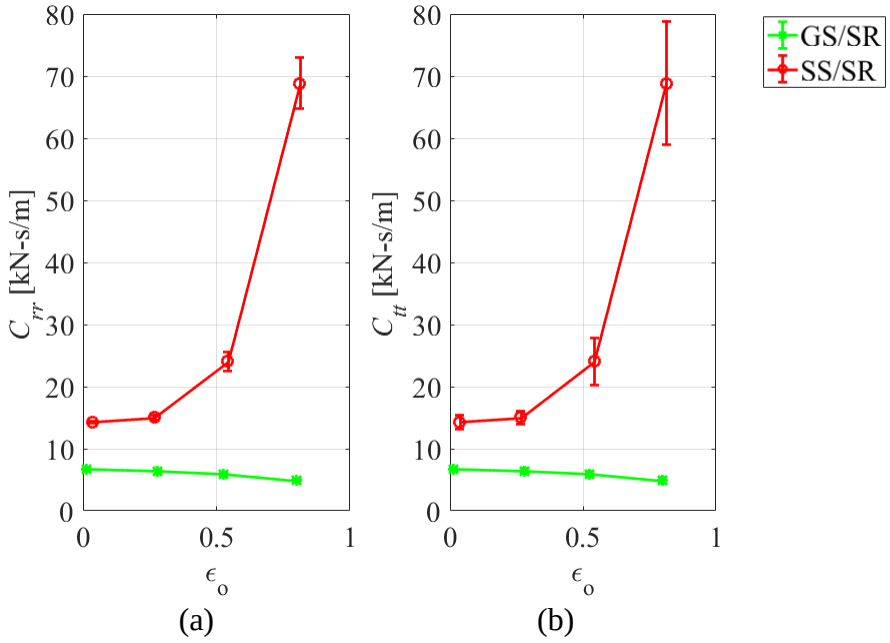

Figure 41 GS/SR and SS/SR; (a) C_{rr} and (b) C_{tt} vs ε_o at 8 krpm, 8.28 bar, and ISO VG 2

10.4 Cross-Coupled Damping

As seen in Fig. 42, C_{rt} and C_{tr} for the SS/SR increases with increasing ε_o and are larger than those of a GS/SR. For a turbulent flow seal, grooves have the effect of reducing the magnitude of C_{rt} and C_{tr}. Additionally, grooves make C_{rt} and C_{tr} less dependent on ε_o.

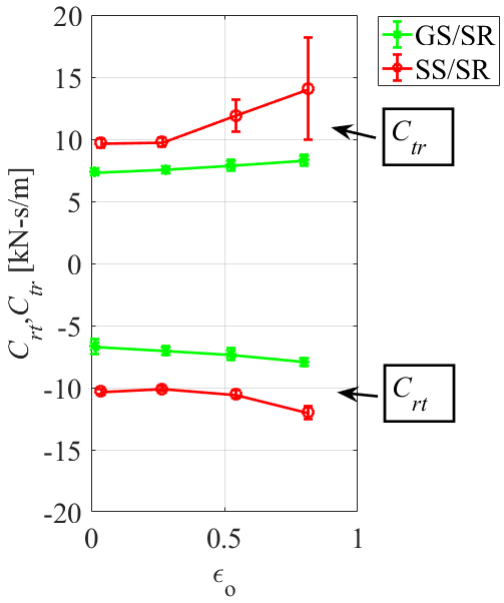

Figure 42 GS/SR and SS/SR; C_{rt} and C_{tr} vs ε_o at 8 krpm, 8.28 bar, and ISO VG 2

10.5 Direct Virtual-Mass

As seen in Fig. 43, M_{rr} and M_{tt} for the SS/SR seal increase with increasing ε_o and are larger than those of a GS/SR. In the turbulent flow seal, grooves have the effect of reducing M_{rr} and M_{tt}. Grooves also reduce the dependence of M_{rr} and M_{tt} on ε_o.

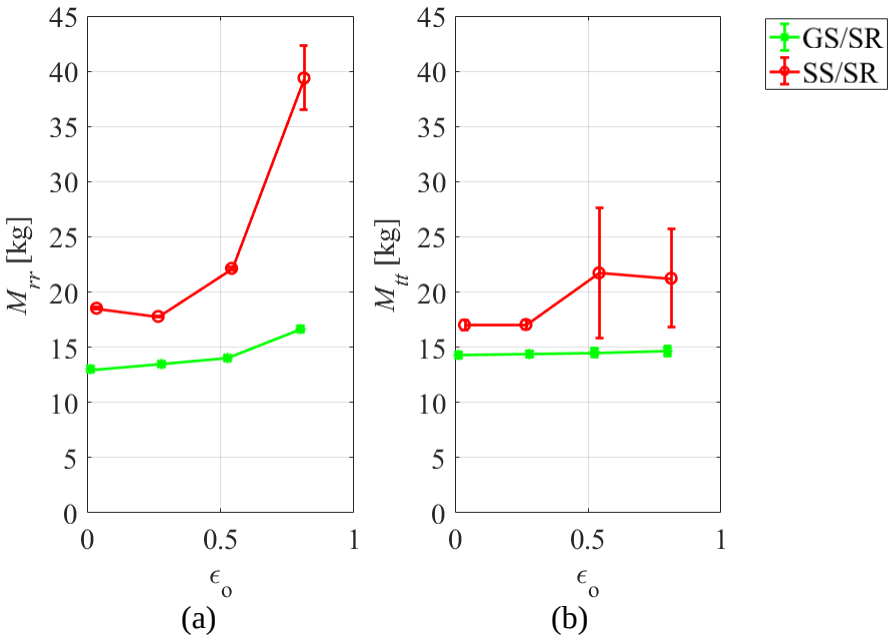

Figure 43 GS/SR and SS/SR; (a) M_{rr} and (b) M_{tt}, vs ε_o at 8 krpm, 8.28 bar, and ISO VG 2

10.6 Cross-Coupled Virtual-Mass

As seen in Fig. 44, M_{rt} and M_{tr} for the SS/SR increases in magnitude with increasing ε_o and are larger than those of a GS/SR. M_{rt} and M_{tr} are generally opposite in sign, within the uncertainty values, for both the SS/SR and the GS/SR. For the SS/SR $M_{tr} > 0$ and $M_{rt} < 0$ which has a destabilizing effect. For the GS/SR $M_{tr} < 0$ and $M_{rt} > 0$ which has a stabilizing effect, however, measurement uncertainty is often significant. In the turbulent flow seal, grooves have the effect of reducing M_{rt} and M_{tr}. Grooves also reduce the dependence of M_{rt} and M_{tr} on ε_o.

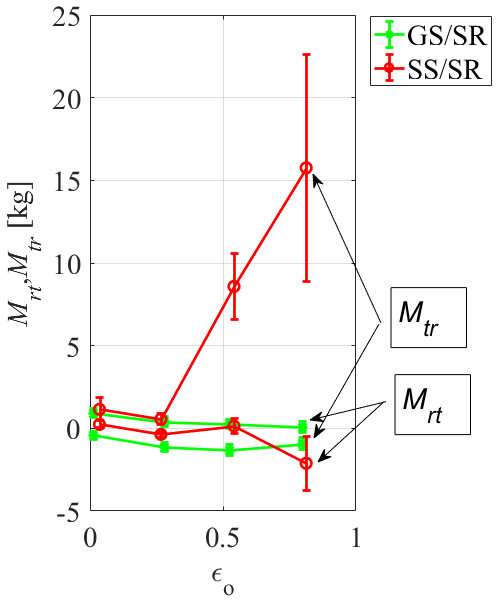

Figure 44 GS/SR and SS/SR; M_{rt} and M_{tr} vs ε_o at 8 krpm, 8.28 bar, and ISO VG 2

11. PREDICTED CHARACTERISTICS OF TURBULENT FLOW SEALS

Static and Rotordynamic characteristics are predicted with the code developed by San Andrés et. al. [18]. Table 4 shows the percent difference between the predicted and measured characteristics of the tested seal. Torres [14] similarly found a significant difference between the predicted and measured characteristics with these relatively low ΔPs and ωs. For zero pre-swirl (radial injection), Torres found predictions improved as ΔP and ω increased. With high pre-swirl levels tested here (and by Torres), predicted values did not improve noticeably at higher ΔPs and ωs.

Table 4 Predicted [18] vs measured percent difference for ISO VG 2

ISO VG 2	Predicted vs Measured Percent Difference		
	Minimum	Maximum	Average
K	5.6%	667%	199%
k	116%	148%	134%
C	101%	131%	115%
c	3.1%	10,000%	1,170%
M	1.3%	27%	12%
$\dot{Q}$	35%	61%	49%

This seal code uses several empirical coefficients. Predictions might be improved by introducing new coefficients.

12. PREDICTED CHARACTERISTICS OF LAMINAR FLOW SEALS

For the laminar flow seal, a code based on the work by San Andrés and Delgado [21] was used to predict static and rotordynamic characteristics. This code does not account for viscous heating of the fluid. Fluid properties input to the code were determined two ways. The first using the measured inlet temperature, the second using the average fluid temperature within the seal.

12.1 Leakage Rates

As seen in Fig. 45(a), predicted $\dot{Q}$ based on the measured inlet temperature does not increase with increasing ω as does the measured $\dot{Q}$. When the average fluid temperature is used, the predicted values follows the measured trend. In Fig. 45(b), predicted $\dot{Q}$ follows the measured trend of increasing $\dot{Q}$ with increasing ΔP. As seen in Fig. 45(c), predicted $\dot{Q}$ follows the measured trend of increasing $\dot{Q}$ with increasing ε_o. The code generally predicts lower $\dot{Q}$ than was measured. Using the average measured fluid temperature improves $\dot{Q}$ predictions.

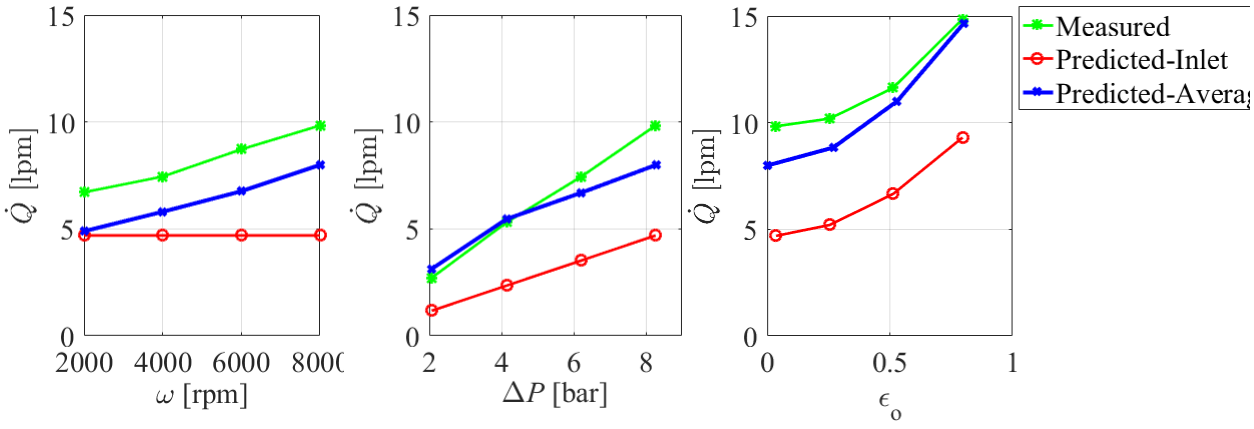

Figure 45 Predicted [21] and measured $\dot{Q}$ with VG 100 vs (a) ω at 8.28 bar and ε_o = 0.00 (b) ΔP at 8 krpm and ε_o = 0.00 (c) ε_o at 8.28 bar and 8 krpm

12.2 Direct Stiffness

As seen in Fig. 46, *K* is not well predicted. The code does not predict the negative *K* that was measured. Using the average measured fluid temperature did not have a noticeable impact on the predicted *K*.

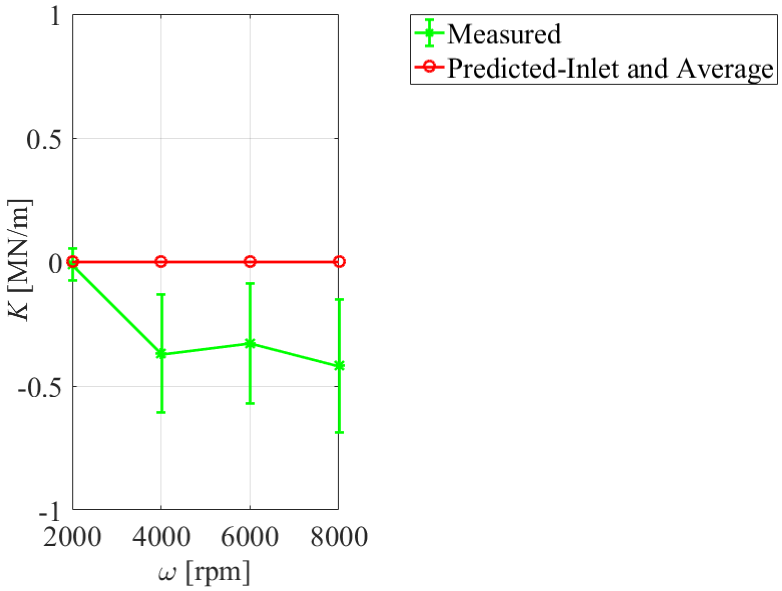

Figure 46 Predicted [21] and measured *K* for ISO VG 100 vs ω at 8.28 bar

12.3 Cross-Coupled Stiffness

As seen in Fig. 47, predicted *k* is generally higher than measured. The measured trend of increasing *k* with increasing ω is predicted by the code. Using the average fluid temperature improves the predicted values.

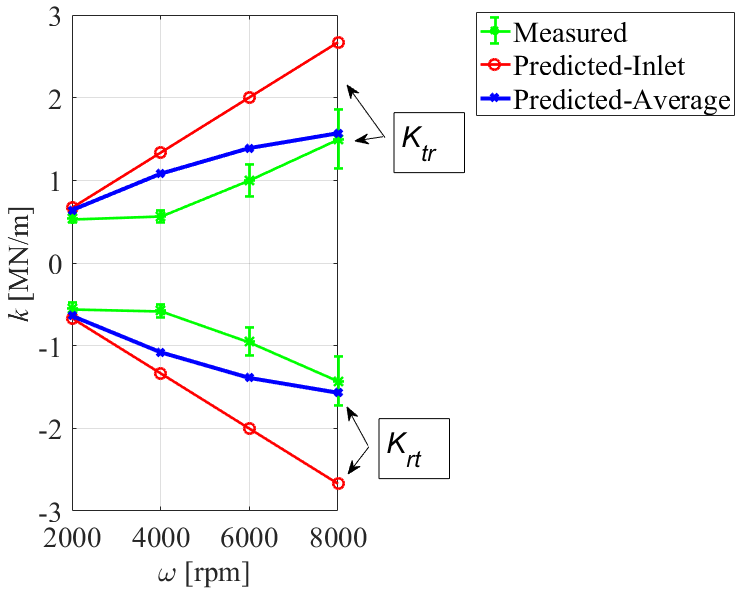

Figure 47 Predicted [21] and measured *k* for ISO VG 100 vs ω at 8.28 bar

12.4 Direct Damping

As seen in Fig. 48, predicted C_{rr} and C_{tt} are lower than measured and follow the measured trend. Using the average measured fluid temperature did not improve the predicted C_{rr} and C_{tt}.

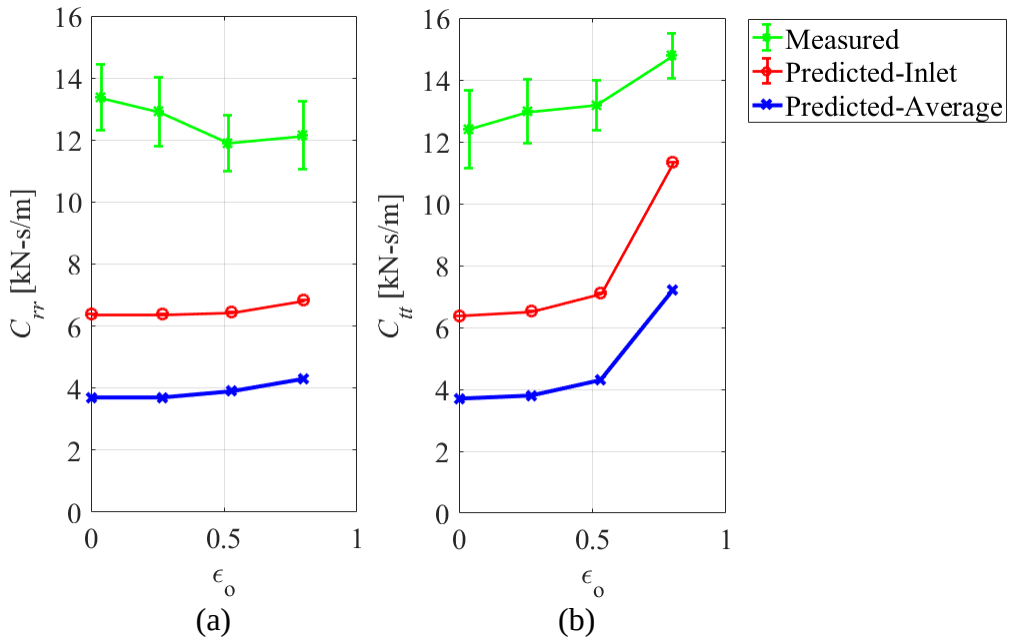

Figure 48 Predicted [21] and measured (a) C_{rr} and (b) C_{tt} for ISO VG 100 vs ε_o at 8 krpm and 8.28 bar

12.5 Cross-Coupled Damping

As seen in Fig. 49, predicted C_{rt} and C_{tr} were significantly lower (close to zero) than the measured values. Using the average measured fluid temperature did not have a noticeable impact on the predicted C_{rt} and C_{tr}.

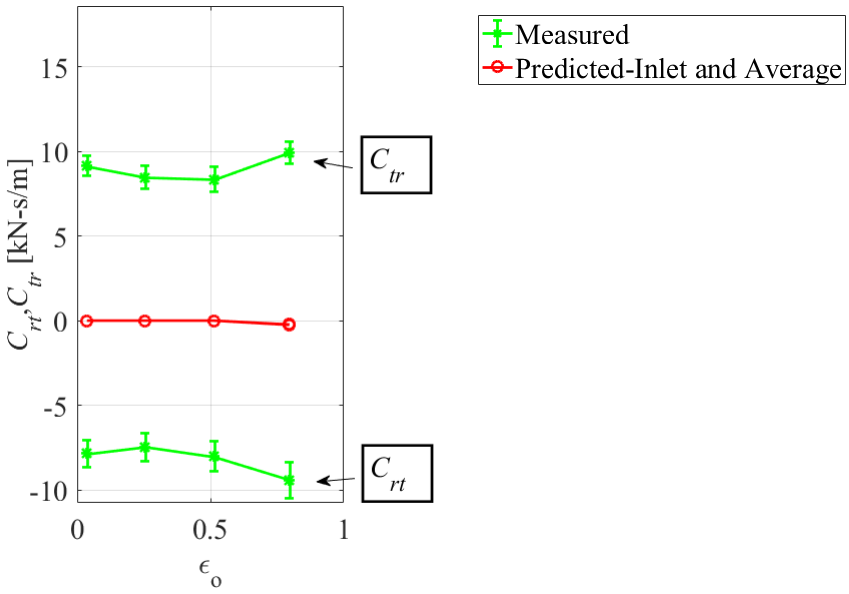

Figure 49 Predicted [21] and measured C_{rt} and C_{tr} for ISO VG 100 vs ε_o at 8 krpm and 8.28 bar

12.6 Direct Virtual-Mass

As seen in Fig. 50, predicted M_{rr} and M_{tt} values are less than measured and do not follow the trend of increasing M_{rr} and M_{tt} with increasing ε_o. Using the average measured fluid temperature did not have a noticeable impact on the predicted M_{rr} and M_{tt}.

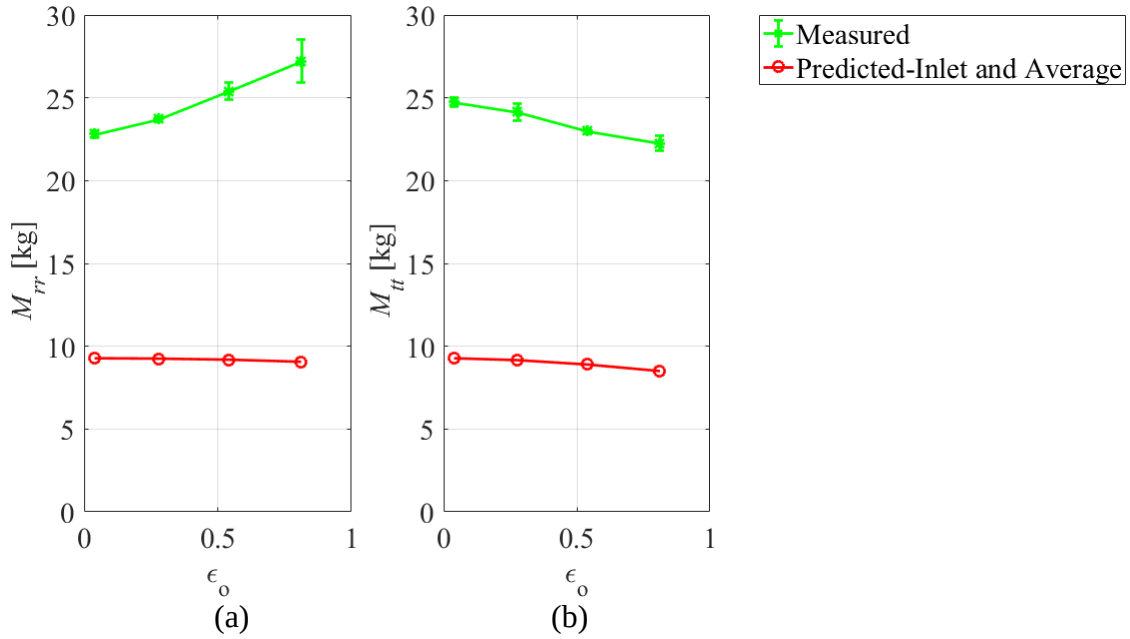

Figure 50 Predicted [21] and measured (a) M_{rr} and (b) M_{tt} for ISO VG 100 vs ε_o at 2 krpm and 2.07 bar

12.7 Cross-Coupled Virtual-Mass

As seen in Fig. 51, measured M_{rt} and M_{tr} were small and comparisons to the predicted value is difficult due to the small values and large error bars. Using the average measured fluid temperature did not have a noticeable impact on the predicted M_{rt} and M_{tr}.

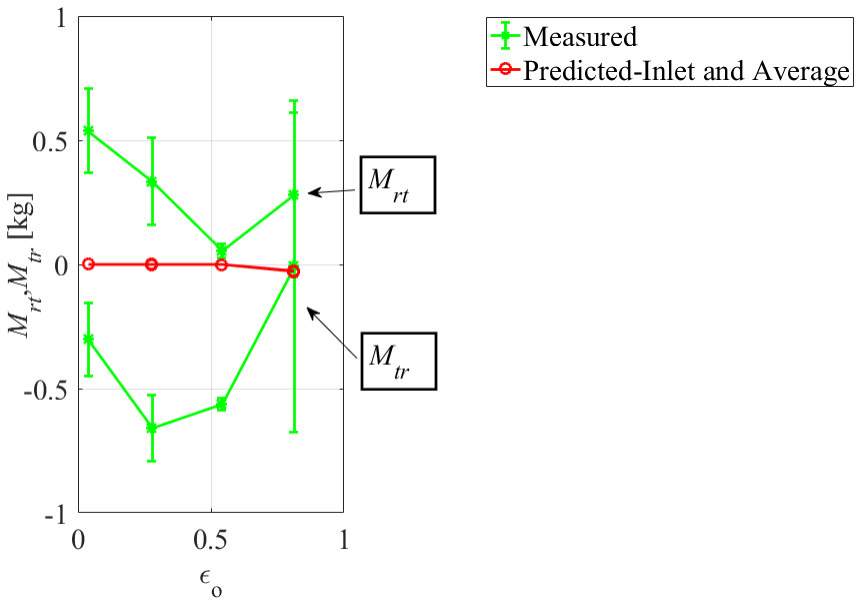

Figure 51 Predicted [21] and measured M_{rt} and M_{tr} for ISO VG 100 vs ε_o at 2 krpm and 2.07 bar

12.8 Discussion for Laminar Flow Predictions

Improvements to these predictions can be accomplished by adjusting μ for an anticipated ΔT, with the exception of C_{rr} and C_{tt} which did not improve with the average measured fluid temperature. Reducing the groove depth input to the code improves predictions of C_{rt} and C_{tr}, M_{rr} and M_{tt}, and M_{rt} and M_{tr}. A study of how much to adjust the groove depth is beyond the scope of this work.

13. SUMMARY AND CONCLUSIONS

As shown in Fig. 2, the circumferentially-grooved stator/smooth-rotor seal (GS/SR) tested had 15 square grooves with groove length, groove depth, and lands between grooves measuring 1.52 mm. Radial clearance (C_r) was 0.1905 mm and length to diameter ratio (L/D) was 0.5 for the seal. This seal was tested with three different viscosity (μ) liquids; ISO VG 2, ISO VG 46, and ISO VG 100 oils at 46.1°C. Tests were conducted at rotor speeds (ω) of 2, 4, 6, and 8 krpm; pressure drops (ΔP) of 2.07, 4.14, 6.21, and 8.28 bar; and eccentricity ratios (ε_o) of 0.00, 0.27, 0.53, and 0.80. To introduce fluid rotation at the seal inlet, fluid was injected with a component in the circumferential direction.

For the low μ test liquid (VG 2) the flow was turbulent at all test points. Flow for the high μ (VG 100) was laminar for all test points. With the medium μ test liquid (VG 46), the flow varied between laminar and turbulent. Temperature rise (ΔT) for VG 2 was small, less than 4°C. For VG 100, ΔT was significant, as high as 29°C at 8 krpm and 2.07 bar.

Flow rate ($\dot{Q}$) decreased with increasing μ, and increased with increasing ΔP and increasing ε_o. For VG 2, $\dot{Q}$ decreased with increasing ω. With VG 100, $\dot{Q}$ increased with increasing ω due to viscous heating of the liquid.

Direct stiffness (K_{rr} and K_{tt}) were generally negative. Cross-coupled stiffness (K_{rt} and K_{tr}) increase in magnitude with increasing ω and were generally destabilizing (opposite in sign). Direct damping (C_{rr} and C_{tt}) increase with increasing μ and increasing ΔP. Cross-coupled damping (C_{rt} and C_{tr}) are opposite in sign (act as gyroscopic damping, not dissipative damping) and increase with increasing ω. Direct virtual-mass (M_{rr} and M_{tt}) increase with increasing μ and increasing ε_o. M_{rr} and M_{tt} decrease with increasing ω. Cross-coupled virtual-mass (M_{rt} and M_{tr}) were small in magnitude relative to the direct term, on the same order as the uncertainty values, and opposite in sign.

Effective stiffness (K_{eff}) is often negative, decreases with increasing ω, and typically decreases with increasing μ. Effective damping (C_{eff}) increases with increasing μ. Whirl frequency ratio (WFR) tends towards ~0.2 as ω increases.

Static and rotordynamic characteristics generally changed significantly going from VG 2 to VG 100. Some results for VG 46 were unexpected and significantly different from those of

VG 2 and VG 100. At low ω, VG 46 has a low phase angle (ϕ), small K_{rt} and K_{tr}, and low WFR. As ω increases for VG 46, ϕ, K_{rt} and K_{tr}, and WFR all increase. The low ϕ and low WFR at low ω is similar to that of a plain journal bearing. This behavior was not observed in the VG 2 or VG 100 test results.

For an Electric Submersible Pump (ESP) with GS/SR seals, a rotordynamic analysis at both the high and low expected μ values is recommended. As μ increases, C_{eff} increases which improves stability characteristics. However, increasing μ also decreases K_{eff} which lowers the natural frequencies of the rotor system, which is detrimental to rotor stability.

For turbulent flow seals, grooves have the effect of reducing all rotordynamic coefficients. Additionally, grooves reduce the dependence of the rotordynamic coefficients on ε_o.

Static and rotordynamic characteristics of the turbulent GS/SR were poorly predicted using [18]. For the laminar GS/SR, static and some rotordynamic (K_{rt}, K_{tr} and C_{rr}, C_{tt}) characteristics were reasonably well predicted using [21].

Future work should focus on (a) improving the pre-swirl measurements for the VG 46 and VG 100 test cases; (b) improvements to laminar seal prediction codes to include viscous heating effects; and (c) improvements to turbulent seal prediction codes to include updated experimental coefficients.

REFERENCES

[1] Childs, D. W., 2013, *Turbomachinery Rotordynamics with Case Studies*, Minter Spring, Wellborn.

[2] Black, H., 1969, "Effects of Hydraulic Forces in Annular Pressure Seals on the Vibrations of Centrifugal Pump Rotors," Journal Mechanical Engineering Science, **11**, pp. 206–213.

[3] Lomakin, A., 1958, "Calculation of the Critical Number of Revolutions and the Conditions Necessary for Dynamic Stability of Rotors in High-Pressure Hydraulic Machines When Taking into Account Forces Originating in Sealings," Journal for Power and Mechanical Engineering, (In Russian), pp. 1–5.

[4] Nelson, C. C., and Nguyen, D., 1988, "Analysis of Eccentric Annular Incompressible Seals: Part 1 - A New Solution Using Fast Fourier Transoformations for Determining Hydrodynamic Forces," ASME Journal of Tribology, **110**, pp. 254–359.

[5] Nelson, C. C., and Nguyen, D., 1988, "Analysis of Eccentric Annular Incompressible Seals: Part 2 - Effects of Eccentricity on Rotordynamic Coefficients," ASME Journal of Tribology, **110**, pp. 361–366.

[6] Childs, D. W., 1983, "Finite-Length Solutions for Rotordynamic Coefficients of Turbulent Annular Seals," Journal of Lubrication Technology, **105**, pp. 437–444.

[7] Lund, J., 1966, "Self-Excited, Stationary Whirl Orbits of a Journal in a Sleeve Bearing," Rensselaer Polytechnic Institute.

[8] San Andrés, L. A., 1991, "Effects of Eccentricity on the Forced Response of a Hybrid Bearing," Tribology Transactions, **34**(4), pp. 537–544.

[9] Black, H., Allaire, P., and Barrett, L., 1981, "Inlet Flow Swirl in Short Turbulent Seal Dynamics," *Ninth International Conference on Fluid Sealing*, Noordwijkerhout, Netherlands.

[10] Iwatsubo, T., Sheng, B., and Matsumoto, T., 1989, "An Experimental Study on the Static and Dynamic Characteristics of Pump Annular Seals," *Rotordynamic Instability Problems in High-Performance Turbomachinery*, NASA, Lewis Research Center, pp. 229–251.

[11] Childs, D. W., Norrbin, C. S., and Phillips, S., 2014, "A Lateral Rotordynamics Primer on Electric Submersible Pumps (ESPs) for Deep Subsea Applications," *43rd Turbomachinery & 30th Pump Users Symposia*, Houston TX.

[12] Marquette, O., Childs, D. W., and Phillips, S., 1997, "Theory Versus Experement for Leakage and Rotordynamic Coefficients of Circumferentially Grooved Liquid Annular Seals with L/D of 0.45," *ASME Fluids Engineering Division Summer Meeting*,

Vancouver, BC, Canada.

[13] Moreland, J. A., 2016, "Influence of Pre-Swirl and Eccentricity in Smooth Stator/Groved Rotor Liquid Annular Seals, Measured Static and Rotordynamic Characteristics," M.S. Thesis, Texas A&M University.

[14] Torres, J. M., 2016, "Static and Rotordynamic Charicteristics of Liquid Annular Seals with Circumferentially-Grooved Stator and Smooth Rotor Using Three Levels of Circumferential Inlet-Fluid Rotation," M.S. Thesis, Texas A&M University.

[15] Florjancic, S., and McCloskey, T., 1991, "Measurement and Prediction of Full Scale Annular Seal Coefficients," *Eighth International Pump Users Symposium*, Houston TX.

[16] Marquette, O., and Childs, D. W., 1996, "An Extended Three-Control-Volume Theory for Circumferentially-Grooved Liquid Seals," ASME Journal of Tribology, **118**, pp. 276–285.

[17] Arghir, M., and Frene, J., 2004, "A Bulk-Flow Analysis of Static and Dynamic Characteristics of Eccentric Circumferentially-Grooved Liquid Annular Seals," ASME Journal of Tribology, **126**, pp. 316–325.

[18] San Andrés, L. A., Wu, T., Maeda, H., and Ono, T., 2017, "A Computational Fluid Dynamics Modified Bulk FLow Analysis for Circumferentially Shallow Grooved Liquid Seals," *Proceedings of ASME Turbo Expo*.

[19] Semanate, J. E., and San Andrés, L. A., 1994, "Thermal Analysis of Locked Multi-Ring Oil Seals," Tribology International, **27**(3), pp. 197–206.

[20] Childs, D. W., Graviss, M., and Rodriguez, L., 2007, "Influence of Groove Size on the Static and Rotordynamic Characteristics of Short, Laminar-Flow Annular Seals," ASME Journal of Tribology, **129**, pp. 398–406.

[21] San Andrés, L. A., and Delgado, A., 2012, "A Novel Bulk-Flow Model for Improved Predictions of Force Coefficients in Grooved Oil Seals Operating Eccentrically," ASME Journal of Engineering for Gas Turbines and Power, **134**(52509).

[22] Kaul, A., 1999, "Design and Development of a Test Setup for the Experimental Determination of the Rotordynamic and Leakage Characteristics of Annular Bushing Oil Seals," Texas A&M University.

[23] Glienicke, J., 1966, "Experimental Investigation of the Stiffness and Damping Coefficients of Turbine Bearings and Their Application to Instability Prediction," Proceedings of IMechE 1966-67, (181), pp. 116–129.

[24] Rouvas, C., and Childs, D. W., 1993, "A Parameter Identification Method for the Rotordynamic Coefficients of a High Reynolds Number Hydrostatic Bearing," ASME Journal of Vibration and Acoustics, **115**, pp. 264–270.

[25] Childs, D. W., and Hale, K., 1994, “A Test Apparatus and Facility to Identify the Rotordynamic Coefficients of High-Speed Hydrostatic Bearings,” ASME Journal of Tribology, **116**, pp. 337–343.

[26] Beckwith, T., Marangoni, R., and Lienhard, V., 2007, *Mechanical Measurements*, Pearson Education, Inc., Upper Saddle River, NJ.

APPENDIX A
TABULATED RESULTS

International Standards Organization Viscosity Grade 2 Test Liquid

Table A. 1 Static results of CGS with ISO VG 2 (ω, Δ*P*, ε_o, *Q*, PSR, Re_z, Re_θ, and *Re*)

Test Point	Measured ω	Measured Δ*P*	Measured ε_o	$\dot{Q}$	v_{inlet}	Pre-swirl Ratio	Re_z	Re_θ	*Re*
	[RPM]	[bar]	[-]	[lpm]	[m/s]	[-]	[-]	[-]	[-]
1	2002	2.04	0.04	24.1	5.9	0.55	1.08E+03	7.98E+03	8.06E+03
2	2002	2.05	0.29	24.4	5.7	0.54	1.07E+03	7.77E+03	7.85E+03
3	2002	2.05	0.55	25.5	5.8	0.54	1.12E+03	7.77E+03	7.85E+03
4	2002	2.06	0.82	28.1	6.0	0.56	1.24E+03	7.86E+03	7.96E+03
5	2003	4.16	0.04	37.2	7.6	0.71	1.64E+03	7.84E+03	8.01E+03
6	2003	4.14	0.27	37.9	7.5	0.70	1.69E+03	7.92E+03	8.10E+03
7	2003	4.08	0.54	39.5	7.3	0.69	1.75E+03	7.90E+03	8.09E+03
8	2002	4.13	0.80	42.7	7.2	0.68	1.85E+03	7.70E+03	7.92E+03
9	2002	6.21	0.03	48.4	8.9	0.84	2.15E+03	7.92E+03	8.21E+03
10	2002	6.26	0.27	49.0	8.6	0.81	2.15E+03	7.81E+03	8.11E+03
11	2002	6.19	0.54	51.3	8.4	0.79	2.28E+03	7.89E+03	8.22E+03
12	2002	6.19	0.81	55.0	8.4	0.78	2.42E+03	7.84E+03	8.21E+03
13	2002	8.39	0.02	58.6	8.9	0.84	2.61E+03	7.93E+03	8.35E+03
14	2002	8.31	0.27	59.1	7.8	0.74	2.62E+03	7.88E+03	8.30E+03
15	2002	8.25	0.53	61.3	7.5	0.71	2.73E+03	7.93E+03	8.39E+03
16	2003	8.20	0.82	66.0	7.7	0.72	2.93E+03	7.91E+03	8.43E+03
17	4007	2.01	0.14	18.5	7.6	0.36	8.33E+02	1.60E+04	1.60E+04
18	4007	2.04	0.33	20.0	7.7	0.36	8.95E+02	1.59E+04	1.60E+04
19	4010	2.08	0.54	21.6	7.6	0.36	9.62E+02	1.59E+04	1.59E+04
20	4011	2.08	0.80	23.3	7.9	0.37	1.04E+03	1.59E+04	1.60E+04
21	4011	4.13	0.10	34.5	9.7	0.46	1.53E+03	1.58E+04	1.59E+04
22	4012	4.09	0.31	35.1	9.6	0.45	1.55E+03	1.57E+04	1.58E+04
23	4013	4.07	0.57	37.0	9.6	0.45	1.67E+03	1.61E+04	1.62E+04
24	4012	4.16	0.82	40.3	9.7	0.46	1.79E+03	1.58E+04	1.59E+04
25	4014	6.28	0.01	45.6	11.5	0.54	2.01E+03	1.57E+04	1.58E+04
26	4015	6.16	0.28	45.8	11.1	0.52	2.05E+03	1.60E+04	1.61E+04
27	4017	6.25	0.52	48.5	11.3	0.53	2.16E+03	1.59E+04	1.60E+04
28	4017	6.14	0.81	51.5	11.3	0.53	2.30E+03	1.60E+04	1.61E+04
29	4016	8.31	0.04	54.8	12.1	0.56	2.42E+03	1.57E+04	1.59E+04
30	4017	8.29	0.27	55.5	11.5	0.54	2.48E+03	1.59E+04	1.61E+04
31	4017	8.26	0.53	58.0	11.4	0.53	2.57E+03	1.58E+04	1.60E+04
32	4018	8.32	0.79	62.1	10.7	0.50	2.78E+03	1.60E+04	1.62E+04

Test Point	Measured ω	Measured ΔP	Measured ε_o	$\dot{Q}$	v_{inlet}	Pre-swirl Ratio	Re_z	Re_θ	Re
	[RPM]	[bar]	[-]	[lpm]	[m/s]	[-]	[-]	[-]	[-]
33	6004	2.07	0.06	17.7	10.4	0.32	7.84E+02	2.37E+04	2.37E+04
34	6006	2.03	0.32	17.7	10.3	0.32	7.83E+02	2.36E+04	2.37E+04
35	6011	2.09	0.55	19.1	10.1	0.32	8.51E+02	2.37E+04	2.37E+04
36	6015	2.05	0.80	20.8	10.2	0.32	9.31E+02	2.39E+04	2.39E+04
37	6017	4.09	0.05	30.5	11.2	0.35	1.39E+03	2.43E+04	2.44E+04
38	6019	4.15	0.28	31.4	11.2	0.35	1.41E+03	2.40E+04	2.40E+04
39	6020	4.12	0.53	32.9	11.3	0.35	1.50E+03	2.44E+04	2.44E+04
40	6020	4.08	0.82	35.4	11.6	0.36	1.60E+03	2.41E+04	2.42E+04
41	6018	6.28	0.00	41.0	12.5	0.39	1.80E+03	2.35E+04	2.36E+04
42	6019	6.18	0.29	41.3	12.2	0.38	1.84E+03	2.37E+04	2.38E+04
43	6020	6.22	0.54	43.3	12.3	0.39	1.94E+03	2.40E+04	2.40E+04
44	6020	6.22	0.78	46.1	12.5	0.39	2.04E+03	2.36E+04	2.37E+04
45	6019	8.26	0.01	49.3	12.7	0.40	2.18E+03	2.36E+04	2.37E+04
46	6020	8.28	0.27	50.0	12.3	0.38	2.24E+03	2.39E+04	2.40E+04
47	6020	8.25	0.55	52.3	12.3	0.38	2.35E+03	2.40E+04	2.41E+04
48	6020	8.27	0.79	56.1	13.4	0.42	2.54E+03	2.42E+04	2.43E+04
49	8000	2.06	0.03	14.6	14.8	0.35	6.77E+02	3.30E+04	3.30E+04
50	8001	2.12	0.27	14.8	14.6	0.34	6.87E+02	3.29E+04	3.29E+04
51	8001	2.11	0.53	15.6	14.4	0.34	7.20E+02	3.27E+04	3.27E+04
52	8001	2.08	0.78	16.8	14.2	0.33	7.71E+02	3.26E+04	3.26E+04
53	7998	4.15	0.04	27.3	13.6	0.32	1.28E+03	3.33E+04	3.34E+04
54	7998	4.22	0.26	28.1	13.5	0.32	1.29E+03	3.26E+04	3.26E+04
55	7998	4.18	0.53	29.4	13.5	0.32	1.33E+03	3.21E+04	3.21E+04
56	7998	4.15	0.80	31.7	13.3	0.31	1.43E+03	3.19E+04	3.20E+04
57	7998	6.17	0.03	37.7	14.4	0.34	1.75E+03	3.30E+04	3.30E+04
58	7999	6.24	0.25	38.4	14.2	0.33	1.75E+03	3.23E+04	3.23E+04
59	7999	6.22	0.52	40.1	14.2	0.33	1.83E+03	3.24E+04	3.25E+04
60	7999	6.23	0.81	43.3	14.3	0.34	1.95E+03	3.19E+04	3.20E+04
61	7999	8.28	0.01	46.8	14.9	0.35	2.16E+03	3.27E+04	3.28E+04
62	7999	8.37	0.28	47.8	14.5	0.34	2.18E+03	3.24E+04	3.24E+04
63	7999	8.24	0.52	49.3	14.5	0.34	2.25E+03	3.24E+04	3.25E+04
64	7999	8.35	0.80	53.6	14.7	0.35	2.44E+03	3.23E+04	3.24E+04

Table A. 2 Static results of CGS with ISO VG 2 (T_{in}, T_{out}, F_{sr}, uncertainty in F_{sr}, F_{st}, uncertainty in F_{st}, ϕ, and uncertainty in ϕ)

Test Point	Inlet Temperature	Average Outlet Temperature	F_{sr}	UF_{sr}	F_{st}	UF_{st}	ϕ	$U\phi$
	[°C]	[°C]	[N]	±[N]	[N]	±[N]	[degrees]	±[degrees]
1	46.9	46.7	0	0.8	0	0.5	-	-
2	45.2	45.4	11	1.1	-9	1.3	39	4.9
3	45.4	45.1	26	0.6	-21	1.1	40	1.6
4	46.0	45.8	36	1.6	-30	4.2	39	4.2
5	45.8	45.7	0	1.1	0	5.7	-	-
6	46.4	46.3	22	6.9	-25	4.4	49	10.2
7	46.2	46.1	34	1.3	-48	1.8	55	1.4
8	44.5	44.9	44	1.4	-68	0.8	57	0.9
9	46.3	46.4	0	1.1	0	2.1	-	-
10	45.6	45.5	23	2.3	-40	2.7	60	2.9
11	46.2	46.1	37	0.5	-85	1.3	66	0.4
12	45.8	45.7	44	0.5	-120	1.5	70	0.3
13	46.4	46.4	0	1.4	0	2.1	-	-
14	45.9	46.2	8	28.7	-68	15.8	83	23.8
15	46.4	46.4	23	1.1	-128	2.3	80	0.5
16	46.2	46.2	32	0.8	-187	0.8	80	0.2
17	46.6	47.0	0	12	0	6	-	-
18	46.7	46.8	6	1.5	-10	2.7	61	9.4
19	46.3	46.5	11	5.6	-21	1.2	61	12.1
20	46.6	46.7	12	2.5	-33	1.1	70	3.8
21	46.0	46.2	0	9.3	0	4.3	-	-
22	45.7	45.9	18	8.8	-22	7.9	51	17.2
23	47.2	47.2	23	8.7	-45	4.4	63	9.1
24	46.2	46.3	24	0.5	-65	1.1	69	0.5
25	45.6	45.9	0	0.9	0	1.8	-	-
26	46.6	46.8	15	1.4	-45	1.7	71	1.8
27	46.3	46.5	22	1.2	-83	0.6	75	0.8
28	46.6	46.7	24	2.2	-118	0.8	78	1.0
29	45.7	45.9	0	3	0	2.9	-	-
30	46.5	46.7	26	1	-63	1.3	68	0.9
31	45.8	46.2	34	1.2	-121	2.5	75	0.6
32	46.5	46.7	31	0.5	-175	0.5	80	0.2

Test Point	Inlet Temperature	Average Outlet Temperature	F_{sr}	UF_{sr}	F_{st}	UF_{st}	ϕ	$U\phi$
	[°C]	[°C]	[N]	±[N]	[N]	±[N]	[degrees]	±[degrees]
33	45.7	46.7	0	1.3	0	1	-	-
34	45.5	46.7	-2	1.9	-28	1.9	94	3.9
35	45.8	46.8	-1	16.4	-64	5.1	91	14.7
36	46.1	47.3	-10	5.7	-91	0.9	96	3.5
37	47.2	47.9	0	7.8	0	2.3	-	-
38	46.4	47.2	-4	2.6	-33	2.3	96	4.4
39	47.3	48.1	-15	27.6	-63	6.1	104	23.9
40	46.8	47.4	-28	4.7	-101	2.4	106	2.5
41	45.4	46.0	0	0.9	0	2	-	-
42	45.9	46.6	-1	1.3	-50	2.4	91	1.5
43	46.5	47.0	-9	1	-88	3.3	96	0.7
44	45.7	46.3	-21	0.7	-125	1.7	100	0.3
45	45.6	46.4	0	1.6	0	2.9	-	-
46	46.3	46.8	2	1.1	-62	2.5	88	1.0
47	46.6	47.1	-5	0.4	-120	0.9	92	0.2
48	47.1	47.6	-17	3.4	-169	1.6	96	1.1
49	47.1	50.1	0	9.3	0	2.4	-	-
50	46.7	50.1	-11	12.9	-64	0.4	100	11.2
51	46.5	49.9	-27	1	-122	1.1	102	0.5
52	46.4	49.6	-55	1.9	-164	1	108	0.6
53	48.3	50.2	0	2.7	0	4.7	-	-
54	47.0	49.0	-14	0.6	-49	2.9	106	1.1
55	46.0	48.2	-32	10.1	-103	3.5	107	5.2
56	45.9	47.9	-78	4.8	-152	2.5	117	1.5
57	47.8	49.5	0	13	0	3.1	-	-
58	46.6	48.3	-27	0.6	-46	1.6	120	1.0
59	46.9	48.5	-58	1	-99	2.6	120	0.8
60	46.2	47.7	-96	1	-166	4.5	120	0.7
61	47.5	49.0	0	1.1	0	3.7	-	-
62	46.9	48.3	-23	1.5	-66	3	109	1.4
63	47.0	48.4	-48	1.9	-119	2.4	112	0.9
64	46.9	48.2	-83	1.2	-194	1.4	113	0.3

Table A. 3 Stiffness coefficients and uncertainties of CGS with ISO VG 2

Test Point	K_{rr} [MN/m]	UK_{rr} ±[MN/m]	K_{tt} [MN/m]	UK_{tt} ±[MN/m]	K_{tr} [MN/m]	UK_{tr} ±[MN/m]	K_{rt} [MN/m]	UK_{rt} ±[MN/m]
1	-0.2	0.15	-0.2	0.12	0.3	0.06	-0.3	0.06
2	-0.2	0.13	-0.1	0.13	0.2	0.06	-0.3	0.06
3	-0.1	0.13	-0.1	0.1	0.3	0.05	-0.3	0.07
4	-0.2	0.13	-0.2	0.05	0.1	0.08	-0.2	0.09
5	0.0	0.11	0.1	0.13	0.6	0.06	-0.6	0.08
6	0.0	0.08	0.0	0.07	0.5	0.05	-0.6	0.04
7	-0.1	0.11	0.0	0.04	0.3	0.04	-0.5	0.05
8	-0.2	0.1	0.0	0.06	0.3	0.1	-0.5	0.03
9	0.2	0.07	0.2	0.05	0.8	0.04	-0.8	0.04
10	0.1	0.03	0.2	0.07	0.9	0.04	-0.9	0.03
11	-0.1	0.07	0.1	0.03	0.7	0.06	-0.8	0.03
12	-0.2	0.08	0.0	0.04	0.4	0.13	-0.8	0.04
13	0.3	0.08	0.3	0.09	1.2	0.05	-1.1	0.04
14	0.1	0.07	0.3	0.06	1.2	0.04	-1.1	0.03
15	-0.1	0.04	0.2	0.06	1.1	0.07	-1.2	0.05
16	-0.1	0.1	0.0	0.05	0.4	0.13	-1.1	0.09
17	-0.3	0.1	-0.4	0.09	0.4	0.07	-0.4	0.15
18	-0.3	0.09	-0.3	0.04	0.4	0.08	-0.4	0.12
19	-0.3	0.03	-0.4	0.11	0.4	0.07	-0.4	0.1
20	-0.3	0.14	-0.4	0.05	0.3	0.12	-0.4	0.09
21	-0.2	0.06	-0.2	0.09	0.6	0.1	-0.6	0.12
22	-0.2	0.12	-0.2	0.02	0.5	0.06	-0.6	0.06
23	-0.3	0.12	-0.2	0.01	0.4	0.07	-0.6	0.06
24	-0.3	0.09	-0.2	0.06	0.3	0.08	-0.5	0.04
25	0.0	0.06	0.0	0.05	0.9	0.06	-0.8	0.05
26	-0.1	0.04	-0.1	0.06	0.8	0.05	-0.9	0.04
27	-0.2	0.08	-0.1	0.04	0.6	0.05	-0.8	0.03
28	-0.4	0.08	-0.2	0.06	0.4	0.08	-0.8	0.07
29	0.1	0.05	0.1	0.03	1.2	0.09	-1.1	0.06
30	0.0	0.05	0.1	0.06	1.2	0.05	-1.1	0.04
31	-0.2	0.06	0.0	0.05	0.9	0.06	-1.1	0.04
32	-0.3	0.13	-0.1	0.09	0.6	0.11	-1.2	0.16

Test Point	K_{rr} [MN/m]	UK_{rr} ±[MN/m]	K_{tt} [MN/m]	UK_{tt} ±[MN/m]	K_{tr} [MN/m]	UK_{tr} ±[MN/m]	K_{rt} [MN/m]	UK_{rt} ±[MN/m]
33	-0.5	0.08	-0.6	0.1	0.7	0.07	-0.6	0.08
34	-0.5	0.11	-0.6	0.07	0.8	0.08	-0.7	0.12
35	-0.6	0.01	-0.5	0.22	0.9	0.02	-0.8	0.09
36	-0.7	0.09	-0.7	0.22	0.6	0.1	-0.8	0.13
37	-0.4	0.04	-0.5	0.1	0.8	0.06	-0.7	0.14
38	-0.5	0.11	-0.5	0.04	0.6	0.1	-0.8	0.17
39	-0.6	0.06	-0.6	0.08	0.7	0.14	-0.7	0.13
40	-0.5	0.14	-0.5	0.06	0.6	0.17	-0.6	0.1
41	-0.3	0.06	-0.4	0.07	1.0	0.09	-0.9	0.12
42	-0.4	0.03	-0.4	0.09	0.9	0.09	-0.9	0.06
43	-0.5	0.06	-0.4	0.08	0.8	0.11	-0.9	0.07
44	-0.6	0.05	-0.5	0.09	0.7	0.11	-0.8	0.1
45	-0.3	0.05	-0.3	0.08	1.2	0.1	-1.1	0.08
46	-0.3	0.06	-0.3	0.09	1.2	0.07	-1.1	0.06
47	-0.5	0.08	-0.4	0.08	0.9	0.1	-1.1	0.06
48	-0.6	0.09	-0.4	0.09	0.7	0.09	-1.1	0.11
49	-0.7	0.09	-0.7	0.14	1.3	0.12	-1.3	0.06
50	-0.7	0.09	-0.8	0.14	1.3	0.08	-1.3	0.08
51	-1.0	0.05	-0.9	0.16	1.3	0.06	-1.2	0.09
52	-1.3	0.04	-1.0	0.16	1.0	0.08	-1.1	0.11
53	-0.8	0.12	-0.8	0.18	1.2	0.17	-1.1	0.2
54	-0.8	0.18	-0.9	0.13	1.3	0.16	-1.2	0.18
55	-0.9	0.16	-0.9	0.12	1.4	0.17	-1.3	0.21
56	-1.1	0.03	-1.0	0.25	1.1	0.17	-1.2	0.16
57	-0.8	0.1	-0.8	0.09	1.1	0.05	-1.1	0.1
58	-0.9	0.03	-0.9	0.1	1.1	0.07	-1.0	0.14
59	-1.0	0.05	-0.9	0.1	1.2	0.05	-1.0	0.14
60	-1.0	0.06	-1.0	0.15	1.2	0.12	-1.1	0.1
61	-0.7	0.07	-0.7	0.08	1.4	0.07	-1.2	0.07
62	-0.8	0.05	-0.7	0.08	1.1	0.07	-1.2	0.08
63	-1.0	0.05	-0.7	0.11	1.0	0.09	-1.1	0.07
64	-0.9	0.08	-0.9	0.13	1.2	0.1	-1.2	0.09

Table A. 4 Damping coefficients and uncertainties of CGS with ISO VG 2

Test Point	C_{rr} [kN-s/m]	UC_{rr} ±[kN-s/m]	C_{tt} [kN-s/m]	UC_{tt} ±[kN-s/m]	C_{tr} [kN-s/m]	UC_{tr} ±[kN-s/m]	C_{rt} [kN-s/m]	UC_{rt} ±[kN-s/m]
1	4.0	0.58	4.1	0.43	1.7	0.23	-1.4	0.16
2	4.0	0.47	4.0	0.36	1.7	0.17	-1.5	0.18
3	4.0	0.67	3.8	0.33	1.7	0.12	-1.5	0.12
4	3.7	0.64	3.5	0.24	2.0	0.15	-1.8	0.13
5	4.8	0.56	4.9	0.45	1.9	0.14	-1.5	0.32
6	4.7	0.59	4.8	0.32	2.1	0.14	-1.6	0.24
7	4.5	0.48	4.5	0.25	2.3	0.11	-1.8	0.17
8	3.8	0.39	4.2	0.31	2.5	0.3	-2.2	0.26
9	5.3	0.44	5.5	0.29	2.4	0.21	-2.1	0.23
10	5.1	0.23	5.5	0.4	2.3	0.1	-2.2	0.26
11	4.7	0.3	5.2	0.18	2.8	0.15	-2.1	0.21
12	3.8	0.33	4.8	0.22	2.9	0.43	-2.7	0.21
13	5.9	0.29	6.1	0.29	2.9	0.24	-2.5	0.15
14	5.7	0.23	6.0	0.27	2.8	0.15	-2.5	0.22
15	4.9	0.25	5.8	0.23	2.9	0.17	-2.6	0.23
16	4.0	0.43	5.2	0.2	3.3	0.43	-3.2	0.19
17	4.2	0.43	4.4	0.26	3.3	0.33	-2.9	0.33
18	4.2	0.39	4.2	0.04	3.4	0.26	-2.9	0.3
19	4.0	0.21	4.3	0.22	3.4	0.37	-3.2	0.37
20	3.6	0.32	3.7	0.13	3.5	0.42	-3.7	0.21
21	4.9	0.29	5.2	0.24	3.4	0.39	-3.0	0.43
22	5.1	0.48	5.0	0.01	3.7	0.16	-3.2	0.25
23	4.7	0.42	4.7	0	3.9	0.23	-3.4	0.23
24	4.0	0.33	4.6	0.13	4.0	0.4	-3.9	0.3
25	5.7	0.29	5.8	0.19	3.8	0.36	-3.4	0.33
26	5.3	0.23	5.8	0.2	3.9	0.23	-3.5	0.31
27	5.2	0.3	5.5	0.12	4.0	0.19	-3.7	0.29
28	4.3	0.42	5.2	0.19	4.5	0.38	-4.2	0.41
29	6.1	0.19	6.3	0.19	4.2	0.34	-3.8	0.26
30	5.8	0.18	6.3	0.24	4.1	0.16	-3.8	0.29
31	5.6	0.2	6.1	0.27	4.2	0.17	-4.0	0.24
32	4.5	0.6	5.8	0.33	4.9	0.24	-4.6	0.26

Test Point	C_{rr} [kN-s/m]	UC_{rr} ±[kN-s/m]	C_{tt} [kN-s/m]	UC_{tt} ±[kN-s/m]	C_{tr} [kN-s/m]	UC_{tr} ±[kN-s/m]	C_{rt} [kN-s/m]	UC_{rt} ±[kN-s/m]
33	4.3	0.2	4.5	0.28	4.7	0.27	-4.2	0.25
34	4.4	0.43	4.3	0.16	4.7	0.35	-4.2	0.26
35	4.2	0.16	4.5	0.53	4.7	0.24	-4.5	0.2
36	4.2	0.19	4.3	0.49	5.1	0.31	-5.2	0.17
37	5.2	0.23	5.6	0.19	5.4	0.4	-4.8	0.43
38	5.3	0.36	5.5	0.04	5.5	0.44	-4.8	0.41
39	5.0	0.24	5.2	0.17	5.6	0.51	-5.2	0.43
40	4.5	0.47	4.6	0.33	5.9	0.45	-5.6	0.42
41	6.0	0.22	6.3	0.27	5.4	0.4	-4.9	0.54
42	5.9	0.18	6.2	0.37	5.7	0.36	-5.1	0.26
43	5.5	0.12	6.0	0.4	5.9	0.31	-5.4	0.27
44	4.7	0.23	5.6	0.34	6.2	0.35	-5.9	0.4
45	6.6	0.24	6.9	0.25	5.8	0.41	-5.2	0.47
46	6.4	0.23	6.9	0.42	5.9	0.25	-5.4	0.22
47	5.9	0.21	6.7	0.43	6.0	0.38	-5.6	0.32
48	4.9	0.42	6.2	0.34	6.5	0.43	-6.1	0.48
49	4.1	0.24	4.5	0.36	5.9	0.45	-5.3	0.15
50	4.1	0.15	4.5	0.35	5.9	0.31	-5.4	0.17
51	4.2	0.09	4.6	0.41	6.1	0.25	-5.9	0.19
52	4.2	0.2	4.3	0.41	6.7	0.27	-6.7	0.41
53	5.9	0.42	6.3	0.48	6.0	0.63	-5.5	0.61
54	5.9	0.53	6.0	0.31	6.0	0.57	-5.6	0.46
55	5.5	0.56	6.0	0.47	6.2	0.75	-5.9	0.49
56	4.9	0	5.8	0.76	6.9	0.79	-6.9	0.51
57	6.2	0.23	6.6	0.24	7.4	0.34	-6.6	0.5
58	6.0	0.13	6.6	0.33	7.4	0.36	-6.8	0.59
59	5.5	0.15	6.4	0.35	7.5	0.4	-7.1	0.67
60	4.6	0.23	5.7	0.41	7.9	0.48	-7.8	0.34
61	6.7	0.2	7.1	0.19	7.4	0.25	-6.7	0.58
62	6.4	0.05	7.2	0.38	7.6	0.25	-7.0	0.37
63	5.9	0.33	6.9	0.44	7.9	0.42	-7.3	0.46
64	4.9	0.34	6.3	0.49	8.3	0.42	-7.9	0.29

Table A. 5 Virtual-mass coefficients and uncertainties of CGS with ISO VG 2

Test Point	M_{rr} [kg]	UM_{rr} ±[kg]	M_{tt} [kg]	UM_{tt} ±[kg]	M_{tr} [kg]	UM_{tr} ±[kg]	M_{rt} [kg]	UM_{rt} ±[kg]
1	12.6	0.52	13.6	0.44	0.2	0.21	0.2	0.2
2	12.5	0.47	13.4	0.46	0.2	0.22	0.3	0.22
3	14.1	0.47	13.5	0.37	0.3	0.17	0.4	0.27
4	16.5	0.48	13.9	0.18	-0.3	0.28	0.0	0.31
5	13.5	0.38	14.7	0.46	0.3	0.23	0.3	0.28
6	14.3	0.3	14.5	0.25	0.3	0.19	0.3	0.16
7	15.1	0.39	14.6	0.14	0.3	0.16	0.6	0.19
8	17.0	0.35	15.3	0.21	0.1	0.35	0.4	0.12
9	14.1	0.24	15.2	0.19	0.0	0.16	0.6	0.13
10	14.3	0.12	15.4	0.26	0.0	0.14	0.1	0.11
11	15.5	0.26	15.3	0.1	0.3	0.22	0.4	0.12
12	17.4	0.29	16.0	0.16	-0.2	0.48	0.2	0.15
13	14.2	0.29	15.3	0.33	0.2	0.19	0.5	0.15
14	14.4	0.24	15.5	0.22	0.2	0.14	0.3	0.1
15	15.6	0.16	15.7	0.2	0.2	0.24	0.1	0.17
16	17.9	0.36	16.0	0.19	-0.4	0.48	-0.1	0.31
17	11.6	0.35	12.4	0.31	-0.7	0.27	0.6	0.52
18	12.1	0.34	12.6	0.15	-0.2	0.29	0.5	0.43
19	13.1	0.1	12.9	0.39	-0.4	0.26	0.3	0.36
20	16.3	0.49	13.3	0.19	0.4	0.44	0.8	0.32
21	13.3	0.22	14.4	0.31	-0.4	0.36	0.6	0.43
22	13.7	0.45	14.3	0.08	0.0	0.21	1.0	0.21
23	14.9	0.43	14.4	0.05	0.2	0.24	0.8	0.2
24	16.5	0.32	15.0	0.23	-0.1	0.3	0.9	0.15
25	14.0	0.21	15.2	0.18	-0.4	0.23	0.9	0.17
26	14.4	0.15	15.2	0.23	-0.3	0.2	0.5	0.14
27	15.0	0.28	15.4	0.14	0.1	0.18	0.7	0.1
28	16.9	0.29	15.7	0.23	-0.4	0.29	0.6	0.26
29	14.2	0.19	15.5	0.13	-0.2	0.34	0.6	0.21
30	14.5	0.16	15.6	0.2	-0.1	0.19	0.5	0.14
31	15.2	0.2	15.7	0.18	0.2	0.21	0.2	0.14
32	17.7	0.46	16.1	0.33	-0.6	0.38	-0.5	0.57

Test Point	M_{rr} [kg]	UM_{rr} ±[kg]	M_{tt} [kg]	UM_{tt} ±[kg]	M_{tr} [kg]	UM_{tr} ±[kg]	M_{rt} [kg]	UM_{rt} ±[kg]
33	9.5	0.29	10.2	0.35	-0.1	0.25	0.4	0.3
34	10.3	0.38	10.4	0.24	0.3	0.29	0.4	0.45
35	11.8	0.02	11.2	0.78	-0.4	0.08	0.2	0.34
36	14.4	0.33	11.8	0.78	-0.2	0.36	-0.2	0.48
37	12.5	0.16	13.5	0.36	-0.9	0.23	0.9	0.49
38	12.7	0.41	13.4	0.16	-0.8	0.36	0.9	0.6
39	13.7	0.21	13.7	0.28	-0.6	0.51	1.0	0.47
40	16.6	0.5	14.1	0.21	0.0	0.61	1.0	0.36
41	13.0	0.2	14.2	0.25	-0.5	0.34	1.0	0.42
42	13.5	0.11	14.3	0.33	-0.7	0.33	0.9	0.2
43	14.4	0.21	14.6	0.28	-0.5	0.41	0.7	0.24
44	16.5	0.19	15.0	0.31	-0.5	0.38	0.5	0.36
45	13.6	0.18	14.7	0.29	-0.7	0.37	0.9	0.29
46	14.3	0.21	14.8	0.33	-0.4	0.27	0.6	0.2
47	14.9	0.28	14.9	0.28	-0.5	0.35	0.3	0.23
48	17.1	0.33	15.3	0.33	-0.7	0.34	0.3	0.41
49	9.7	0.32	10.5	0.5	0.0	0.44	-0.4	0.22
50	10.0	0.33	10.7	0.49	0.3	0.3	-0.3	0.27
51	11.2	0.18	10.9	0.58	-0.1	0.22	-0.3	0.32
52	13.0	0.16	11.4	0.56	0.0	0.3	-0.3	0.4
53	10.1	0.45	11.3	0.66	-0.3	0.59	0.2	0.72
54	10.5	0.65	11.3	0.45	0.3	0.57	0.5	0.63
55	12.1	0.57	12.2	0.44	-0.3	0.59	0.2	0.76
56	15.3	0.11	12.9	0.89	-1.6	0.62	0.2	0.58
57	12.5	0.35	13.8	0.32	-1.1	0.18	1.1	0.36
58	12.6	0.12	13.8	0.35	-1.2	0.25	1.0	0.51
59	13.8	0.17	14.0	0.36	-1.2	0.19	0.8	0.49
60	16.4	0.21	14.5	0.54	-0.8	0.43	0.4	0.37
61	13.0	0.26	14.3	0.3	-0.4	0.25	0.9	0.27
62	13.5	0.17	14.4	0.3	-1.1	0.26	0.4	0.3
63	14.0	0.17	14.5	0.4	-1.3	0.31	0.3	0.26
64	16.7	0.27	14.7	0.47	-0.9	0.36	0.1	0.33

Table A. 6 WFR, Keff, Ceff, and uncertainties of CGS with ISO VG 2

Test Point	*WFR* [-]	*UWFR* ±[-]	K_{eff} [MN/m]	UK_{eff} ±[MN/m]	C_{eff} [kN-s/m]	UC_{eff} ±[kN-s/m]
1	0.35	0.06	-0.42	0.10	2.6	0.41
2	0.24	0.06	-0.38	0.10	3.0	0.36
3	0.33	0.06	-0.41	0.09	2.6	0.43
4	0.24	0.08	-0.46	0.08	2.7	0.44
5	0.60	0.07	-0.22	0.09	1.9	0.43
6	0.58	0.05	-0.26	0.06	2.0	0.37
7	0.42	0.05	-0.29	0.06	2.6	0.32
8	0.42	0.08	-0.34	0.07	2.2	0.35
9	0.73	0.04	0.00	0.05	1.5	0.3
10	0.80	0.04	-0.06	0.05	1.1	0.26
11	0.72	0.04	-0.17	0.05	1.4	0.24
12	0.62	0.10	-0.23	0.07	1.5	0.39
13	0.91	0.04	0.17	0.07	0.6	0.26
14	0.96	0.04	0.09	0.05	0.2	0.21
15	1.03	0.05	-0.08	0.05	-0.2	0.26
16	0.76	0.11	-0.12	0.08	0.8	0.45
17	0.24	0.05	-1.16	0.12	3.3	0.32
18	0.24	0.04	-1.16	0.10	3.2	0.26
19	0.24	0.04	-1.24	0.13	3.1	0.21
20	0.21	0.05	-1.43	0.13	2.9	0.25
21	0.29	0.04	-1.25	0.14	3.6	0.26
22	0.27	0.02	-1.21	0.10	3.7	0.26
23	0.24	0.03	-1.26	0.10	3.6	0.23
24	0.23	0.03	-1.39	0.12	3.3	0.21
25	0.35	0.02	-1.08	0.11	3.8	0.2
26	0.36	0.02	-1.13	0.09	3.6	0.17
27	0.32	0.02	-1.20	0.09	3.6	0.17
28	0.27	0.03	-1.31	0.13	3.4	0.26
29	0.43	0.02	-0.88	0.10	3.6	0.19
30	0.45	0.02	-0.95	0.08	3.4	0.17
31	0.41	0.02	-1.13	0.08	3.4	0.19
32	0.38	0.05	-1.16	0.12	3.1	0.41

Test Point	*WFR* [-]	*UWFR* ±[-]	K_{eff} [MN/m]	UK_{eff} ±[MN/m]	C_{eff} [kN-s/m]	UC_{eff} ±[kN-s/m]
33	0.24	0.06	-1.66	0.16	3.4	0.19
34	0.28	0.03	-1.86	0.18	3.1	0.26
35	0.31	0.03	-2.22	0.21	3.0	0.29
36	0.25	0.03	-2.62	0.23	3.2	0.29
37	0.22	0.02	-2.41	0.21	4.2	0.19
38	0.21	0.03	-2.44	0.22	4.3	0.24
39	0.23	0.03	-2.62	0.23	4.0	0.21
40	0.21	0.04	-2.98	0.23	3.6	0.33
41	0.25	0.02	-2.49	0.22	4.6	0.21
42	0.24	0.02	-2.53	0.16	4.7	0.23
43	0.24	0.02	-2.69	0.16	4.4	0.23
44	0.25	0.02	-2.97	0.19	3.9	0.24
45	0.27	0.02	-2.41	0.21	5.0	0.2
46	0.27	0.01	-2.51	0.14	4.9	0.25
47	0.26	0.02	-2.65	0.18	4.7	0.25
48	0.25	0.02	-2.95	0.23	4.2	0.29
49	0.35	0.03	-3.08	0.30	2.8	0.23
50	0.35	0.02	-3.29	0.27	2.8	0.2
51	0.33	0.02	-3.65	0.27	2.9	0.22
52	0.30	0.03	-4.14	0.30	2.9	0.24
53	0.23	0.03	-3.51	0.47	4.7	0.35
54	0.25	0.03	-3.63	0.43	4.5	0.34
55	0.28	0.03	-4.35	0.46	4.2	0.4
56	0.27	0.03	-5.17	0.52	4.0	0.41
57	0.22	0.01	-4.13	0.31	5.0	0.18
58	0.21	0.02	-4.17	0.32	5.0	0.2
59	0.23	0.02	-4.58	0.36	4.6	0.21
60	0.27	0.02	-5.25	0.33	3.8	0.25
61	0.23	0.01	-4.35	0.30	5.4	0.15
62	0.21	0.01	-4.37	0.23	5.4	0.2
63	0.21	0.01	-4.52	0.31	5.1	0.28
64	0.26	0.02	-5.13	0.30	4.2	0.31

International Standards Organization Viscosity Grade 46 Test Liquid

Table A. 7 Static results of CGS with ISO VG 46 (ω, Δ*P*, ε_o, *Q*, PSR, Re_z, Re_θ, and *Re*)

Test Point	Measured ω	Measured Δ*P*	Measured ε_o	$\dot{Q}$	v_{inlet}	Pre-swirl Ratio	Re_z	Re_θ	*Re*
	[RPM]	[bar]	[-]	[lpm]	[m/s]	[-]	[-]	[-]	[-]
1	2003	2.08	0.01	4.0	7.7	0.72	1.39E+01	6.18E+02	6.18E+02
2	2003	2.09	0.28	4.5	8.5	0.80	1.61E+01	6.41E+02	6.41E+02
3	2003	2.02	0.54	5.4	7.4	0.69	2.03E+01	6.73E+02	6.73E+02
4	2003	2.10	0.80	7.0	4.6	0.43	2.66E+01	6.81E+02	6.81E+02
5	2004	4.13	0.02	8.3	4.8	0.45	3.25E+01	7.00E+02	7.01E+02
6	2004	4.17	0.29	8.9	5.2	0.49	3.47E+01	6.94E+02	6.94E+02
7	2004	4.16	0.52	10.2	4.9	0.46	3.87E+01	6.78E+02	6.79E+02
8	2004	4.14	0.76	12.7	4.7	0.44	4.85E+01	6.81E+02	6.82E+02
9	2004	6.24	0.06	11.6	4.8	0.45	4.26E+01	6.54E+02	6.56E+02
10	2005	6.35	0.27	12.5	5.1	0.48	4.63E+01	6.60E+02	6.61E+02
11	2004	6.31	0.53	14.9	4.9	0.46	5.68E+01	6.80E+02	6.83E+02
12	2004	6.17	0.81	18.5	4.9	0.46	7.07E+01	6.79E+02	6.83E+02
13	2005	8.35	0.02	15.4	4.8	0.45	5.85E+01	6.78E+02	6.80E+02
14	2005	8.25	0.26	16.5	5.2	0.49	6.52E+01	7.02E+02	7.05E+02
15	2005	8.30	0.53	19.1	4.9	0.46	7.31E+01	6.81E+02	6.85E+02
16	2005	8.28	0.79	23.2	5.2	0.49	8.56E+01	6.58E+02	6.64E+02
17	4007	2.07	0.02	4.2	13.1	0.61	1.61E+01	1.38E+03	1.38E+03
18	4008	2.07	0.27	4.5	13.6	0.64	1.76E+01	1.40E+03	1.40E+03
19	4008	2.03	0.52	5.3	14.4	0.67	2.11E+01	1.41E+03	1.41E+03
20	4008	2.03	0.81	7.0	14.6	0.69	2.78E+01	1.42E+03	1.42E+03
21	4009	4.16	0.03	8.1	15.0	0.70	3.11E+01	1.37E+03	1.37E+03
22	4008	4.18	0.25	8.5	14.8	0.69	3.22E+01	1.35E+03	1.35E+03
23	4009	4.10	0.52	10.1	13.9	0.65	3.90E+01	1.38E+03	1.38E+03
24	4008	4.19	0.80	13.4	8.8	0.41	5.30E+01	1.41E+03	1.42E+03
25	4009	6.16	0.01	11.9	8.7	0.41	4.71E+01	1.41E+03	1.41E+03
26	4009	6.30	0.27	12.9	8.7	0.41	5.12E+01	1.41E+03	1.41E+03
27	4009	6.33	0.52	15.0	8.6	0.40	5.80E+01	1.38E+03	1.38E+03
28	4008	6.12	0.81	19.1	8.7	0.41	7.63E+01	1.42E+03	1.42E+03
29	4009	8.43	0.03	15.3	8.3	0.39	5.77E+01	1.34E+03	1.34E+03
30	4009	8.17	0.27	16.2	8.2	0.38	6.22E+01	1.37E+03	1.37E+03
31	4010	8.27	0.53	19.3	8.5	0.40	7.50E+01	1.39E+03	1.39E+03
32	4008	8.27	0.79	23.8	8.6	0.40	9.12E+01	1.37E+03	1.37E+03

Test Point	Measured ω	Measured ΔP	Measured ε_o	$\dot{Q}$	v_{inlet}	Pre-swirl Ratio	Re_z	Re_θ	Re
	[RPM]	[bar]	[-]	[lpm]	[m/s]	[-]	[-]	[-]	[-]
33	6003	2.06	0.04	4.4	18.7	0.61	1.98E+01	2.42E+03	2.42E+03
34	5981	2.05	0.26	4.6	13.0	0.62	1.96E+01	2.25E+03	2.25E+03
35	6004	2.07	0.53	5.5	13.6	0.62	2.46E+01	2.37E+03	2.37E+03
36	6004	2.11	0.79	7.2	13.6	0.58	3.16E+01	2.35E+03	2.35E+03
37	6006	4.13	0.02	8.4	13.1	0.58	3.61E+01	2.29E+03	2.29E+03
38	5985	4.19	0.25	8.9	13.2	0.41	3.58E+01	2.15E+03	2.15E+03
39	6005	4.23	0.52	10.8	13.0	0.43	4.59E+01	2.27E+03	2.28E+03
40	6004	4.06	0.79	13.2	12.6	0.43	5.45E+01	2.21E+03	2.21E+03
41	6006	6.30	0.02	11.9	12.4	0.41	4.72E+01	2.12E+03	2.12E+03
42	6007	6.15	0.27	12.6	12.7	0.41	5.08E+01	2.15E+03	2.16E+03
43	6006	6.22	0.53	15.3	12.3	0.41	6.33E+01	2.21E+03	2.21E+03
44	6004	6.13	0.81	19.9	12.0	0.39	8.43E+01	2.26E+03	2.27E+03
45	5987	8.38	0.01	15.8	23.6	0.39	6.24E+01	2.10E+03	2.10E+03
46	6007	8.22	0.27	16.4	24.7	0.40	6.60E+01	2.15E+03	2.15E+03
47	6006	8.28	0.53	19.7	24.7	0.38	8.02E+01	2.17E+03	2.17E+03
48	6005	8.31	0.81	25.3	24.4	0.37	1.04E+02	2.19E+03	2.19E+03
49	7999	2.08	0.03	4.7	15.7	0.55	2.48E+01	3.78E+03	3.78E+03
50	7999	2.10	0.27	4.8	15.6	0.58	2.52E+01	3.75E+03	3.75E+03
51	7972	2.03	0.48	5.3	15.6	0.58	2.62E+01	3.52E+03	3.52E+03
52	7999	2.08	0.79	6.8	16.1	0.57	3.23E+01	3.38E+03	3.38E+03
53	7975	4.11	0.08	8.5	15.8	0.37	3.79E+01	3.16E+03	3.16E+03
54	8001	4.17	0.28	9.2	15.9	0.37	4.29E+01	3.30E+03	3.30E+03
55	8001	4.18	0.53	10.7	16.4	0.37	4.74E+01	3.14E+03	3.14E+03
56	8000	4.06	0.81	13.9	16.6	0.38	6.29E+01	3.22E+03	3.22E+03
57	8003	6.20	0.02	12.2	17.0	0.37	5.14E+01	3.01E+03	3.01E+03
58	8004	6.12	0.26	13.0	16.4	0.37	5.62E+01	3.08E+03	3.08E+03
59	8003	6.26	0.53	16.0	16.6	0.39	7.00E+01	3.11E+03	3.11E+03
60	8002	6.30	0.80	19.4	16.2	0.39	8.11E+01	2.97E+03	2.98E+03
61	7975	8.11	0.05	16.2	18.7	0.40	7.00E+01	3.06E+03	3.06E+03
62	7976	8.32	0.21	16.8	13.0	0.39	7.10E+01	2.99E+03	2.99E+03
63	8003	8.28	0.53	19.7	13.6	0.39	8.25E+01	2.97E+03	2.97E+03
64	8001	8.11	0.81	24.8	13.6	0.38	1.05E+02	3.02E+03	3.03E+03

Table A. 8 Static results of CGS with ISO VG 46 (T_{in}, T_{out}, F_{sr}, uncertainty in F_{sr}, F_{st}, uncertainty in F_{st}, ϕ, and uncertainty in ϕ)

Test Point	Inlet Temperature	Average Outlet Temperature	F_{sr}	UF_{sr}	F_{st}	UF_{st}	ϕ	$U\phi$
	[°C]	[°C]	[N]	±[N]	[N]	±[N]	[degrees]	±[degrees]
1	44.7	44.6	0	0.9	0	0.2	-	-
2	45.2	45.9	15	1.2	-2	1.6	6	5.9
3	46.8	46.6	28	0.4	1	2.9	-3	5.8
4	46.6	47.4	38	1.1	5	8.3	-7	12.4
5	47.6	47.8	0	1.3	0	0.9	-	-
6	47.1	47.7	16	-0.8	5	4	-19	13.2
7	46.6	47.1	28	0.9	4	2.1	-8	4.2
8	46.8	47.1	41	3.5	9	21.5	-12	28.9
9	46.0	46.0	0	0.7	0	1.4	-	-
10	46.0	46.4	21	1.1	5	0.8	-12	2.2
11	46.8	47.1	39	1	3	0.2	-4	0.4
12	46.8	47.0	56	0.5	5	0.3	-5	0.3
13	46.6	47.1	0	1.1	0	1.1	-	-
14	47.6	47.8	29	0.3	4	0.4	-8	0.7
15	46.7	47.2	48	0.5	8	1.6	-9	1.8
16	45.8	46.4	68	0.5	5	1	-4	0.9
17	45.5	48.9	0	3.2	0	2.6	-	-
18	46.0	49.1	17	0.2	-11	0.5	33	1.1
19	46.1	49.4	23	0.8	-8	1.1	19	2.4
20	46.2	49.8	20	0.7	-6	0.5	17	1.3
21	45.6	48.4	0	0.4	0	0.9	-	-
22	45.5	47.8	13	0.4	-9	0.4	36	1.4
23	46.2	48.3	31	0.4	-15	0.8	26	1.2
24	46.6	49.1	41	0.8	-15	0.6	20	0.9
25	46.9	48.6	0	0.9	0	0.5	-	-
26	46.9	48.8	22	0.4	-11	0.7	26	1.6
27	46.4	48.2	46	0.4	-32	0.5	34	0.5
28	47.1	48.9	57	0.1	-33	1.1	30	0.8
29	45.6	47.6	0	3.7	0	2.9	-	-
30	46.3	47.9	45	1.1	-25	2.8	29	2.8
31	46.6	48.1	71	1.9	-42	2.4	31	1.6
32	46.1	48.0	79	0.5	-19	1.2	13	0.8

Test Point	Inlet Temperature	Average Outlet Temperature	F_{sr}	UF_{sr}	F_{st}	UF_{st}	ϕ	$U\phi$
	[°C]	[°C]	[N]	±[N]	[N]	±[N]	[degrees]	±[degrees]
33	47.0	55.2	0	0.5	0	0.8	-	-
34	45.6	53.1	17	1	-27	2	58	4.4
35	46.6	54.4	7	2.7	-15	3.5	64	2.1
36	45.9	54.8	-7	9.9	-19	8.1	111	3.5
37	46.8	52.7	0	2.4	0	2.3	-	-
38	45.4	51.1	11	0.9	-20	1	61	3.2
39	47.0	52.2	32	0.9	-31	1	44	4.1
40	46.1	51.7	31	1.8	-35	2	49	11.1
41	45.4	50.2	0	22.9	0	20.3	-	-
42	46.1	50.4	25	0.6	-26	1.3	46	1.5
43	46.8	50.9	56	1.4	-61	1.4	48	0.6
44	47.5	51.5	59	1.1	-93	1.8	57	1.0
45	45.9	49.6	0	1.4	0	2.2	-	-
46	46.4	50.0	39	2.5	-51	2.3	53	0.9
47	46.8	50.2	68	3.3	-98	1.2	55	0.7
48	46.8	50.6	65	2.6	-127	3.1	63	0.5
49	47.2	62.6	0	14.5	0	13.4	-	-
50	47.5	61.9	15	3.8	-45	2	71	3.0
51	46.7	59.6	30	3.2	-46	2.7	57	3.0
52	45.1	58.8	-33	2.1	-54	2.3	122	2.5
53	45.1	55.8	0	2.4	0	1.7	-	-
54	46.7	56.4	5	0.6	-51	0.5	85	4.2
55	45.5	55.1	34	1.7	-76	1.2	66	2.1
56	46.6	55.4	28	2.6	-107	2.2	76	1.1
57	45.2	53.3	0	7.6	0	7	-	-
58	46.1	53.7	60	23.5	-60	10.6	45	0.4
59	46.7	53.7	92	1.3	-109	1.3	50	0.6
60	45.4	52.7	82	2.5	-125	2.8	57	0.9
61	46.9	52.9	0	0.5	0	0.8	-	-
62	46.0	52.5	68	1	-111	2	59	9.1
63	45.9	52.2	121	2.7	-152	3.5	52	0.4
64	46.5	52.5	117	9.9	-179	8.1	57	0.7

Table A. 9 Stiffness coefficients and uncertainties of CGS with ISO VG 46

Test Point	K_{rr} [MN/m]	UK_{rr} ±[MN/m]	K_{tt} [MN/m]	UK_{tt} ±[MN/m]	K_{tr} [MN/m]	UK_{tr} ±[MN/m]	K_{rt} [MN/m]	UK_{rt} ±[MN/m]
1	-0.3	0.07	-0.3	0.11	0.2	0.08	-0.3	0.04
2	-0.3	0.17	-0.4	0.26	0.0	0.11	-0.1	0.04
3	-0.3	0.2	-0.5	0.33	0.0	0.12	-0.1	0.07
4	-0.3	0.21	-0.5	0.31	0.2	0.1	-0.2	0.07
5	-0.5	0.27	-0.5	0.3	-0.2	0.07	0.1	0.05
6	-0.4	0.31	-0.4	0.11	0.2	0.01	0.1	0.02
7	-0.1	0.1	-0.2	0.11	0.1	0.09	0.0	0.08
8	-0.2	0.11	-0.2	0.16	0.1	0.09	-0.1	0.04
9	-0.1	0.15	-0.1	0.14	-0.1	0.04	0.1	0.06
10	-0.2	0.14	-0.1	0.19	-0.1	0.05	0.1	0.05
11	-0.1	0.08	0.0	0.12	0.2	0.06	0.0	0.06
12	-0.2	0.13	-0.3	0.27	0.2	0.1	0.2	0.18
13	0.1	0.19	0.1	0.16	0.0	0.06	0.0	0.1
14	0.0	0.11	0.0	0.18	-0.1	0.03	-0.1	0.05
15	0.0	0.15	0.0	0.12	0.3	0.09	0.0	0.06
16	-0.2	0.13	0.0	0.12	0.1	0.11	-0.1	0.06
17	-0.4	0.22	-0.4	0.21	0.6	0.15	-0.5	0.14
18	-0.4	0.28	-0.3	0.26	0.3	0.13	-0.5	0.11
19	-0.5	0.22	-0.4	0.21	0.2	0.12	-0.4	0.14
20	-0.5	0.21	-0.5	0.24	0.5	0.14	-0.4	0.14
21	-0.5	0.26	-0.4	0.27	0.3	0.08	-0.3	0.08
22	-0.3	0.29	-0.4	0.25	0.5	0.1	-0.4	0.09
23	-0.3	0.23	-0.3	0.21	0.3	0.14	-0.4	0.13
24	-0.4	0.17	-0.4	0.21	0.4	0.16	-0.4	0.16
25	-0.2	0.28	-0.2	0.28	0.4	0.14	-0.3	0.08
26	-0.2	0.23	-0.3	0.31	0.5	0.07	-0.4	0.09
27	-0.1	0.24	-0.3	0.32	0.4	0.15	-0.5	0.09
28	-0.5	0.16	-0.3	0.21	0.4	0.19	-0.4	0.09
29	0.0	0.51	0.0	0.42	1.0	0.14	-0.9	0.11
30	-0.1	0.24	-0.3	0.36	0.6	0.14	-0.5	0.06
31	-0.1	0.23	-0.3	0.27	0.3	0.21	-0.5	0.08
32	-0.5	0.11	-0.2	0.18	0.3	0.17	-0.4	0.14

Test Point	K_{rr} [MN/m]	UK_{rr} ±[MN/m]	K_{tt} [MN/m]	UK_{tt} ±[MN/m]	K_{tr} [MN/m]	UK_{tr} ±[MN/m]	K_{rt} [MN/m]	UK_{rt} ±[MN/m]
33	-0.5	0.08	-0.6	0.1	0.7	0.07	-0.6	0.08
34	-0.5	0.11	-0.6	0.07	0.8	0.08	-0.7	0.12
35	-0.6	0.01	-0.5	0.22	0.9	0.02	-0.8	0.09
36	-0.7	0.09	-0.7	0.22	0.6	0.1	-0.8	0.13
37	-0.4	0.04	-0.5	0.1	0.8	0.06	-0.7	0.14
38	-0.5	0.11	-0.5	0.04	0.6	0.1	-0.8	0.17
39	-0.6	0.06	-0.6	0.08	0.7	0.14	-0.7	0.13
40	-0.5	0.14	-0.5	0.06	0.6	0.17	-0.6	0.1
41	-0.3	0.06	-0.4	0.07	1.0	0.09	-0.9	0.12
42	-0.4	0.03	-0.4	0.09	0.9	0.09	-0.9	0.06
43	-0.5	0.06	-0.4	0.08	0.8	0.11	-0.9	0.07
44	-0.6	0.05	-0.5	0.09	0.7	0.11	-0.8	0.1
45	-0.3	0.05	-0.3	0.08	1.2	0.1	-1.1	0.08
46	-0.3	0.06	-0.3	0.09	1.2	0.07	-1.1	0.06
47	-0.5	0.08	-0.4	0.08	0.9	0.1	-1.1	0.06
48	-0.6	0.09	-0.4	0.09	0.7	0.09	-1.1	0.11
49	-0.7	0.09	-0.7	0.14	1.3	0.12	-1.3	0.06
50	-0.7	0.09	-0.8	0.14	1.3	0.08	-1.3	0.08
51	-1.0	0.05	-0.9	0.16	1.3	0.06	-1.2	0.09
52	-1.3	0.04	-1.0	0.16	1.0	0.08	-1.1	0.11
53	-0.8	0.12	-0.8	0.18	1.2	0.17	-1.1	0.2
54	-0.8	0.18	-0.9	0.13	1.3	0.16	-1.2	0.18
55	-0.9	0.16	-0.9	0.12	1.4	0.17	-1.3	0.21
56	-1.1	0.03	-1.0	0.25	1.1	0.17	-1.2	0.16
57	-0.8	0.1	-0.8	0.09	1.1	0.05	-1.1	0.1
58	-0.9	0.03	-0.9	0.1	1.1	0.07	-1.0	0.14
59	-1.0	0.05	-0.9	0.1	1.2	0.05	-1.0	0.14
60	-1.0	0.06	-1.0	0.15	1.2	0.12	-1.1	0.1
61	-0.7	0.07	-0.7	0.08	1.4	0.07	-1.2	0.07
62	-0.8	0.05	-0.7	0.08	1.1	0.07	-1.2	0.08
63	-1.0	0.05	-0.7	0.11	1.0	0.09	-1.1	0.07
64	-0.9	0.08	-0.9	0.13	1.2	0.1	-1.2	0.09

Table A. 10 Damping coefficients and uncertainties of CGS with ISO VG 46

Test Point	C_{rr} [kN-s/m]	UC_{rr} ±[kN-s/m]	C_{tt} [kN-s/m]	UC_{tt} ±[kN-s/m]	C_{tr} [kN-s/m]	UC_{tr} ±[kN-s/m]	C_{rt} [kN-s/m]	UC_{rt} ±[kN-s/m]
1	8.1	0.28	8.6	0.34	2.3	0.14	-1.9	0.25
2	8.3	0.53	8.9	0.92	2.6	0.27	-2.1	0.23
3	8.1	0.52	8.5	0.89	2.7	0.37	-2.3	0.3
4	8.7	0.47	8.3	0.92	2.4	0.32	-2.6	0.5
5	9.7	0.94	10.3	1	2.6	0.18	-2.0	0.14
6	9.8	1.02	9.2	0.51	2.1	0.01	-2.1	0.07
7	8.6	0.83	8.2	0.84	2.5	0.28	-2.3	0.4
8	8.8	0.68	8.1	0.79	2.8	0.31	-2.9	0.34
9	9.2	1	9.7	1.08	2.3	0.16	-1.8	0.17
10	9.4	0.9	9.7	0.87	2.7	0.24	-2.1	0.19
11	8.7	0.61	8.6	0.67	2.3	0.27	-2.4	0.18
12	9.4	0.38	8.3	1.97	2.9	0.31	-2.9	1.42
13	9.3	1.03	9.7	1	2.1	0.18	-1.7	0.21
14	9.2	0.96	9.8	1.06	2.6	0.23	-1.8	0.28
15	9.0	0.69	9.0	0.59	2.4	0.25	-2.3	0.23
16	9.9	0.78	8.8	0.84	3.0	0.38	-2.7	0.28
17	8.0	1.05	8.5	1.06	4.0	0.47	-3.4	0.59
18	8.3	1.02	8.3	1.09	3.9	0.37	-3.7	0.49
19	8.1	0.77	7.7	0.77	4.3	0.33	-4.2	0.49
20	8.7	0.63	7.5	0.57	4.3	0.41	-4.8	0.48
21	9.3	1.37	9.8	1.31	4.3	0.24	-3.7	0.22
22	9.3	1.31	9.6	1.14	4.1	0.31	-3.8	0.29
23	8.8	0.89	8.5	0.84	4.0	0.45	-4.1	0.39
24	9.2	0.49	8.3	0.7	4.3	0.52	-4.7	0.44
25	9.3	1.35	9.9	1.31	3.7	0.39	-3.2	0.2
26	9.3	1.13	10.1	1.24	3.9	0.28	-3.4	0.28
27	9.1	0.86	9.5	0.99	3.9	0.49	-3.8	0.27
28	9.7	0.52	9.0	0.76	4.4	0.67	-4.6	0.31
29	9.9	1.64	10.4	1.42	2.8	0.72	-2.3	0.5
30	9.7	1.11	10.6	1.31	3.7	0.54	-3.2	0.19
31	9.5	0.89	10.2	0.85	4.2	0.79	-3.6	0.23
32	9.8	0.32	9.2	0.73	4.7	0.71	-4.6	0.44

Test Point	C_{rr} [kN-s/m]	UC_{rr} ±[kN-s/m]	C_{tt} [kN-s/m]	UC_{tt} ±[kN-s/m]	C_{tr} [kN-s/m]	UC_{tr} ±[kN-s/m]	C_{rt} [kN-s/m]	UC_{rt} ±[kN-s/m]
33	6.6	1.68	7.1	1.53	6.2	0.93	-5.7	0.74
34	6.8	0.02	7.1	1.46	6.0	1.15	-5.9	1.12
35	7.6	0.29	7.6	0.82	6.2	0.27	-6.4	0.93
36	8.0	0.81	7.6	0.54	6.3	0.44	-7.0	0.88
37	8.9	0.89	9.5	1.05	6.3	0.49	-5.6	0.59
38	9.2	0.98	9.1	0.69	5.9	0.43	-5.7	0.51
39	8.5	0.57	8.2	0.69	5.8	0.42	-6.1	0.51
40	8.9	1.07	8.2	0.65	6.4	0.47	-6.8	0.77
41	9.2	1.07	9.8	1.2	5.5	0.29	-4.8	0.42
42	9.1	0.67	9.9	1.1	5.8	0.26	-5.5	0.32
43	8.9	0.42	8.8	0.91	5.9	0.75	-6.1	0.32
44	9.2	0.54	8.4	0.97	6.9	1.07	-6.8	0.37
45	9.7	0.64	10.2	0.66	4.7	0.37	-4.1	0.26
46	9.6	0.86	10.0	0.98	5.9	1.01	-5.0	0.43
47	9.4	0.45	9.4	0.89	5.9	0.82	-5.9	0.33
48	10.1	0.69	8.8	1.33	7.2	0.94	-6.8	0.38
49	6.1	0.41	6.9	0.46	8.3	0.35	-7.5	0.44
50	6.3	0.31	6.7	0.81	8.0	0.28	-8.0	0.71
51	6.4	0.11	6.8	1.26	8.1	1.66	-8.4	1.4
52	8.1	0.91	6.4	0.76	8.6	0.78	-9.8	1.33
53	7.7	1.05	8.1	1.39	9.7	2.37	-8.1	1.99
54	7.9	1.14	8.2	0.8	8.1	0.48	-8.5	0.78
55	7.9	1.02	8.1	0.84	7.1	0.69	-8.9	1.31
56	9.3	0.92	7.8	0.81	8.0	0.68	-9.5	0.89
57	8.5	0.88	9.5	1.4	7.5	0.39	-6.6	0.44
58	8.8	0.6	9.0	1.1	8.0	0.59	-7.3	0.21
59	8.0	0.34	8.3	0.7	7.3	0.5	-8.0	0.49
60	9.8	0.65	8.0	0.82	7.9	0.92	-9.1	0.7
61	8.7	0.72	9.9	1	6.5	0.29	-5.7	0.48
62	9.4	1.05	9.9	1.41	6.5	0.79	-6.2	0.99
63	8.7	0.47	8.9	0.89	7.3	0.57	-8.0	0.52
64	9.9	0.56	8.5	1.15	7.5	1.04	-8.8	0.71

Table A. 11 Virtual-mass coefficients and uncertainties of CGS with ISO VG 46

Test Point	M_{rr} [kg]	UM_{rr} ±[kg]	M_{tt} [kg]	UM_{tt} ±[kg]	M_{tr} [kg]	UM_{tr} ±[kg]	M_{rt} [kg]	UM_{rt} ±[kg]
1	17.1	0.15	18.3	0.22	0.0	0.17	0.4	0.08
2	18.5	0.35	18.8	0.55	-0.5	0.22	0.7	0.07
3	20.8	0.42	18.4	0.69	-0.1	0.25	0.6	0.14
4	23.0	0.44	18.2	0.65	-0.5	0.21	0.1	0.15
5	17.1	0.55	18.5	0.62	0.0	0.15	0.6	0.1
6	18.8	0.65	18.1	0.24	0.5	0.03	1.2	0.05
7	23.1	0.37	20.8	0.39	0.3	0.34	1.5	0.3
8	25.0	0.4	21.4	0.58	-0.8	0.32	-0.3	0.15
9	20.2	0.53	21.8	0.49	0.5	0.13	0.4	0.21
10	21.0	0.5	21.1	0.69	-0.6	0.19	0.7	0.19
11	23.5	0.28	21.4	0.42	0.3	0.23	0.7	0.22
12	25.7	0.56	21.4	1.13	-0.4	0.43	1.5	0.78
13	20.5	0.67	22.0	0.58	0.3	0.2	0.7	0.36
14	21.3	0.39	21.9	0.65	0.1	0.12	0.4	0.17
15	23.8	0.55	21.4	0.44	0.2	0.33	0.8	0.2
16	25.9	0.47	22.2	0.45	-0.4	0.38	1.0	0.21
17	16.8	0.64	18.3	0.62	-0.7	0.44	1.0	0.43
18	18.0	0.87	18.9	0.82	-0.2	0.42	0.8	0.34
19	20.3	0.67	18.9	0.65	0.3	0.38	0.7	0.44
20	22.7	0.64	18.1	0.73	0.3	0.42	0.4	0.44
21	18.3	0.82	19.9	0.83	0.1	0.25	0.2	0.26
22	19.3	0.91	19.5	0.78	-0.3	0.32	0.4	0.26
23	21.3	0.72	19.6	0.65	0.3	0.42	0.8	0.41
24	23.6	0.53	19.0	0.65	0.0	0.48	0.6	0.48
25	19.0	0.86	20.3	0.86	0.9	0.42	-0.2	0.25
26	19.9	0.72	19.9	0.95	0.4	0.23	0.1	0.27
27	21.8	0.75	19.6	1	0.0	0.46	0.5	0.28
28	23.9	0.49	19.5	0.65	-0.1	0.58	0.5	0.27
29	19.4	1.44	20.8	1.2	1.3	0.39	-0.8	0.31
30	20.2	0.73	20.3	1.13	0.8	0.43	0.1	0.2
31	22.2	0.72	19.7	0.83	-0.6	0.65	0.5	0.25
32	24.4	0.33	20.8	0.55	-0.8	0.52	0.5	0.43

Test Point	M_{rr} [kg]	UM_{rr} ±[kg]	M_{tt} [kg]	UM_{tt} ±[kg]	M_{tr} [kg]	UM_{tr} ±[kg]	M_{rt} [kg]	UM_{rt} ±[kg]
33	17.8	0.72	18.2	0.72	-2.2	0.71	1.9	0.76
34	17.4	0.02	17.3	0.8	-1.6	0.98	0.8	0.41
35	19.1	0.39	17.4	0.57	-0.6	0.2	0.8	0.5
36	21.3	0.61	17.0	0.47	-0.4	0.4	0.6	0.6
37	17.2	0.62	18.7	0.62	-1.0	0.31	1.1	0.35
38	18.3	0.55	18.0	0.44	-0.4	0.32	1.2	0.26
39	20.2	0.47	18.5	0.65	-0.4	0.34	1.7	0.39
40	21.7	0.72	18.5	0.57	-0.9	0.51	1.2	0.41
41	19.0	0.87	20.1	0.9	0.1	0.18	0.0	0.24
42	19.0	0.55	19.4	1.15	-0.6	0.31	0.8	0.26
43	20.1	0.59	19.1	0.96	-0.7	0.44	0.9	0.37
44	22.5	0.5	19.1	1.07	-0.5	1.1	0.5	0.3
45	18.1	0.45	19.5	0.61	0.9	0.56	-0.3	0.46
46	18.8	1.09	19.7	0.95	-0.4	0.82	0.4	0.51
47	20.8	0.59	19.5	0.93	-1.0	0.63	0.4	0.23
48	23.3	0.64	21.0	0.93	-1.0	1.24	-0.1	0.51
49	15.0	0.29	16.0	0.28	-0.8	0.31	0.1	0.44
50	16.9	0.44	16.6	0.61	-1.2	0.38	-0.1	0.46
51	18.4	0.88	16.8	0.77	-1.6	0.92	0.7	1.1
52	19.7	0.94	17.7	0.72	-0.9	0.75	2.8	1.06
53	16.7	1.63	18.1	1.22	-2.9	0.83	1.9	0.94
54	19.4	0.73	18.2	0.59	-1.5	0.45	0.6	0.64
55	22.0	1.08	18.1	0.43	-0.9	0.38	-0.5	0.83
56	22.3	0.75	18.5	0.67	0.6	0.4	0.8	0.82
57	19.0	0.25	20.5	0.56	-0.6	0.57	-0.7	0.45
58	19.4	0.55	19.8	0.46	-1.7	0.36	-0.4	0.42
59	22.0	0.92	19.0	0.53	-1.3	0.47	-0.9	0.69
60	22.2	0.73	19.7	0.65	1.8	0.62	0.6	0.51
61	19.1	0.36	19.7	0.63	0.3	0.67	-1.6	0.38
62	20.1	0.78	18.6	0.96	-0.4	0.84	-1.4	0.4
63	23.1	0.88	19.3	0.73	-0.7	0.52	-0.9	0.55
64	21.9	0.56	20.2	1.08	2.1	0.68	0.3	0.84

Table A. 12 WFR, Keff, Ceff, and uncertainties of CGS with ISO VG 46

Test Point	*WFR* [-]	*UWFR* ±[-]	K_{eff} [MN/m]	UK_{eff} ±[MN/m]	C_{eff} [kN-s/m]	UC_{eff} ±[kN-s/m]
1	0.13	0.03	-0.63	0.07	7.3	0.31
2	0.00	0.00	-0.68	0.16	8.2	0.59
3	0.00	0.00	-0.78	0.20	8.0	0.61
4	0.09	0.07	-0.81	0.20	7.6	0.59
5	0.07	0.02	-0.80	0.20	9.3	0.72
6	0.00	0.00	-0.77	0.17	8.8	0.57
7	0.00	0.00	-0.60	0.09	8.1	0.66
8	0.07	0.03	-0.58	0.11	7.9	0.57
9	0.04	0.02	-0.59	0.11	9.1	0.75
10	0.04	0.03	-0.58	0.12	9.2	0.65
11	0.03	0.08	-0.54	0.08	8.0	0.5
12	0.00	0.00	-0.68	0.21	7.9	1.12
13	0.00	0.00	-0.45	0.13	9.4	0.77
14	0.00	0.00	-0.48	0.11	9.1	0.73
15	0.05	0.05	-0.49	0.11	8.3	0.52
16	0.03	0.05	-0.55	0.10	8.9	0.64
17	0.16	0.03	-1.91	0.23	7.0	0.79
18	0.11	0.03	-1.97	0.26	7.4	0.78
19	0.08	0.03	-2.11	0.21	7.2	0.59
20	0.13	0.03	-2.18	0.22	7.0	0.49
21	0.07	0.02	-2.11	0.23	8.8	0.96
22	0.10	0.02	-2.14	0.24	8.5	0.88
23	0.08	0.03	-2.19	0.22	7.9	0.65
24	0.11	0.03	-2.29	0.21	7.8	0.5
25	0.09	0.02	-2.22	0.24	8.7	0.96
26	0.11	0.02	-2.23	0.24	8.6	0.85
27	0.11	0.03	-2.24	0.26	8.3	0.69
28	0.10	0.03	-2.32	0.22	8.4	0.52
29	0.22	0.03	-2.46	0.41	7.9	1.1
30	0.13	0.02	-2.30	0.28	8.8	0.88
31	0.09	0.03	-2.24	0.27	8.9	0.67
32	0.08	0.03	-2.36	0.21	8.7	0.48

Test Point	*WFR* [-]	*UWFR* ±[-]	K_{eff} [MN/m]	UK_{eff} ±[MN/m]	C_{eff} [kN-s/m]	UC_{eff} ±[kN-s/m]
33	0.18	0.06	-3.30	0.48	5.7	1.19
34	0.11	0.09	-3.12	0.57	6.2	0.86
35	0.08	0.02	-3.83	0.37	6.9	0.47
36	0.12	0.03	-4.17	0.38	6.9	0.54
37	0.09	0.02	-3.79	0.35	8.4	0.71
38	0.10	0.02	-3.89	0.30	8.2	0.62
39	0.08	0.02	-4.29	0.31	7.7	0.48
40	0.08	0.03	-4.49	0.39	7.8	0.66
41	0.16	0.02	-4.43	0.40	8.0	0.81
42	0.12	0.02	-4.30	0.40	8.4	0.66
43	0.10	0.02	-4.30	0.42	7.9	0.54
44	0.09	0.06	-4.51	0.50	7.9	0.68
45	0.27	0.03	-4.58	0.28	7.3	0.55
46	0.15	0.03	-4.43	0.54	8.3	0.73
47	0.12	0.03	-4.51	0.42	8.2	0.55
48	0.00	0.00	-4.84	0.44	8.5	0.85
49	0.23	0.03	-4.25	0.30	5.0	0.36
50	0.18	0.03	-4.86	0.47	5.3	0.48
51	0.19	0.07	-5.55	1.04	5.4	0.78
52	0.17	0.04	-6.20	0.79	6.1	0.64
53	0.11	0.05	-4.32	1.57	7.1	0.96
54	0.10	0.04	-5.99	0.57	7.2	0.74
55	0.06	0.04	-7.33	0.81	7.4	0.73
56	0.13	0.02	-7.53	0.61	7.4	0.64
57	0.24	0.03	-7.40	0.36	6.9	0.85
58	0.14	0.02	-7.25	0.41	7.7	0.65
59	0.10	0.03	-7.80	0.53	7.2	0.45
60	0.13	0.02	-8.11	0.62	7.7	0.54
61	0.31	0.04	-7.70	0.41	6.3	0.67
62	0.24	0.04	-7.93	0.78	7.3	0.94
63	0.13	0.03	-8.20	0.58	7.6	0.55
64	0.15	0.03	-8.43	0.71	7.8	0.67

International Standards Organization Viscosity Grade 100 Test Liquid

Table A. 13 Static results of CGS with ISO VG 100 (ω, Δ*P*, ε_o, *Q*, PSR, Re_z, Re_θ, and *Re*)

Test Point	Measured ω	Measured Δ*P*	Measured ε_o	$\dot{Q}$	v_{inlet}	Pre-swirl Ratio	Re_z	Re_θ	*Re*
	[RPM]	[bar]	[-]	[lpm]	[m/s]	[-]	[-]	[-]	[-]
1	2006	2.08	0.04	1.7	4.2	0.40	2.04E+00	2.15E+02	2.15E+02
2	2006	2.07	0.28	1.9	4.1	0.39	2.27E+00	2.16E+02	2.16E+02
3	2005	2.00	0.54	2.4	4.4	0.41	2.90E+00	2.18E+02	2.18E+02
4	2005	2.08	0.81	3.4	7.5	0.70	4.54E+00	2.37E+02	2.37E+02
5	2006	4.12	0.04	3.4	6.3	0.59	4.34E+00	2.26E+02	2.26E+02
6	2006	4.11	0.29	3.8	7.6	0.71	4.77E+00	2.23E+02	2.23E+02
7	2006	4.15	0.52	4.7	7.9	0.74	6.00E+00	2.27E+02	2.27E+02
8	2005	4.10	0.81	6.0	4.7	0.44	7.58E+00	2.23E+02	2.23E+02
9	2006	6.24	0.02	5.0	4.2	0.40	6.41E+00	2.27E+02	2.27E+02
10	2006	6.14	0.29	5.9	4.1	0.38	7.99E+00	2.40E+02	2.40E+02
11	2006	6.30	0.54	7.0	4.5	0.42	9.19E+00	2.34E+02	2.34E+02
12	2005	6.25	0.80	9.0	4.5	0.42	1.17E+01	2.31E+02	2.31E+02
13	2006	8.30	0.02	6.7	6.5	0.61	8.62E+00	2.29E+02	2.29E+02
14	2006	8.25	0.26	7.4	6.6	0.62	9.74E+00	2.35E+02	2.35E+02
15	2006	8.50	0.49	8.9	5.2	0.49	1.16E+01	2.32E+02	2.32E+02
16	2004	8.40	0.79	11.4	4.9	0.46	1.43E+01	2.25E+02	2.25E+02
17	4005	2.08	0.02	2.0	10.9	0.51	2.97E+00	5.18E+02	5.18E+02
18	4005	2.09	0.29	2.3	11.5	0.54	3.30E+00	5.16E+02	5.16E+02
19	4005	2.12	0.50	2.8	12.8	0.60	4.23E+00	5.39E+02	5.39E+02
20	4004	2.07	0.83	3.8	15.4	0.72	5.93E+00	5.52E+02	5.52E+02
21	4006	4.27	0.03	4.1	14.4	0.68	6.06E+00	5.26E+02	5.26E+02
22	4006	4.08	0.28	4.3	15.5	0.73	6.50E+00	5.35E+02	5.35E+02
23	4006	4.28	0.52	5.3	13.1	0.61	7.71E+00	5.22E+02	5.22E+02
24	4005	4.33	0.77	6.7	11.4	0.53	9.61E+00	5.08E+02	5.08E+02
25	4006	6.18	0.03	5.9	14.8	0.70	8.52E+00	5.15E+02	5.15E+02
26	4006	6.11	0.28	6.4	13.1	0.61	9.35E+00	5.21E+02	5.21E+02
27	4005	6.36	0.53	7.6	11.0	0.51	1.06E+01	5.01E+02	5.01E+02
28	4005	6.17	0.81	10.1	7.1	0.33	1.47E+01	5.17E+02	5.17E+02
29	4006	8.24	0.03	7.5	13.7	0.64	1.04E+01	4.95E+02	4.96E+02
30	4006	8.28	0.27	8.4	14.8	0.70	1.23E+01	5.18E+02	5.18E+02
31	4006	8.27	0.54	9.8	7.2	0.34	1.37E+01	4.95E+02	4.95E+02
32	4005	8.22	0.77	12.9	7.1	0.33	1.86E+01	5.16E+02	5.16E+02

Test Point	Measured ω	Measured Δ*P*	Measured ε_o	$\dot{Q}$	v_{inlet}	Pre-swirl Ratio	Re_z	Re_θ	Re
	[RPM]	[bar]	[-]	[lpm]	[m/s]	[-]	[-]	[-]	[-]
33	6014	2.00	0.03	2.5	11.3	0.35	4.66E+00	1.01E+03	1.01E+03
34	6016	1.97	0.29	2.6	13.7	0.43	4.90E+00	1.01E+03	1.01E+03
35	6015	2.05	0.51	2.9	10.1	0.32	5.00E+00	9.12E+02	9.12E+02
36	6014	1.99	0.77	3.9	11.3	0.35	6.87E+00	9.52E+02	9.52E+02
37	6015	4.04	0.02	4.4	11.5	0.36	7.48E+00	9.10E+02	9.10E+02
38	6016	4.21	0.26	4.9	11.6	0.36	8.42E+00	9.14E+02	9.14E+02
39	6017	4.11	0.51	5.8	11.9	0.37	9.76E+00	8.98E+02	8.98E+02
40	6017	4.06	0.79	7.6	12.8	0.40	1.26E+01	8.86E+02	8.86E+02
41	6018	6.29	0.03	6.8	12.2	0.38	1.10E+01	8.68E+02	8.68E+02
42	6019	6.25	0.24	7.0	12.5	0.39	1.12E+01	8.59E+02	8.59E+02
43	6019	6.18	0.53	8.6	13.5	0.42	1.39E+01	8.63E+02	8.63E+02
44	6017	6.23	0.79	11.2	16.4	0.51	1.81E+01	8.62E+02	8.62E+02
45	6019	8.15	0.04	8.7	13.0	0.40	1.38E+01	8.48E+02	8.48E+02
46	6018	8.36	0.29	9.3	13.9	0.44	1.46E+01	8.36E+02	8.36E+02
47	6018	8.13	0.52	10.8	15.6	0.49	1.69E+01	8.35E+02	8.35E+02
48	6017	8.24	0.81	13.8	21.4	0.67	2.07E+01	8.01E+02	8.01E+02
49	8007	1.90	0.05	2.7	15.1	0.35	6.75E+00	1.77E+03	1.77E+03
50	8007	1.98	0.29	3.0	14.9	0.35	7.54E+00	1.81E+03	1.81E+03
51	8007	2.09	0.54	3.7	14.6	0.34	8.96E+00	1.74E+03	1.74E+03
52	8005	1.97	0.81	4.5	14.7	0.34	1.07E+01	1.70E+03	1.70E+03
53	8006	4.13	0.03	5.3	15.0	0.35	1.14E+01	1.52E+03	1.52E+03
54	8006	4.04	0.27	5.6	15.0	0.35	1.18E+01	1.51E+03	1.51E+03
55	8005	4.04	0.55	6.7	15.2	0.36	1.32E+01	1.40E+03	1.40E+03
56	8004	4.16	0.81	8.4	21.9	0.51	1.57E+01	1.33E+03	1.33E+03
57	8006	6.09	0.04	7.4	19.2	0.45	1.46E+01	1.39E+03	1.39E+03
58	8005	6.24	0.26	8.0	20.4	0.48	1.54E+01	1.36E+03	1.36E+03
59	8005	6.32	0.50	9.3	22.4	0.53	1.68E+01	1.28E+03	1.28E+03
60	8004	6.18	0.79	11.7	26.2	0.62	2.07E+01	1.25E+03	1.25E+03
61	8006	8.19	0.04	9.8	21.0	0.49	1.80E+01	1.30E+03	1.30E+03
62	8005	8.37	0.26	10.2	22.6	0.53	1.81E+01	1.26E+03	1.26E+03
63	8005	8.29	0.51	11.6	25.4	0.60	1.99E+01	1.21E+03	1.21E+03
64	8002	8.22	0.80	14.9	26.1	0.61	2.50E+01	1.19E+03	1.19E+03

Table A. 14 Static results of CGS with ISO VG 100 (T_{in}, T_{out}, F_{sr}, uncertainty in F_{sr}, F_{st}, uncertainty in F_{st}, ϕ, and uncertainty in ϕ)

Test Point	Inlet Temperature	Average Outlet Temperature	F_{sr}	UF_{sr}	F_{st}	UF_{st}	ϕ	$U\phi$
	[°C]	[°C]	[N]	±[N]	[N]	±[N]	[degrees]	±[degrees]
1	45.1	43.8	0	2.4	0	10	-	-
2	45.1	44.0	19	3.2	-35	3.6	62	4.8
3	45.4	44.3	28	12.2	-66	7.3	67	9.2
4	47.6	46.8	38	0.9	-83	1.6	66	0.7
5	45.9	45.8	0	0.6	0	3.2	-	-
6	46.0	44.9	18	8.6	-47	7.7	69	9.6
7	47.0	45.0	31	-0.7	-71	3.2	66	1.1
8	45.7	45.4	48	-0.3	-95	5.5	63	1.3
9	45.6	46.3	0	7.6	0	2.6	-	-
10	47.6	47.3	20	4.1	-26	1.3	52	5.8
11	46.2	47.3	40	2.3	-50	3.2	51	2.4
12	46.2	46.7	56	6.1	-67	2.4	50	3.2
13	45.6	46.8	0	0.1	0	2.6	-	-
14	46.6	47.3	17	6.4	-14	0.7	41	10.9
15	46.1	47.0	35	1.5	-26	0.6	37	1.3
16	45.4	46.1	59	4.3	-63	4.1	47	2.8
17	45.6	53.2	0	1	0	0.8	-	-
18	45.0	53.5	20	0.9	-19	0.5	44	1.5
19	47.3	53.8	18	2.8	-19	1.3	46	4.8
20	47.1	55.2	-9	0.9	-33	3.8	106	2.2
21	45.9	53.7	0	3.2	0	5.6	-	-
22	47.1	53.6	19	5.8	-35	1.9	62	7.5
23	46.1	53.1	27	4.7	-30	3.8	49	6.2
24	45.1	52.6	13	4.6	-21	1.4	59	9.4
25	45.9	52.7	0	1.5	0	4.2	-	-
26	46.8	52.5	18	3.2	-33	7.5	62	7.0
27	45.5	51.6	33	8.9	-27	7.7	40	10.9
28	47.0	52.0	24	9.4	-8	16.5	18	36.4
29	45.3	51.2	0	2.4	0	1.5	-	-
30	47.2	51.9	16	2.4	-15	1.7	43	5.3
31	45.6	50.9	41	1.3	-19	2.3	25	2.7
32	47.6	51.3	38	0.6	-5	1.9	7	2.9

Test Point	Inlet Temperature	Average Outlet Temperature	F_{sr}	UF_{sr}	F_{st}	UF_{st}	ϕ	$U\phi$
	[°C]	[°C]	[N]	±[N]	[N]	±[N]	[degrees]	±[degrees]
33	46.3	64.7	0	2.2	0	10.1	-	-
34	49.4	62.6	1	1.6	-11	0.6	87	7.9
35	45.8	60.4	-5	0.6	-4	0.7	140	5.8
36	45.6	62.3	-39	4.5	-8	3	168	4.5
37	45.6	60.4	0	2.2	0	2.5	-	-
38	46.0	60.3	19	8.5	-38	8.5	63	11.5
39	46.2	59.5	23	1.2	-32	1	55	1.6
40	46.4	58.7	-10	4.8	-14	3.2	124	14.5
41	45.7	58.2	0	2.4	0	5.1	-	-
42	45.6	57.8	23	2.9	-43	3.6	62	3.6
43	47.0	57.1	38	0.7	-39	1.9	46	1.5
44	47.4	56.8	18	2.1	-13	0.4	35	3.3
45	46.5	56.6	0	3.2	0	3.2	-	-
46	46.2	56.2	17	2.8	-53	3.5	72	2.9
47	46.9	55.6	37	0.3	-51	4.5	54	2.4
48	45.5	54.7	20	7.4	-18	2.3	42	11.0
49	47.6	74.8	0	1.4	0	7	-	-
50	47.0	75.9	16	1.8	-57	2.1	74	1.8
51	48.5	73.9	-5	1.9	-14	1.7	109	7.1
52	49.6	72.5	-54	2.6	-36	2.9	147	2.5
53	46.2	69.6	0	1.2	0	6.2	-	-
54	47.7	68.5	2	2.8	-64	2.8	88	2.5
55	47.2	65.8	-3	1.2	-43	3.8	95	1.7
56	45.7	64.4	-56	3.4	-27	2.5	154	2.5
57	47.6	65.3	0	13.4	0	10.2	-	-
58	47.8	64.2	13	2.4	-62	2.4	78	2.2
59	46.6	62.4	33	1.6	-79	1.1	68	1.1
60	46.5	61.3	-11	5.3	-43	0.5	104	6.7
61	47.6	62.3	0	2.5	0	1.7	-	-
62	46.9	61.5	19	2	-58	2.3	72	1.9
63	46.2	60.2	43	1.5	-83	1.8	63	1.0
64	46.5	59.3	17	3.6	-39	0.4	67	4.5

Table A. 15 Stiffness coefficients and uncertainties of CGS with ISO VG 100

	K_{rr}	UK_{rr}	K_{tt}	UK_{tt}	K_{tr}	UK_{tr}	K_{rt}	UK_{rt}
Test Point	[MN/m]	±[MN/m]	[MN/m]	±[MN/m]	[MN/m]	±[MN/m]	[MN/m]	±[MN/m]
1	0.0	0.07	-0.1	0.08	0.8	0.05	-0.8	0.05
2	-0.1	0.08	-0.1	0.1	0.8	0.06	-0.8	0.07
3	-0.1	0.13	-0.1	0.09	0.7	0.06	-0.8	0.05
4	0.1	0.28	-0.1	0.12	0.5	0.16	-0.6	0.09
5	0.0	0.05	0.0	0.08	0.9	0.05	-0.8	0.05
6	-0.1	0.1	-0.1	0.08	0.6	0.04	-0.8	0.03
7	-0.1	0.13	-0.1	0.1	0.5	0.05	-0.7	0.03
8	0.0	0.23	-0.1	0.15	0.5	0.1	-0.7	0.12
9	0.0	0.06	0.0	0.07	0.8	0.04	-0.8	0.04
10	0.0	0.12	-0.1	0.08	0.4	0.06	-0.5	0.05
11	0.0	0.16	-0.1	0.12	0.5	0.09	-0.5	0.06
12	0.1	0.25	-0.1	0.12	0.6	0.13	-0.5	0.05
13	0.0	0.07	0.0	0.11	0.5	0.05	-0.6	0.07
14	0.0	0.11	0.0	0.06	0.4	0.05	-0.4	0.04
15	0.0	0.16	0.0	0.12	0.5	0.12	-0.4	0.04
16	0.2	0.21	0.0	0.11	0.7	0.18	-0.5	0.05
17	0.0	0.13	0.0	0.12	0.7	0.18	-0.7	0.19
18	-0.1	0.15	-0.1	0.13	0.4	0.1	-0.7	0.14
19	-0.4	0.09	-0.3	0.14	0.3	0.12	-0.7	0.14
20	0.3	0.5	-0.3	0.08	1.3	0.28	-0.6	0.19
21	0.0	0.16	-0.1	0.19	1.1	0.14	-1.1	0.14
22	0.0	0.18	0.0	0.14	0.5	0.16	-0.9	0.14
23	-0.2	0.14	-0.5	0.18	0.1	0.13	-0.6	0.16
24	-0.3	0.24	-0.4	0.13	0.9	0.19	-0.7	0.19
25	-0.2	0.22	-0.3	0.25	1.0	0.09	-0.9	0.1
26	-0.2	0.21	0.0	0.14	0.5	0.15	-0.7	0.11
27	-0.3	0.18	-0.4	0.22	-0.1	0.18	-0.5	0.14
28	-0.1	0.25	-0.3	0.16	1.0	0.27	-0.5	0.18
29	-0.4	0.24	-0.4	0.25	0.6	0.07	-0.6	0.08
30	-0.2	0.24	-0.2	0.19	0.6	0.11	-0.5	0.1
31	-0.4	0.19	-0.1	0.22	0.0	0.1	-0.4	0.14
32	-0.3	0.19	-0.3	0.17	0.7	0.17	-0.5	0.07

Test Point	K_{rr} [MN/m]	UK_{rr} ±[MN/m]	K_{tt} [MN/m]	UK_{tt} ±[MN/m]	K_{tr} [MN/m]	UK_{tr} ±[MN/m]	K_{rt} [MN/m]	UK_{rt} ±[MN/m]
33	0.2	0.43	0.3	0.52	1.2	0.14	-1.3	0.11
34	-0.5	0.28	-0.4	0.16	0.4	0.2	-0.7	0.18
35	-1.2	0.22	-0.7	0.22	0.6	0.18	-0.7	0.15
36	-0.7	0.37	-0.9	0.2	1.5	0.21	-0.6	0.19
37	0.3	0.29	0.3	0.28	1.3	0.31	-1.2	0.31
38	-0.2	0.34	-0.2	0.16	0.6	0.33	-1.0	0.21
39	-0.8	0.22	-0.5	0.24	0.1	0.15	-0.9	0.24
40	-0.9	0.34	-0.9	0.25	1.0	0.32	-0.8	0.17
41	-0.2	0.25	-0.2	0.27	1.2	0.21	-1.2	0.19
42	-0.1	0.3	-0.1	0.23	0.9	0.32	-1.1	0.19
43	-0.6	0.23	-0.3	0.22	0.0	0.22	-0.9	0.26
44	-1.0	0.29	-0.7	0.26	0.7	0.35	-0.9	0.18
45	-0.3	0.24	-0.3	0.25	1.0	0.19	-1.0	0.16
46	0.0	0.28	-0.2	0.23	1.0	0.29	-1.0	0.19
47	-0.4	0.3	-0.2	0.21	0.1	0.28	-1.0	0.26
48	-0.5	0.53	-0.6	0.3	0.9	0.33	-1.1	0.28
49	0.2	0.17	0.1	0.21	1.9	0.14	-1.6	0.24
50	0.2	0.24	0.2	0.39	1.2	0.49	-1.4	0.32
51	-0.7	0.26	-0.5	0.21	0.8	0.41	-1.0	0.24
52	-0.6	0.48	-1.0	0.27	2.1	0.49	-1.0	0.39
53	0.5	0.44	0.4	0.5	2.1	0.29	-2.0	0.25
54	0.2	0.29	-0.1	0.46	0.6	0.45	-1.3	0.4
55	-1.3	0.17	-0.8	0.4	-0.1	0.18	-1.2	0.27
56	-1.4	0.78	-1.2	0.25	1.4	0.41	-0.7	0.38
57	-0.5	0.43	-0.6	0.31	1.4	0.44	-1.3	0.31
58	-0.2	0.27	-0.2	0.26	1.4	0.41	-1.3	0.26
59	-0.6	0.27	-0.4	0.34	0.4	0.36	-1.4	0.31
60	-1.6	0.57	-1.0	0.2	0.9	0.39	-1.0	0.3
61	-0.4	0.27	-0.4	0.32	1.5	0.35	-1.4	0.3
62	-0.2	0.29	-0.3	0.3	1.7	0.42	-1.4	0.3
63	-0.4	0.29	-0.3	0.34	0.5	0.46	-1.5	0.34
64	-1.5	0.53	-1.0	0.27	0.8	0.42	-1.3	0.28

Table A. 16 Damping coefficients and uncertainties of CGS with ISO VG 100

Test Point	C_{rr} [kN-s/m]	UC_{rr} ±[kN-s/m]	C_{tt} [kN-s/m]	UC_{tt} ±[kN-s/m]	C_{tr} [kN-s/m]	UC_{tr} ±[kN-s/m]	C_{rt} [kN-s/m]	UC_{rt} ±[kN-s/m]
1	11.4	0.72	12.2	0.73	2.9	0.12	-2.4	0.17
2	11.4	0.61	12.2	0.66	2.5	0.16	-2.7	0.21
3	12.3	0.43	12.1	0.53	3.1	0.16	-2.3	0.22
4	13.6	1.03	11.8	0.62	2.8	0.44	-2.7	0.3
5	11.9	0.31	12.7	0.42	2.8	0.15	-2.4	0.18
6	12.6	0.41	13.1	0.52	3.3	0.15	-2.3	0.26
7	13.5	0.44	13.0	0.64	3.3	0.1	-2.5	0.22
8	15.8	1.52	13.6	0.73	2.4	0.46	-3.2	0.39
9	13.4	0.21	14.4	0.28	2.9	0.09	-2.5	0.23
10	13.3	0.37	13.8	0.57	3.3	0.13	-2.5	0.26
11	14.0	0.47	14.1	0.73	2.8	0.3	-2.8	0.35
12	16.1	1.71	14.1	0.64	2.8	0.45	-2.6	0.43
13	14.4	0.32	15.5	0.32	3.3	0.12	-2.9	0.31
14	14.5	0.4	14.6	0.39	2.7	0.17	-3.5	0.36
15	14.4	0.41	14.1	0.57	2.8	0.37	-3.1	0.39
16	16.9	1.64	14.8	0.61	2.9	0.45	-2.8	0.27
17	8.8	0.57	9.4	0.58	4.4	0.47	-3.9	0.54
18	9.4	0.56	10.3	0.68	5.1	0.53	-4.3	0.49
19	10.1	0.31	10.8	0.56	5.8	0.35	-5.0	0.47
20	13.7	1.68	11.0	0.47	5.7	0.51	-6.0	0.74
21	11.2	0.56	11.9	0.61	3.8	0.31	-3.4	0.51
22	11.2	0.6	11.6	0.68	5.2	0.8	-3.9	0.4
23	11.8	0.39	12.5	0.85	6.1	0.62	-5.1	0.46
24	14.1	1.23	12.6	0.53	6.0	0.39	-6.1	0.7
25	12.9	0.64	13.9	0.6	4.5	0.29	-3.9	0.41
26	13.1	0.53	12.2	0.61	5.1	0.47	-4.4	0.31
27	13.5	0.4	13.5	0.82	6.4	0.62	-5.2	0.45
28	15.4	2.01	13.1	0.57	5.7	0.32	-5.1	0.51
29	14.4	0.77	15.3	0.77	5.2	0.24	-4.4	0.43
30	13.7	0.78	13.7	0.57	4.5	0.26	-4.5	0.29
31	14.7	0.34	13.0	0.83	6.1	0.4	-5.4	0.43
32	15.1	0.92	13.0	0.62	5.8	0.31	-5.7	0.32

Test Point	C_{rr} [kN-s/m]	UC_{rr} ±[kN-s/m]	C_{tt} [kN-s/m]	UC_{tt} ±[kN-s/m]	C_{tr} [kN-s/m]	UC_{tr} ±[kN-s/m]	C_{rt} [kN-s/m]	UC_{rt} ±[kN-s/m]
33	7.8	1.56	8.2	1.84	6.4	0.63	-5.6	0.56
34	8.9	0.8	9.5	0.92	6.9	0.6	-6.2	0.73
35	10.3	0.44	10.2	1.01	7.9	0.82	-6.8	0.89
36	11.1	1.12	10.0	0.72	8.1	0.83	-8.1	1.28
37	10.4	0.84	11.1	0.8	6.1	0.73	-5.4	0.77
38	11.3	1.14	11.3	1.02	6.4	0.79	-5.7	0.89
39	11.8	0.67	11.2	1.19	7.4	0.36	-6.3	0.8
40	13.2	1.68	11.3	0.69	7.9	0.64	-8.0	0.85
41	12.1	1.39	13.0	1.5	7.1	0.6	-6.2	0.81
42	12.5	1.34	12.6	1.11	6.3	0.86	-5.9	0.85
43	12.7	0.78	11.7	1.14	7.0	0.55	-6.5	0.93
44	14.1	1.38	11.7	0.79	7.9	0.78	-7.7	0.72
45	12.7	1.46	13.6	1.51	7.3	0.51	-6.5	0.67
46	13.4	1.38	12.8	0.99	6.3	0.76	-6.0	0.85
47	13.5	0.93	12.2	1.14	6.9	0.7	-6.4	0.92
48	16.1	1.95	12.6	0.91	8.2	0.97	-7.9	0.89
49	7.5	0.62	8.1	0.66	8.8	0.17	-7.5	0.26
50	7.8	0.68	8.2	0.92	8.8	1.1	-7.8	0.75
51	8.7	0.49	8.7	0.59	9.2	0.91	-8.8	0.78
52	9.8	1.03	8.7	0.65	9.5	1.07	-9.8	1.28
53	9.3	1.23	10.0	1.37	8.9	0.58	-7.8	0.71
54	10.5	0.75	9.7	0.95	9.3	1.04	-7.9	0.97
55	11.6	0.43	10.6	1.09	9.5	0.4	-8.0	0.79
56	13.1	1.23	11.1	0.66	9.8	0.51	-9.7	1.2
57	11.4	0.45	12.3	0.69	9.9	1.57	-8.6	1.58
58	12.0	1	12.1	0.77	8.5	0.69	-8.0	0.89
59	12.5	0.69	11.4	0.94	8.5	0.64	-8.0	0.87
60	13.7	0.92	11.7	0.53	9.7	0.54	-9.7	1.21
61	12.4	1.06	13.4	1.26	9.2	0.62	-7.9	0.81
62	13.0	1.17	12.9	0.99	8.5	0.69	-7.5	0.82
63	13.2	0.77	11.9	0.95	8.3	0.74	-8.0	0.89
64	14.8	1.16	12.2	0.68	9.9	0.63	-9.4	1.05

Table A. 17 Virtual-mass coefficients and uncertainties of CGS with ISO VG 100

Test Point	M_{rr} [kg]	UM_{rr} ±[kg]	M_{tt} [kg]	UM_{tt} ±[kg]	M_{tr} [kg]	UM_{tr} ±[kg]	M_{rt} [kg]	UM_{rt} ±[kg]
1	22.8	0.22	24.8	0.26	-0.3	0.15	0.5	0.17
2	23.7	0.28	24.2	0.37	-0.7	0.21	0.3	0.25
3	25.4	0.4	23.0	0.27	-0.6	0.2	0.1	0.15
4	27.2	1.24	22.2	0.52	0.0	0.72	0.3	0.38
5	21.7	0.15	23.6	0.27	-0.2	0.17	0.3	0.14
6	23.1	0.32	23.3	0.26	-0.2	0.14	0.8	0.09
7	25.6	0.43	22.9	0.31	-0.4	0.17	0.3	0.11
8	27.8	0.73	22.9	0.47	-0.8	0.33	-0.9	0.38
9	21.5	0.19	23.5	0.22	-0.5	0.13	0.6	0.12
10	22.6	0.38	23.5	0.27	-0.2	0.18	1.2	0.15
11	24.6	0.51	23.9	0.38	-0.1	0.27	0.5	0.19
12	28.3	0.8	24.1	0.38	0.6	0.41	1.0	0.17
13	21.2	0.24	23.2	0.39	-1.0	0.18	0.9	0.26
14	22.9	0.35	23.2	0.21	-1.5	0.16	0.0	0.13
15	25.0	0.5	24.8	0.38	-0.4	0.37	0.4	0.13
16	28.6	0.68	24.6	0.34	0.5	0.58	0.7	0.15
17	20.8	0.41	22.5	0.4	1.3	0.57	-1.0	0.6
18	21.5	0.47	22.5	0.41	0.8	0.33	-1.1	0.46
19	22.6	0.3	21.5	0.44	-0.2	0.37	-0.6	0.44
20	24.8	2.22	20.6	0.35	0.2	1.22	-0.1	0.82
21	19.5	0.5	21.0	0.6	0.8	0.44	-0.6	0.44
22	21.2	0.58	22.5	0.45	1.5	0.51	-0.4	0.44
23	23.2	0.46	22.8	0.58	-0.2	0.4	-0.3	0.51
24	24.9	0.78	21.7	0.41	0.0	0.61	-0.4	0.61
25	19.2	0.53	20.8	0.6	0.0	0.22	0.3	0.25
26	21.9	0.51	21.7	0.34	1.9	0.37	0.6	0.26
27	23.3	0.43	23.4	0.55	-0.1	0.43	0.5	0.34
28	25.4	0.6	22.0	0.39	-0.4	0.66	0.7	0.44
29	19.7	0.58	21.6	0.6	-0.6	0.18	0.6	0.2
30	20.9	0.57	22.2	0.47	0.9	0.27	0.3	0.25
31	24.6	0.46	23.1	0.53	0.2	0.24	0.6	0.34
32	25.4	0.46	22.3	0.4	-0.2	0.41	0.3	0.17

Test Point	M_{rr} [kg]	UM_{rr} ±[kg]	M_{tt} [kg]	UM_{tt} ±[kg]	M_{tr} [kg]	UM_{tr} ±[kg]	M_{rt} [kg]	UM_{rt} ±[kg]
33	19.9	1.02	21.5	1.23	0.9	0.32	-0.7	0.26
34	19.5	0.68	20.6	0.4	-1.0	0.5	1.0	0.43
35	20.2	0.53	19.8	0.54	-0.1	0.44	0.9	0.37
36	23.0	0.94	18.9	0.5	0.6	0.53	1.5	0.48
37	19.6	0.65	21.4	0.65	-0.7	0.7	1.0	0.71
38	20.4	0.82	22.3	0.38	-0.2	0.79	1.5	0.5
39	21.5	0.54	22.1	0.59	0.6	0.37	1.0	0.58
40	23.2	0.84	20.3	0.6	-0.4	0.78	0.5	0.41
41	20.7	0.6	22.6	0.67	-1.3	0.52	1.5	0.47
42	21.1	0.74	22.6	0.57	-0.6	0.77	1.5	0.47
43	22.5	0.57	22.8	0.53	0.7	0.54	1.1	0.63
44	23.2	0.71	20.8	0.62	-0.7	0.86	0.8	0.44
45	21.4	0.59	23.5	0.61	-0.8	0.47	1.1	0.4
46	22.3	0.69	22.5	0.57	-0.1	0.7	1.7	0.47
47	23.3	0.73	23.3	0.5	0.9	0.67	1.3	0.64
48	24.6	1.46	21.7	0.83	-0.8	0.91	0.4	0.79
49	16.9	0.22	18.7	0.27	0.0	0.18	0.3	0.31
50	17.9	0.34	18.6	0.55	0.1	0.69	0.8	0.44
51	20.1	0.36	18.9	0.29	-0.3	0.57	1.9	0.34
52	21.8	0.68	17.9	0.37	0.6	0.68	1.4	0.55
53	18.7	0.61	20.2	0.7	-1.0	0.4	1.3	0.35
54	19.0	0.38	19.4	0.61	-0.5	0.59	2.3	0.53
55	20.2	0.24	19.8	0.56	0.5	0.25	1.5	0.38
56	21.5	1.09	19.1	0.35	-0.3	0.57	1.2	0.53
57	17.3	0.56	18.9	0.41	-2.2	0.57	2.4	0.41
58	19.3	0.38	20.3	0.36	-0.5	0.57	1.6	0.37
59	21.2	0.38	21.1	0.47	0.7	0.5	1.2	0.43
60	21.8	0.8	20.2	0.29	-0.7	0.54	0.7	0.42
61	19.6	0.37	21.6	0.45	-0.7	0.49	1.0	0.41
62	20.4	0.41	21.9	0.42	-0.4	0.58	1.4	0.41
63	22.1	0.41	21.8	0.47	0.8	0.64	1.2	0.48
64	22.1	0.75	20.6	0.38	-0.6	0.59	0.8	0.4

Table A. 18 WFR, Keff, Ceff, and uncertainties of CGS with ISO VG 100

Test Point	*WFR* [-]	*UWFR* ±[-]	K_{eff} [MN/m]	UK_{eff} ±[MN/m]	C_{eff} [kN-s/m]	UC_{eff} ±[kN-s/m]
1	0.31	0.02	-0.54	0.06	8.1	0.54
2	0.31	0.02	-0.59	0.07	8.2	0.48
3	0.27	0.01	-0.59	0.09	8.8	0.36
4	0.22	0.04	-0.55	0.17	9.9	0.73
5	0.33	0.01	-0.44	0.05	8.3	0.31
6	0.26	0.01	-0.50	0.07	9.5	0.35
7	0.21	0.01	-0.56	0.09	10.4	0.4
8	0.20	0.01	-0.57	0.16	11.7	0.87
9	0.28	0.01	-0.41	0.05	10.1	0.22
10	0.16	0.01	-0.43	0.08	11.3	0.36
11	0.18	0.02	-0.57	0.11	11.5	0.53
12	0.18	0.03	-0.58	0.16	12.3	0.93
13	0.17	0.01	-0.34	0.07	12.4	0.3
14	0.13	0.01	-0.37	0.07	12.7	0.34
15	0.15	0.01	-0.49	0.11	12.2	0.49
16	0.18	0.03	-0.49	0.14	12.9	0.97
17	0.17	0.03	-2.06	0.18	7.5	0.51
18	0.13	0.02	-2.01	0.19	8.5	0.49
19	0.11	0.02	-1.96	0.16	9.3	0.39
20	0.16	0.04	-1.55	0.37	10.1	0.96
21	0.22	0.02	-2.08	0.19	9.0	0.48
22	0.13	0.02	-1.98	0.23	9.8	0.51
23	0.05	0.02	-2.06	0.18	11.3	0.6
24	0.14	0.03	-1.90	0.24	11.5	0.73
25	0.16	0.01	-2.01	0.21	11.2	0.47
26	0.11	0.01	-1.93	0.18	11.3	0.47
27	0.00	0.00	-2.04	0.22	12.8	0.53
28	0.11	0.03	-2.09	0.19	12.5	1.13
29	0.09	0.01	-1.99	0.21	13.5	0.56
30	0.09	0.01	-2.12	0.18	12.5	0.51
31	0.00	0.00	-2.03	0.21	13.3	0.47
32	0.10	0.01	-2.11	0.16	12.6	0.61

Test Point	*WFR* [-]	*UWFR* ±[-]	K_{eff} [MN/m]	UK_{eff} ±[MN/m]	C_{eff} [kN-s/m]	UC_{eff} ±[kN-s/m]
33	0.24	0.04	-4.18	0.53	6.0	1.22
34	0.10	0.03	-4.27	0.37	8.3	0.66
35	0.09	0.02	-4.27	0.45	9.3	0.55
36	0.15	0.02	-4.05	0.55	8.9	0.73
37	0.19	0.03	-4.26	0.43	8.7	0.68
38	0.11	0.03	-4.81	0.46	10.0	0.82
39	0.04	0.03	-5.01	0.37	10.7	0.7
40	0.12	0.02	-4.53	0.42	10.8	0.98
41	0.15	0.02	-4.64	0.41	10.7	1.05
42	0.13	0.03	-4.95	0.46	10.9	0.92
43	0.03	0.05	-5.17	0.41	11.4	0.74
44	0.10	0.03	-4.76	0.42	11.6	0.87
45	0.12	0.02	-4.87	0.36	11.6	1.07
46	0.12	0.02	-5.13	0.38	11.6	0.97
47	0.05	0.03	-5.36	0.46	12.0	0.79
48	0.11	0.03	-4.68	0.61	12.8	1.13
49	0.26	0.03	-5.51	0.22	5.8	0.48
50	0.20	0.05	-5.67	0.65	6.5	0.67
51	0.13	0.03	-6.79	0.55	7.6	0.48
52	0.20	0.04	-6.70	0.78	7.4	0.76
53	0.26	0.03	-6.22	0.61	7.2	0.95
54	0.11	0.04	-6.23	0.65	8.9	0.78
55	0.03	0.04	-7.75	0.51	10.4	0.58
56	0.10	0.03	-7.43	0.79	10.9	0.77
57	0.14	0.03	-5.54	1.00	10.2	0.52
58	0.13	0.02	-7.23	0.55	10.5	0.69
59	0.08	0.03	-8.51	0.55	10.9	0.64
60	0.09	0.03	-7.94	0.69	11.6	0.61
61	0.14	0.02	-7.77	0.52	11.1	0.87
62	0.14	0.02	-8.44	0.54	11.1	0.82
63	0.09	0.03	-8.86	0.58	11.4	0.7
64	0.09	0.03	-8.12	0.66	12.2	0.73

Predicted Values

Table A. 19 Predicted (flow rate and stiffness) characteristics with ISO VG 2 at centered position

Test Point	Specified ω [RPM]	Specified ΔP [bar]	Specified ε_o [-]	$\dot{Q}$ [lpm]	K_{rr}/K_{tt} [MN/m]	$K_{rt}/-K_{tr}$ [MN/m]
1	2000	2.068	0	43.6	0.5	1.1
5	2000	4.137	0	70.0	1.3	2.4
9	2000	6.205	0	89.7	2.0	4.0
13	2000	8.274	0	107.0	2.6	4.8
17	4000	2.068	0	32.1	0.0	2.2
21	4000	4.137	0	57.7	0.8	2.8
25	4000	6.205	0	78.9	1.7	3.9
29	4000	8.274	0	95.9	2.4	4.9
33	6000	2.068	0	25.2	-0.9	4.3
37	6000	4.137	0	47.1	-0.2	4.5
41	6000	6.205	0	67.3	0.6	5.0
45	6000	8.274	0	83.9	1.4	5.4
49	8000	2.068	0	20.9	-1.9	7.1
53	8000	4.137	0	39.3	-1.4	7.3
57	8000	6.205	0	56.7	-0.8	7.4
61	8000	8.274	0	73.2	0.0	7.7

Table A. 20 Predicted (damping and direct virtual-mass) characteristics with ISO VG 2 at centered position

Test Point	Specified ω [RPM]	Specified ΔP [bar]	Specified ε_o [-]	C_{rr}/C_{tt} [kN-s/m]	$C_{rt}/-C_{tr}$ [kN-s/m]	M_{rr}/M_{tt} [kg]
1	2000	2.068	0	12.2	-0.1	12.1
5	2000	4.137	0	15.7	-1.8	13.1
9	2000	6.205	0	18.4	-3.2	14.2
13	2000	8.274	0	20.4	-2.8	17.3
17	4000	2.068	0	14.7	3.5	12.6
21	4000	4.137	0	18.7	2.1	12.1
25	4000	6.205	0	21.9	0.5	11.8
29	4000	8.274	0	24.0	-0.5	11.9
33	6000	2.068	0	17.6	6.2	12.7
37	6000	4.137	0	20.7	5.6	12.6
41	6000	6.205	0	23.8	4.6	12.4
45	6000	8.274	0	26.3	3.9	12.4
49	8000	2.068	0	20.9	8.5	12.6
53	8000	4.137	0	23.2	8.3	12.7
57	8000	6.205	0	25.6	7.9	12.7
61	8000	8.274	0	28.1	7.3	12.6

Table A. 21 Predicted (flow rate and stiffness) characteristics with ISO VG 46 laminar

Test Point	Specified ω [RPM]	Specified ΔP [bar]	Specified ε_o [-]	$\dot{Q}$ [lpm]	K_{rr} [MN/m]	K_{tt} [MN/m]	K_{tr} [MN/m]	K_{rt} [MN/m]
1	2000	2.068	0	3.4	0.00	0.00	0.22	-0.22
2	2000	2.068	0.27	3.8	0.00	0.00	0.23	-0.22
3	2000	2.068	0.53	4.8	0.00	0.00	0.24	-0.23
4	2000	2.068	0.8	6.6	0.04	0.00	0.38	-0.24
5	2000	4.137	0	6.8	0.00	0.00	0.22	-0.22
6	2000	4.137	0.27	7.5	0.00	0.00	0.23	-0.22
7	2000	4.137	0.53	9.6	0.00	0.00	0.24	-0.23
8	2000	4.137	0.8	13.2	0.01	0.00	0.40	-0.24
9	2000	6.205	0	10.2	0.00	0.00	0.22	-0.22
10	2000	6.205	0.27	11.3	0.00	0.00	0.23	-0.22
11	2000	6.205	0.53	14.4	0.00	0.00	0.24	-0.23
12	2000	6.205	0.8	19.8	0.00	0.00	0.40	-0.24
13	2000	8.274	0	13.5	0.00	0.00	0.22	-0.22
14	2000	8.274	0.27	15.0	0.00	0.00	0.23	-0.22
15	2000	8.274	0.53	19.2	0.00	0.00	0.24	-0.23
16	2000	8.274	0.8	26.5	0.00	0.00	0.40	-0.24
17	4000	2.068	0	3.4	0.00	0.00	0.45	-0.45
18	4000	2.068	0.27	3.8	0.00	0.00	0.45	-0.45
19	4000	2.068	0.53	4.8	0.00	0.00	0.47	-0.45
20	4000	2.068	0.8	6.7	0.12	0.01	0.75	-0.49
21	4000	4.137	0	6.8	0.00	0.00	0.45	-0.45
22	4000	4.137	0.27	7.5	0.00	0.00	0.45	-0.45
23	4000	4.137	0.53	9.6	0.00	0.00	0.47	-0.45
24	4000	4.137	0.8	13.2	0.09	0.00	0.77	-0.49
25	4000	6.205	0	10.2	0.00	0.00	0.45	-0.45
26	4000	6.205	0.27	11.3	0.00	0.00	0.45	-0.45
27	4000	6.205	0.53	14.4	0.00	0.00	0.47	-0.45
28	4000	6.205	0.8	19.9	0.05	0.00	0.78	-0.49
29	4000	8.274	0	13.5	0.00	0.00	0.45	-0.45
30	4000	8.274	0.27	15.0	0.00	0.00	0.45	-0.45
31	4000	8.274	0.53	19.2	0.00	0.00	0.47	-0.45
32	4000	8.274	0.8	26.5	0.02	0.00	0.79	-0.49

Table A. 22 Predicted damping characteristics with ISO VG 46 laminar flow

Test Point	Specified ω [RPM]	Specified ΔP [bar]	Specified ε_o [-]	C_{rr} [kN-s/m]	C_{tt} [kN-s/m]	C_{tr} [kN-s/m]	C_{rt} [kN-s/m]
1	2000	2.068	0	2.14	2.14	0.00	0.00
2	2000	2.068	0.27	2.20	2.15	0.00	0.00
3	2000	2.068	0.53	2.39	2.17	0.00	0.00
4	2000	2.068	0.8	3.91	2.32	0.05	0.05
5	2000	4.137	0	2.14	2.14	0.00	0.00
6	2000	4.137	0.27	2.20	2.15	0.00	0.00
7	2000	4.137	0.53	2.39	2.17	0.00	0.00
8	2000	4.137	0.8	4.03	2.33	0.01	0.01
9	2000	6.205	0	2.14	2.14	0.00	0.00
10	2000	6.205	0.27	2.20	2.15	0.00	0.00
11	2000	6.205	0.53	2.39	2.17	0.00	0.00
12	2000	6.205	0.8	4.06	2.34	0.00	0.00
13	2000	8.274	0	2.14	2.14	0.00	0.00
14	2000	8.274	0.27	2.20	2.15	0.00	0.00
15	2000	8.274	0.53	2.39	2.17	0.00	0.00
16	2000	8.274	0.8	4.06	2.34	0.00	0.00
17	4000	2.068	0	2.14	2.14	0.00	0.00
18	4000	2.068	0.27	2.20	2.15	0.00	0.00
19	4000	2.068	0.53	2.39	2.17	0.00	0.00
20	4000	2.068	0.8	3.84	2.31	0.07	0.07
21	4000	4.137	0	2.14	2.14	0.00	0.00
22	4000	4.137	0.27	2.20	2.15	0.00	0.00
23	4000	4.137	0.53	2.39	2.17	0.00	0.00
24	4000	4.137	0.8	3.91	2.32	0.05	0.05
25	4000	6.205	0	2.14	2.14	0.00	0.00
26	4000	6.205	0.27	2.20	2.15	0.00	0.00
27	4000	6.205	0.53	2.39	2.17	0.00	0.00
28	4000	6.205	0.8	3.98	2.33	0.03	0.02
29	4000	8.274	0	2.14	2.14	0.00	0.00
30	4000	8.274	0.27	2.20	2.15	0.00	0.00
31	4000	8.274	0.53	2.39	2.17	0.00	0.00
32	4000	8.274	0.8	4.03	2.33	0.01	0.01

Table A. 23 Predicted virtual-mass characteristics with ISO VG 46 laminar flow

Test Point	Specified ω [RPM]	Specified ΔP [bar]	Specified ε_o [-]	M_{rr} [kg]	M_{tt} [kg]	M_{tr} [kg]	M_{rt} [kg]
1	2000	2.068	0	9.00	9.00	0.00	0.00
2	2000	2.068	0.27	8.89	8.97	0.00	0.00
3	2000	2.068	0.53	8.63	8.91	0.00	0.00
4	2000	2.068	0.8	8.27	8.81	0.01	0.01
5	2000	4.137	0	9.00	9.00	0.00	0.00
6	2000	4.137	0.27	8.89	8.97	0.00	0.00
7	2000	4.137	0.53	8.63	8.91	0.00	0.00
8	2000	4.137	0.8	8.29	8.81	0.00	0.00
9	2000	6.205	0	9.00	9.00	0.00	0.00
10	2000	6.205	0.27	8.89	8.97	0.00	0.00
11	2000	6.205	0.53	8.63	8.91	0.00	0.00
12	2000	6.205	0.8	8.29	8.81	0.00	0.00
13	2000	8.274	0	9.00	9.00	0.00	0.00
14	2000	8.274	0.27	8.89	8.97	0.00	0.00
15	2000	8.274	0.53	8.63	8.91	0.00	0.00
16	2000	8.274	0.8	8.29	8.81	0.00	0.00
17	4000	2.068	0	9.00	9.00	0.00	0.00
18	4000	2.068	0.27	8.89	8.97	0.00	0.00
19	4000	2.068	0.53	8.63	8.91	0.00	0.00
20	4000	2.068	0.8	8.25	8.80	0.02	0.02
21	4000	4.137	0	9.00	9.00	0.00	0.00
22	4000	4.137	0.27	8.89	8.97	0.00	0.00
23	4000	4.137	0.53	8.63	8.91	0.00	0.00
24	4000	4.137	0.8	8.27	8.81	0.01	0.01
25	4000	6.205	0	9.00	9.00	0.00	0.00
26	4000	6.205	0.27	8.89	8.97	0.00	0.00
27	4000	6.205	0.53	8.63	8.91	0.00	0.00
28	4000	6.205	0.8	8.28	8.81	0.00	0.00
29	4000	8.274	0	9.00	9.00	0.00	0.00
30	4000	8.274	0.27	8.89	8.97	0.00	0.00
31	4000	8.274	0.53	8.63	8.91	0.00	0.00
32	4000	8.274	0.8	8.29	8.81	0.00	0.00

Table A. 24 Predicted (flow rate and stiffness) characteristics with ISO VG 100

Test Point	Specified ω	Specified ΔP	Specified ε_o	$\dot{Q}$	K_{rr}	K_{tt}	K_{tr}	K_{rt}
	[RPM]	[bar]	[-]	[lpm]	[MN/m]	[MN/m]	[MN/m]	[MN/m]
1	2000	2.068	0	1.2	0.00	0.00	0.67	-0.67
2	2000	2.068	0.27	1.3	0.00	0.00	0.67	-0.67
3	2000	2.068	0.53	1.7	0.00	0.00	0.68	-0.70
4	2000	2.068	0.8	2.3	0.02	0.20	0.72	-1.11
5	2000	4.137	0	2.3	0.00	0.00	0.67	-0.67
6	2000	4.137	0.27	2.6	0.00	0.00	0.67	-0.67
7	2000	4.137	0.53	3.3	0.00	0.00	0.68	-0.70
8	2000	4.137	0.8	4.6	0.01	0.17	0.72	-1.13
9	2000	6.205	0	3.5	0.00	0.00	0.67	-0.67
10	2000	6.205	0.27	3.9	0.00	0.00	0.67	-0.67
11	2000	6.205	0.53	5.0	0.00	0.00	0.68	-0.70
12	2000	6.205	0.8	6.9	0.00	0.13	0.73	-1.14
13	2000	8.274	0	4.7	0.00	0.00	0.67	-0.67
14	2000	8.274	0.27	5.2	0.00	0.00	0.67	-0.67
15	2000	8.274	0.53	6.7	0.00	0.00	0.68	-0.70
16	2000	8.274	0.8	9.2	0.00	0.09	0.73	-1.16
17	4000	2.068	0	1.2	0.00	0.00	1.34	-1.34
18	4000	2.068	0.27	1.3	0.00	0.00	1.34	-1.34
19	4000	2.068	0.53	1.7	0.00	0.02	1.35	-1.39
20	4000	2.068	0.8	2.4	0.04	0.43	1.43	-2.19
21	4000	4.137	0	2.3	0.00	0.00	1.34	-1.34
22	4000	4.137	0.27	2.6	0.00	0.00	1.34	-1.34
23	4000	4.137	0.53	3.3	0.00	0.00	1.35	-1.41
24	4000	4.137	0.8	4.7	0.03	0.40	1.44	-2.22
25	4000	6.205	0	3.5	0.00	0.00	1.34	-1.34
26	4000	6.205	0.27	3.9	0.00	0.00	1.34	-1.34
27	4000	6.205	0.53	5.0	0.00	0.00	1.35	-1.41
28	4000	6.205	0.8	6.9	0.02	0.37	1.45	-2.24
29	4000	8.274	0	4.7	0.00	0.00	1.34	-1.34
30	4000	8.274	0.27	5.2	0.00	0.00	1.34	-1.34
31	4000	8.274	0.53	6.7	0.00	0.00	1.35	-1.41
32	4000	8.274	0.8	9.2	0.02	0.33	1.45	-2.26

Test Point	Specified ω [RPM]	Specified ΔP [bar]	Specified ε_o [-]	$\dot{Q}$ [lpm]	K_{rr} [MN/m]	K_{tt} [MN/m]	K_{tr} [MN/m]	K_{rt} [MN/m]
33	6000	2.068	0	1.2	0.00	0.00	2.00	-2.00
34	6000	2.068	0.27	1.3	0.00	0.00	2.01	-2.01
35	6000	2.068	0.53	1.8	0.01	0.04	2.02	-2.07
36	6000	2.068	0.8	2.7	0.07	0.73	2.13	-3.20
37	6000	4.137	0	2.3	0.00	0.00	2.00	-2.00
38	6000	4.137	0.27	2.6	0.00	0.00	2.01	-2.01
39	6000	4.137	0.53	3.4	0.00	0.01	2.03	-2.10
40	6000	4.137	0.8	4.7	0.06	0.61	2.16	-3.32
41	6000	6.205	0	3.5	0.00	0.00	2.00	-2.00
42	6000	6.205	0.27	3.9	0.00	0.00	2.01	-2.01
43	6000	6.205	0.53	5.0	0.00	0.00	2.03	-2.11
44	6000	6.205	0.8	7.0	0.05	0.60	2.16	-3.33
45	6000	8.274	0	4.7	0.00	0.00	2.00	-2.00
46	6000	8.274	0.27	5.2	0.00	0.00	2.01	-2.01
47	6000	8.274	0.53	6.7	0.00	0.00	2.03	-2.11
48	6000	8.274	0.8	9.2	0.04	0.57	2.17	-3.35
49	8000	2.068	0	1.2	0.00	0.00	2.67	-2.67
50	8000	2.068	0.27	1.3	0.00	0.00	2.67	-2.68
51	8000	2.068	0.53	2.0	0.01	0.07	2.68	-2.70
52	8000	2.068	0.8	2.9	0.11	1.33	2.80	-4.05
53	8000	4.137	0	2.3	0.00	0.00	2.67	-2.67
54	8000	4.137	0.27	2.6	0.00	0.00	2.68	-2.69
55	8000	4.137	0.53	3.4	0.00	0.04	2.70	-2.78
56	8000	4.137	0.8	4.9	0.08	0.86	2.87	-4.39
57	8000	6.205	0	3.5	0.00	0.00	2.67	-2.67
58	8000	6.205	0.27	3.9	0.00	0.00	2.68	-2.69
59	8000	6.205	0.53	5.0	0.00	0.01	2.70	-2.81
60	8000	6.205	0.8	7.1	0.07	0.81	2.88	-4.43
61	8000	8.274	0	4.7	0.00	0.00	2.67	-2.67
62	8000	8.274	0.27	5.2	0.00	0.00	2.68	-2.69
63	8000	8.274	0.53	6.7	0.00	0.00	2.70	-2.82
64	8000	8.274	0.8	9.3	0.06	0.80	2.89	-4.44

Table A. 25 Predicted damping characteristics with ISO VG 100

Test Point	Specified ω	Specified ΔP	Specified ε_o	C_{rr}	C_{tt}	C_{tr}	C_{rt}
	[RPM]	[bar]	[-]	[kN-s/m]	[kN-s/m]	[kN-s/m]	[kN-s/m]
1	2000	2.068	0	6.38	6.38	0.00	0.00
2	2000	2.068	0.27	6.39	6.53	0.00	0.00
3	2000	2.068	0.53	6.45	7.11	0.00	0.00
4	2000	2.068	0.8	6.83	11.33	-0.23	-0.25
5	2000	4.137	0	6.38	6.38	0.00	0.00
6	2000	4.137	0.27	6.39	6.53	0.00	0.00
7	2000	4.137	0.53	6.45	7.11	0.00	0.00
8	2000	4.137	0.8	6.87	11.50	-0.18	-0.19
9	2000	6.205	0	6.38	6.38	0.00	0.00
10	2000	6.205	0.27	6.39	6.53	0.00	0.00
11	2000	6.205	0.53	6.45	7.11	0.00	0.00
12	2000	6.205	0.8	6.90	11.65	-0.14	-0.14
13	2000	8.274	0	6.38	6.38	0.00	0.00
14	2000	8.274	0.27	6.39	6.53	0.00	0.00
15	2000	8.274	0.53	6.45	7.11	0.00	0.00
16	2000	8.274	0.8	6.92	11.78	-0.09	-0.10
17	4000	2.068	0	6.38	6.38	0.00	0.00
18	4000	2.068	0.27	6.39	6.53	0.00	0.00
19	4000	2.068	0.53	6.41	7.05	-0.04	-0.05
20	4000	2.068	0.8	6.76	11.20	-0.27	-0.33
21	4000	4.137	0	6.38	6.38	0.00	0.00
22	4000	4.137	0.27	6.39	6.53	0.00	0.00
23	4000	4.137	0.53	6.45	7.11	0.00	0.00
24	4000	4.137	0.8	6.83	11.33	-0.23	-0.25
25	4000	6.205	0	6.38	6.38	0.00	0.00
26	4000	6.205	0.27	6.39	6.53	0.00	0.00
27	4000	6.205	0.53	6.45	7.11	0.00	0.00
28	4000	6.205	0.8	6.86	11.41	-0.21	-0.22
29	4000	8.274	0	6.38	6.38	0.00	0.00
30	4000	8.274	0.27	6.39	6.53	0.00	0.00
31	4000	8.274	0.53	6.45	7.11	0.00	0.00
32	4000	8.274	0.8	6.87	11.50	-0.18	-0.19

Test Point	Specified ω [RPM]	Specified ΔP [bar]	Specified ε_o [-]	C_{rr} [kN-s/m]	C_{tt} [kN-s/m]	C_{tr} [kN-s/m]	C_{rt} [kN-s/m]
33	6000	2.068	0	6.38	6.38	0.00	0.00
34	6000	2.068	0.27	6.39	6.53	0.00	0.00
35	6000	2.068	0.53	6.36	7.00	-0.06	-0.09
36	6000	2.068	0.8	6.54	10.99	-0.34	-0.56
37	6000	4.137	0	6.38	6.38	0.00	0.00
38	6000	4.137	0.27	6.39	6.53	0.00	0.00
39	6000	4.137	0.53	6.43	7.08	-0.02	-0.02
40	6000	4.137	0.8	6.80	11.28	-0.24	-0.28
41	6000	6.205	0	6.38	6.38	0.00	0.00
42	6000	6.205	0.27	6.39	6.53	0.00	0.00
43	6000	6.205	0.53	6.45	7.11	0.00	0.00
44	6000	6.205	0.8	6.83	11.33	-0.23	-0.25
45	6000	8.274	0	6.38	6.38	0.00	0.00
46	6000	8.274	0.27	6.39	6.53	0.00	0.00
47	6000	8.274	0.53	6.45	7.11	0.00	0.00
48	6000	8.274	0.8	6.85	11.37	-0.21	-0.23
49	8000	2.068	0	6.38	6.38	0.00	0.00
50	8000	2.068	0.27	6.37	6.52	-0.01	-0.01
51	8000	2.068	0.53	6.22	6.95	-0.08	-0.19
52	8000	2.068	0.8	6.28	10.58	-0.46	-0.85
53	8000	4.137	0	6.38	6.38	0.00	0.00
54	8000	4.137	0.27	6.39	6.53	0.00	0.00
55	8000	4.137	0.53	6.41	7.05	-0.04	-0.05
56	8000	4.137	0.8	6.76	11.20	-0.27	-0.33
57	8000	6.205	0	6.38	6.38	0.00	0.00
58	8000	6.205	0.27	6.39	6.53	0.00	0.00
59	8000	6.205	0.53	6.44	7.09	-0.01	-0.01
60	8000	6.205	0.8	6.81	11.29	-0.24	-0.27
61	8000	8.274	0	6.38	6.38	0.00	0.00
62	8000	8.274	0.27	6.39	6.53	0.00	0.00
63	8000	8.274	0.53	6.45	7.11	0.00	0.00
64	8000	8.274	0.8	6.83	11.33	-0.23	-0.25

Table A. 26 Predicted virtual-mass characteristics with ISO VG 100

Test Point	Specified ω	Specified ΔP	Specified ε_o	M_{rr}	M_{tt}	M_{tr}	M_{rt}
	[RPM]	[bar]	[-]	[kg]	[kg]	[kg]	[kg]
1	2000	2.068	0	9.28	9.28	0.00	0.00
2	2000	2.068	0.27	9.25	9.16	0.00	0.00
3	2000	2.068	0.53	9.19	8.90	0.00	0.00
4	2000	2.068	0.8	9.06	8.50	-0.03	-0.03
5	2000	4.137	0	9.28	9.28	0.00	0.00
6	2000	4.137	0.27	9.25	9.16	0.00	0.00
7	2000	4.137	0.53	9.19	8.90	0.00	0.00
8	2000	4.137	0.8	9.08	8.52	-0.01	-0.01
9	2000	6.205	0	9.28	9.28	0.00	0.00
10	2000	6.205	0.27	9.25	9.16	0.00	0.00
11	2000	6.205	0.53	9.19	8.90	0.00	0.00
12	2000	6.205	0.8	9.08	8.53	-0.01	-0.01
13	2000	8.274	0	9.28	9.28	0.00	0.00
14	2000	8.274	0.27	9.25	9.16	0.00	0.00
15	2000	8.274	0.53	9.19	8.90	0.00	0.00
16	2000	8.274	0.8	9.09	8.54	0.00	0.00
17	4000	2.068	0	9.28	9.28	0.00	0.00
18	4000	2.068	0.27	9.25	9.16	0.00	0.00
19	4000	2.068	0.53	9.17	8.88	-0.02	-0.01
20	4000	2.068	0.8	9.01	8.48	-0.05	-0.04
21	4000	4.137	0	9.28	9.28	0.00	0.00
22	4000	4.137	0.27	9.25	9.16	0.00	0.00
23	4000	4.137	0.53	9.19	8.90	0.00	0.00
24	4000	4.137	0.8	9.06	8.50	-0.03	-0.03
25	4000	6.205	0	9.28	9.28	0.00	0.00
26	4000	6.205	0.27	9.25	9.16	0.00	0.00
27	4000	6.205	0.53	9.19	8.90	0.00	0.00
28	4000	6.205	0.8	9.07	8.51	-0.02	-0.02
29	4000	8.274	0	9.28	9.28	0.00	0.00
30	4000	8.274	0.27	9.25	9.16	0.00	0.00
31	4000	8.274	0.53	9.19	8.90	0.00	0.00
32	4000	8.274	0.8	9.08	8.52	-0.01	-0.01

Test Point	Specified ω [RPM]	Specified ΔP [bar]	Specified ε_o [-]	M_{rr} [kg]	M_{tt} [kg]	M_{tr} [kg]	M_{rt} [kg]
33	6000	2.068	0	9.28	9.28	0.00	0.00
34	6000	2.068	0.27	9.25	9.16	0.00	0.00
35	6000	2.068	0.53	9.12	8.86	-0.03	-0.02
36	6000	2.068	0.8	8.72	8.40	-0.12	-0.05
37	6000	4.137	0	9.28	9.28	0.00	0.00
38	6000	4.137	0.27	9.25	9.16	0.00	0.00
39	6000	4.137	0.53	9.18	8.89	-0.01	-0.01
40	6000	4.137	0.8	9.04	8.50	-0.04	-0.03
41	6000	6.205	0	9.28	9.28	0.00	0.00
42	6000	6.205	0.27	9.25	9.16	0.00	0.00
43	6000	6.205	0.53	9.19	8.90	0.00	0.00
44	6000	6.205	0.8	9.06	8.50	-0.03	-0.03
45	6000	8.274	0	9.28	9.28	0.00	0.00
46	6000	8.274	0.27	9.25	9.16	0.00	0.00
47	6000	8.274	0.53	9.19	8.90	0.00	0.00
48	6000	8.274	0.8	9.07	8.51	-0.02	-0.02
49	8000	2.068	0	9.28	9.28	0.00	0.00
50	8000	2.068	0.27	9.24	9.16	0.00	0.00
51	8000	2.068	0.53	8.95	8.83	-0.05	-0.01
52	8000	2.068	0.8	8.40	8.29	-0.17	0.04
53	8000	4.137	0	9.28	9.28	0.00	0.00
54	8000	4.137	0.27	9.25	9.16	0.00	0.00
55	8000	4.137	0.53	9.17	8.88	-0.02	-0.01
56	8000	4.137	0.8	9.01	8.48	-0.05	-0.04
57	8000	6.205	0	9.28	9.28	0.00	0.00
58	8000	6.205	0.27	9.25	9.16	0.00	0.00
59	8000	6.205	0.53	9.19	8.89	0.00	0.00
60	8000	6.205	0.8	9.05	8.50	-0.03	-0.03
61	8000	8.274	0	9.28	9.28	0.00	0.00
62	8000	8.274	0.27	9.25	9.16	0.00	0.00
63	8000	8.274	0.53	9.19	8.90	0.00	0.00
64	8000	8.274	0.8	9.06	8.50	-0.03	-0.03

APPENDIX B

WHIRL FREQUENCY RATIO DEFINITION

The WFR (Φ) as formulated by San Andrés [8] which accounts for cross-coupled virtual-mass is defined as

$$\Phi^4 I_4 + \Phi^2 (I_2 - 1) + \Phi_o^2 = 0 \tag{B.1}$$

where I_4 in Eq. (B.1) is

$$I_4 = \omega^2 \frac{I_1^2 + M_{XY} M_{YX}}{C_{XX} C_{YY} - C_{XY} C_{YX}} \tag{B.2}$$

and where I_2 in Eq. (B.1) is

$$I_2 = \frac{K_{XY} M_{YX} + K_{YX} M_{XY} - I_1 (K_{XX} + K_{YY}) + 2 K_{XY} I_1}{C_{XX} C_{YY} - C_{XY} C_{YX}} \tag{B.3}$$

and where I_1 in Eq.'s (B.2) and (B.3) is

$$I_1 = \frac{C_{YX} M_{XY} + C_{XY} M_{YX}}{C_{XX} + C_{YY}} \tag{B.4}$$

and where Φ_0 in Eq. (B.1) is

$$\Phi_0^2 = \frac{(K_{eq} - K_{XX})(K_{eq} - K_{YY}) - K_{XY} K_{YX}}{\omega^2 (C_{XX} C_{YY} - C_{XY} C_{YX})} \tag{B.5}$$

where K_{eq} in Eq. (B.2) is

$$K_{eq} = \frac{K_{XX} C_{YY} + K_{YY} C_{XX} - K_{XY} C_{YX} - K_{YX} C_{XY}}{C_{XX} + C_{YY}} \tag{B.6}$$

APPENDIX C

UNCERTAINTY ANALYSIS

Seal tests conducted in this report used nearly identical equipment, with only minor modifications, as Moreland [13]. The uncertainty analysis used the same method and techniques; Moreland's discussion on uncertainty analysis is given here:

"Instrument error is assumed to be negligible and only repeatability is calculated for the uncertainty of measurements. A 95% confidence interval is used to calculate the uncertainties for static measurements and the dynamic stiffness values. The true mean, μ, of a set of sample measurements, x_i, lies within the confidence interval

$$\bar{x} - t_{\alpha/2,\nu}\frac{S_x}{\sqrt{n}} < \mu < \bar{x} + t_{\alpha/2,\nu}\frac{S_x}{\sqrt{n}} \tag{C.1}$$

where $\bar{x}$ is the sample mean, $t_{\alpha 2/,\nu}$ is the Student's *t*-distribution value, the level of significance is α=1−c, c = 0.95 is the level of confidence, the degrees of freedom are ν=1−n, and n is the number of samples. The standard deviation is

$$S_x = \sqrt{\frac{\left(\sum_{i=1}^{n} x_i^2\right) - n\bar{x}^2}{n-1}} \tag{C.2}$$

Recalling Eqs. (21)-(23) of Section 7.2 used to calculate the rotordynamic coefficients from curve fits to the dynamic stiffness data, the confidence intervals on the rotordynamic coefficients are determined using a statistical test described in [26]. The true slope of a least-squares regression lies within the c% confidence interval

$$b \pm t_{\alpha/2,\nu}\frac{s_{y/x}}{s_{xx}} \tag{C.3}$$

where the standard error of the y-data about the curve fit is

$$s_{y/x} = \left(\frac{1}{n-2}\sum_{i=1}^{n}[y_i - y(x_i)]^2\right)^{1/2} \tag{C.4}$$

and the total squared variation of the independent variable, x_i, is

$$S_{xx}^2 = \sum_{i=1}^{n}(x_i - \bar{x})^2 \tag{C.5}$$

Finally, the true intercept lies within the interval

$$a \pm t_{\alpha/2,\nu}s_{y/x}\sqrt{\frac{1}{n} + \frac{\bar{x}^2}{S_{xx}^2}} \tag{C.6}$$

Confidence intervals of the rotordynamic coefficients are propagated into the confidence intervals on the WFR and C_{eff} values. Uncertainty propagation is defined as"

$$u_y = \sqrt{\left(\frac{\partial y}{\partial x_1} u_1\right)^2 + \left(\frac{\partial y}{\partial x_2} u_2\right)^2 + \cdots + \left(\frac{\partial y}{\partial x_n} u_n\right)^2} \quad \text{(C.7)}$$